SUPPLEMENTARY MATERIAL for

"Bi-allelic *ACBD6* variants lead to a neurodevelopmental syndrome with progressive and complex movement disorders"

SUPPLEMENTARY MATERIALS AND METHODS

Supplementary Method 1: Relative real-time PCR

Supplementary Method 2: Minigene splicing assay

Supplementary Method 3: Functional studies in zebrafish

Supplementary Method 4: Functional studies in *Xenopus tropicalis*

Supplementary Method 5: Immunofluorescence and microscopy of peroxisomes

Supplementary Method 6: YnMyr metabolic labelling and proteomics analysis

Supplementary Method 7: *Acbd6* Gene Expression in the Adult Mouse Brain

SUPPLEMENTARY RESULTS

Supplementary Result 1: *ACBD6* variants

Supplementary Results 2: Zebrafish studies

Supplementary Results 3: Loss of *ACBD6* does not impact on peroxisome function

Supplementary Results 4: Proteomics data

SUPPLEMENTARY FIGURES

Supplementary Figure 1: In silico splice prediction and Sanger sequencing on cDNA amplified from patient fibroblasts and relative real time PCR in affected individual and wild-type in family 1.

Supplementary Figure 2. RNA analysis of the *ACBD6* c.664-2A>G variant

Supplementary Figure 3: ***Acbd6*** **Gene Expression in the Adult Mouse Brain**

Supplementary Figure 4: *ACBD6* is conserved across species and zebrafish *acbd6* exhibits high expression during development and similar tissue-specific expression patterns to human

Supplementary Figure 5: Zebrafish *acbd6*-/- exhibited a reduction in mRNA expression, and displayed a hyperactive behavior when changed to dark at 6 dpf.

Supplementary Figure 6: Zebrafish *acbd6*-/- displayed hyperactive behavior when the light on but reduced locomotor activity in the dark period at 12 dpf.

Supplementary Figure 7: Zebrafish *acbd6*-/- displayed abnormal behaviors in 30-minute light-dark cycles at 6 and 12 dpf.

Supplementary Figure 8: Zebrafish *acbd6*-/- displayed abnormal histology in the eye and muscle at 30 dpf.

Supplementary Figure 9: Zebrafish adult acbd6-/- mutants exhibited autism spectrum disorder-like behavior.

Supplementary Figure 10: Zebrafish *acbd6* F_0 knockout showed craniofacial dysmorphism.

Supplementary Figure 11: Zebrafish *acbd6* F_0 knockouts showed a similar but worse abnormal behaviors than stable homozygous mutants at 6 dpf.

Supplementary Figure 12: Zebrafish *acbd6* F_0 knockout showed an overall reduction of locomotor activities at 12 dpf.

Supplementary Figure 13: The *acbd6* F_0 knockout showed an increased motor axonal branches

Supplementary Figure 14: The *acbd6* F_0 knockout showed a progressive muscle degeneration

Supplementary Figure 15: The elevated *mbpa* expression was detected in *acbd6* F_0 knockouts as well as in homozygous mutants, and the downregulated expression of acbd6 mRNA in F0 knockouts was confirmed using RT-qPCR

Supplementary Figure 16: Targeted disruption of *acbd6* exon 1 generates F_0 crispants bearing insertion-deletion changes in vivo.

Supplementary Figure 17: Survival, movement and morphology of abcd6 cripspant tadpoles.

Supplemental Figure 18: Chemical proteomics analysis of *N*-myristoylation in fibroblasts of a ACBD6 deficient patient and a healthy sibling.

Supplemental Figure 19: Chemical and whole proteome analysis of wild-type and *ACBD6* crispant zebrafish.

Supplemental Figure 20: Whole proteome meta-analysis of wild-type and *ACBD6* crispant zebrafish.

Supplemental Figure 21: Chemical and whole proteome analysis of wild-type and *ACBD6* crispant *X. tropicalis*.

Supplemental Figure 22: Whole proteome meta-analysis of wild-type and *ACBD6* crispant *X. tropicalis*.

Supplementary Figure 23: Comparison of overlap in identified (potential) N-myristoylated proteins between Homo sapiens, Danio rerio and Xenopus tropicalis.

SUPPLEMENTARY TABLES

Supplementary Table 1: **Detailed clinical description and *ACBD6* variant characteristics**

Supplementary Table 2: ***ACBD6* variant details including pathogenicity prediction and presence in genomic databases.**

Supplementary Table 3: **The frequency of facial dysmorphic features**

Supplementary Table 4: **Detailed dysmorphic features of the *ACBD6* cohort members with available facial photographs**

Supplementary Table 5: **Peroxisomal VLCFA β-oxidation is normal in *ACBD6*-deficient patient fibroblasts.**

Supplementary Table 6: **Primer list for zebrafish studies**

Supplementary Table 7: **Disorders to consider in the differential diagnosis of *ACBD6*-related disease**

SUPPLEMENTARY CASE REPORTS

SUPPLEMENTARY VIDEO RECORDINGS FROM PATIENTS

SUPPLEMENTARY VIDEO RECORDINGS FROM ZEBRAFISH MODELS

SUPPLEMENTARY VIDEO RECORDINGS FROM *X. TROPICALIS* MODELS

SUPPLEMENTARY REFERENCES

SUPPLEMENTARY MATERIALS AND METHODS

Supplementary method 1: Relative real-time PCR (back)

Total RNA was extracted from case and control fresh blood and fibroblast cells, using Tripure reagent (Roche, Nutley, NJ), iScript cDNA synthesis kit (Bio-Rad, California, USA) was used to synthesise cDNAs. To evaluate the expression of *ACBD6*, the cDNAs were amplified by SYBR green method in Applied Biosystems® 7500 Real-Time PCR Systems (USA) by specific primers (sequences available upon request). The optimal thermal condition with cycle time was as follows: 10 min at 95°C, 35 cycles of 15 s at 95°C, 30 s at 58°C, and 45 s at 72°C. For analysis, the real-time PCR data were normalized to *GAPDH*. We used the ΔΔCT method for the evaluation of gene expression in patients relative to control.

Supplementary method 2: Minigene splicing assay (back)

RNA studies to assay the effect of the c.664-2A>G variant were performed as previously described.[1,2] Briefly, exon 7 (31 bp), as well as flanking intronic 5' (235 bp) and 3' (104 bp) sequence was directly PCR amplified from a control individual and the proband with primers containing an additional *Xho*I and *Bam*HI restriction site (forward primer with *Xho*I restriction site: 5'-aattctcgagTGGAGTAACTGGTCATCCTGT-3' and reverse primer with *Bam*HI restriction site: 5'-attggatccTGCCAGGTACCTATCTAAGCACT-3'). After PCR amplification and clean-up, restriction enzyme digestion of the PCR fragment and pSPL3 exon trapping vector was performed prior to ligation between exon A and exon B of the linearized pSPL3-vector. The vector was transformed into DH5α competent cells (NEB 5-alpha, New England Biolabs), plated and incubated overnight. The wild-type (WT) and mutant-containing vector sequences were Sanger sequence confirmed. To test the effect of the c.694+1G>A variant, site-directed mutagenesis using the WT pSPL3 vector was performed using primers (forward: 5'-CTACATTATGaTAAGAAGTTTCTAAATTATTAAG-3' and reverse: 5'-AGCTGTTTGGCCTTCATTG-3') designed with NEBase Changer version 1.3.3 (New

England Biolabs). Colonies cultured overnight for next-day plasmid isolation were Sanger sequence verified.

Vectors containing homozygous and WT sequence were transfected into HEK 293T cells (ATCC) at a density of $2x10^5$ cells per mL. 1 µg of the respective pSPL3 vectors were transiently transfected using 6 µl of FuGENE 6 Transfection Reagent (Promega). An empty vector and transfection negative reactions were included as controls. The transfected cells were harvested 24 hours after transfection. Total RNA was prepared using miRNAeasy Mini Kit (Qiagen). Approximately 1 µg of RNA was reverse transcribed using a High Capacity RNA-to-cDNA Kit (Applied Biosystems) following the manufacturer's protocols. The cDNA was PCR amplified using vector-specific SD6 forward (5'-TCTGAGTCACCTGGACAACC-3') and SA2 reverse (5'-ATCTCAGTGGTATTTGTGAGC-3') primers. The amplified fragments were visualized on a 1% agarose gel and Sanger sequenced.

Supplementary Methods 3: Functional studies in zebrafish (back)

Sequence comparisons

The GenBank accession numbers of the compared proteins are listed as follows: human ACBD6 (NP_115736.1), mouse ACBD6 (NP_082526.2), Chicken Acbd6 (NP_001264476.1), *Xenopus tropicalis* (*X. tropicalis*) Acbd6 (NP_001089443.1) and zebrafish Acbd6 isoform 1 (NP_001020626.1). Amino acid sequences were aligned and analyzed using ClutalW and viewed by JalView.

Zebrafish *acbd6* mutant and F_0 knockout generated by CRISPR/Cas9 technology

To generate a stable mutant line, the selection of CRISPR/Cas9 target site for *acbd6* and the synthesis of single guide RNAs (sgRNAs, acbd6_1/2/3) were previously described.[3] For F_0 knockout, three target sites were designed for CRISPR/Cas9 mutagenesis using the CRISPOR tool, and sgRNAs (acbd6_4/5/6) were synthesized by Synthego Inc. A 6 µL mixture containing

1 μL of 40 μM Cas9-NLS protein (UC Berkeley QB3 Macrolab, Berkeley, CA, USA), 500 ng of each sgRNA (in 3 μL), and 2 μL of 1 M potassium chloride was injected into the WT Tab-5 genetic background at the one-cell stage. The *slc45a2* sgRNA, which inactivates the pigment formation gene, was used to reduce pigments in larvae for better neuronal development tracking. Only the *slc45a2* sgRNA was injected into the control, while it was co-injected with *acbd6* sgRNAs (*acbd6* F_0) in the *Tg(mnx1:GFP;olig2:DsRed)* line. Supplementary Table 6 lists the sgRNA target sequences.

Rescue constructs and site-directed mutagenesis

The full-length coding sequence of zebrafish *acbd6* was PCR amplified from cDNA prepared from a pool of mRNA extracted from embryos of different stages, using primers listed in Supplementary Table 6. The purified PCR product was digested with *Bam*HI and *Eco*RI restriction enzymes (Thermo Fisher Scientific, CA, USA) and cloned into the pCS2+ vector (kindly gifted by Dr. David Turner, University of Michigan). A human *ACBD6* cDNA clone was purchased from Genscript (Cat # OHu04984), and PCR amplified using primers containing the zebrafish Kozak sequence at 5' and restriction enzyme sites as listed in Supplementary Table 6. The purified product was digested and cloned into the pCS2+ vector. The resulting clone was sequence verified, and the plasmids pCS2+ACBD6 and pCS2+acbd6 were used as templates for mRNA synthesis and other downstream applications. Patient-specific mutations were introduced using pCS2+ACBD6 as a template with a QuickChange II site-directed mutagenesis kit (Agilent Technologies Inc, CA, USA), following the manufacturer's instructions with primers listed in Supplementary Table 6.

***In vitro* transcription of capped mRNA synthesis for rescue and variant test**

To generate zebrafish *acbd6* and human *ACBD6* mRNA (including WT and two variants) pCS2+ plasmids from above were linearized by *Not*I, and the RNA was transcribed *in vitro* using mMessage mMachine SP6 Transcription kit (Invitrogen, CA, USA). For *acbd6* F_0 rescue

experiments, a mixture of WT or variant mRNA was co-injected with a sgRNAs/Cas9-NLS mixture.

RNA extraction and reverse transcription quantitative real-time PCR (RT-qPCR)

Total RNA was extracted from uninjected control and *acbd6* F_0 knockout animals using TRIzol Reagent (Thermo Fischer Scientific, Waltham, MA, USA). The experiment was performed in four biological replicates and each replicate containing 6 animals. The RNA purification was done by using miRNeasy Mini kit (Qiagen, Hilden, Germany) and followed the manufacturer's instructions.

The mRNA was reverse transcribed into cDNA using iScript cDNA-synthesis kit (Bio-Rad, Hercules, CA, USA) according to the manufacturer's instructions. The cDNA was used as a template for RT-qPCR reactions using SYBR Green Supermix (Thermo Fisher Scientific) and the Light Cycler® 96 System (Roche, Pleasanton, CA, USA) according to the manufacturer's instructions. All relative quantifications were done using three independent experimental replicates and three technical replicates per amplification, and the values were normalized to the housekeeping gene *18S*. The primer sequences for RT-qPCR are shown in Supplementary Table 6. The quantification was performed using 2^(-ΔΔCT) method and corresponding age-matched control samples as calibrators.

Morphological phenotyping and imaging

For bright field imaging, animals were anesthetized in Tricaine/MS-222 (Sigma-Aldrich), randomly selected, and manually oriented within an agarose cavity mold or 2% methylcellulose (Sigma, USA). A high-definition Nikon DS-Fi2 camera mounted on a Nikon SMZ18 stereomicroscope (Nikon, Japan) was used for imaging. The head and eye sizes were measured directly from scale-calibrated images using ImageJ software (NIH). The head length was measured by tracing a line from the tip of the snout to the end of the otic vesicle, while eye diameter was used for eye size measurements.

Immunofluorescent analysis

Phalloidin staining was performed as previously described.[4] Briefly, larvae were euthanized with tricaine and fixed in 4% (V/V) paraformaldehyde (PFA) at 6 and 12 dpf. The larvae were washed sequentially with PBSTx and incubated in Alexa Fluor 488 Phalloidin (1:50) (Invitrogen, CA, USA) in PBSTw (1% PBS, 0.1% Tween-20) at room temperature (RT). After a series of washes, the larvae were laterally mounted in 1.5% low melting point agarose (Sigma-Aldrich, MO, USA), and images were acquired using a Zeiss LSM-710 Confocal microscope.

Pentylenetetrazole (PTZ) treatment

At 4 dpf, larvae were transferred to individual wells of a 48-well plate containing E3 medium, which was adjusted to a volume reaching 500 µL after adding pentylentetrazol (PTZ) (P6500, Sigma Aldrich, MO, USA), and then sealed with paraffin film to minimize evaporation. The next day, a fresh PTZ stock solution (200 mM in water) was added to each well to achieve concentrations of 1 mM, 5 mM, 10 mM, 15 mM, and 20 mM, or PTZ-free E3 medium as negative controls. Locomotion tracking was performed immediately after treatment.

Zebrafish behaviour analysis

All behavior tests were conducted at RT. To analyze visual startle response (VSR), larval movements were tracked in Zebrabox behavior chambers (Viewpoint Life Sciences, Montreal, Canada) as previously described.[5] The percentage of responses was calculated from the number of responses to five light stimuli for each larva. For the light-dark transition test, larvae at either 5 or 11 dpf were transferred to 96-well plates, with each well containing a single larva in 150 µL embryo water, which was sealed with paraffin film. The next day, the plate was placed in a Noldus chamber, and the DanioVision system running EthoVision XT software (Noldus Information Technology, Leesburg, VA, USA) was used to record and analyze locomotion activity. Specifically, 6 dpf larvae were given a 30-minute habituation period in the dark followed by a 10-minute light-dark transition for three cycles. In another behavior assay, larvae were given a 30-minute habituation period in the light followed by a 30-minute dark-light transition. The distance traveled in millimeters (mm) for each minute and the velocity in

millimeters per second (mm/s) were recorded. The values for each minute were plotted using GraphPad Prism version 9.5 (GraphPad Software, San Diego, CA, USA). To assess the locomotion activity of larvae treated with PTZ, we recorded the activity of one fish per well in Zebrabox behavior chambers with a recording time bin of 10 minutes for a total of 6 cycles, as described previously.[6] Specifically, each 10-minute time bin comprised 2 minutes of light (100%) and 2 minutes of dark (0%), and the average distance traveled by each larva (from 6 cycles) was plotted using GraphPad Prism.

For adult social behavior, experiments were conducted in an opaque, white, 3-D printed tank with 2 chambers separated by a clear divider. 8-month-old fish were acclimatized for an hour before testing. The room lights were set to half intensity and a light pad on minimum power was used under the testing tank to eliminate shadows. The testing area was kept as quiet as possible during testing, and fresh system water was used for each trial. The fish were allowed to habituate in the test tank for 15 seconds before starting the 10 minute test time.[7] Videos were recorded and analyzed using Noldus EthoVision XT software. The software was used to define the arenas (each chamber of the test tank) and zones of interest (area approaching the clear divider in both chambers). The software was also used to collect data about the time spent inside or outside of the zone, as well as the distances moved both inside and outside of the zone and overall time spent.

Alcian blue staining

Alcian blue staining was performed to visualize the cartilage development in the head of the 8 dpf larvae as per earlier described method.[8] Briefly, 8 dpf larvae were euthanized and fixed in 4% PFA at RT for 2 hours, and then washed with PBSTw followed by bleaching with 3% H_2O_2 and 0.5% KOH for 30 minutes. After additional wash, larvae were stained overnight with 0.01% Alcian blue stain prepared in 60 mM $MgCl_2$ and 70% ethanol. After staining, larvae were washed with washing buffer and rinsed through 0.1% KOH and glycerol series.

Statistical analysis

The statistical analysis was performed using GraphPad Prism. Data are presented as indicated in figure legends. In all the analyses, the significance level was set to 0.05. The *p*-value was determined as below: One-way ANOVA with Tukey's multiple comparisons test for eye and head size, eyes distance, Meckel's cartilage length, and articulation distance comparisons. One-way Brown-Forsythe and Welch ANOVA tests with multiple comparisons corrected by Dunnett's T3 test for all behavioral analysis and RT-qPCR experiments. The unpaired Student *t* test incorporating Welch's correction was used for RT-qPCR experiments of *acbd6* expression in controls, and F_0 knockouts, as well as for assessing distance traveled in adult social behavior tests. For evaluating time spent inside or outside designated zones during adult social behavior tests, the Mann-Whitney test was utilized.

Supplementary methods 4: Functional studies in frog (back)

Outbred Nigerian WT strain *X. tropicalis* were housed and maintained in recirculating systems (MBK Installations) at 25ºC with 15% daily water changes on 12-hour light-dark cycles. Adult *Xenopus* were maintained in translucent dark grey tanks with lily pads providing environmental enrichment. Adult animals were fed thrice daily, five days per week, on a mixed equal diet of Horizon 23 and Eternal 25 pellets (Skretting). Juvenile *X. tropicalis* were fed twice daily seven days per week on a mixed diet consisting of Sera Micron and Spirulina (Sera). Fertilised embryos were obtained from adult *X. tropicalis* as described in Macken *et al.*[9] *X. tropicalis* embryos and tadpoles were maintained in 0.05X Marc's Modified Ringers solution (1X MMR: 0.1M NaCl, 2 mM KCl, 1mM $MgSO_4$, 2mM $CaCl_2$, 5mM HEPES, pH 7.4), in fill and dump set ups with 50% media changes every other day. Animals were staged throughout their early development according to Zahn *et al* .[10] All procedures were conducted in accordance with the Home Office Code of Practice, under PP4353452 with approval from the University of Portsmouth's Animal Welfare and Ethical Review Body.

Generating F_0 *acbd6* crispant animals

The exon structure of the *acbd6* gene in *X. tropicalis* and humans is identical. The target region within *acbd6* exon 1 was identified using Xenbase (genome V10; http://www.xenbase.org), and two single-stranded oligonucleotides (sgRNA68 - taatacgactcactataGGACTCTTCCAGTACCCCAGgttttagagctagaa, sgRNA71 - taatacgactcactataGGAGTGGGACGAGAAGACAGgttttagagctagaa) were selected with high predicted mutagenic activity (values 68 and 71 respectively), minimal predicted off-target events (CRISPRscan, http://www.crisprscan.org) and a high frameshift frequency (inDelphi mESC model: 79.7% (sgRNA68) and 78% (sgRNA71) https://indelphi.giffordlab.mit.edu). sgRNA were synthesised from single-stranded oligonucleotides (Invitrogen) as described in Macken *et al*. Each sgRNA (600 pg) was co-injected with Cas9 protein (2.6 ng, spy Cas9 NLS, NEB), within 1 hour of fertilisation (1-cell stage) into WT strain *X. tropicalis* embryos. CRISPR/Cas9 experiments include un-injected control tadpoles and *tyr*$^{-/-}$ control tadpoles (sgRNA71(2) - taatacgactcactataGCTGTTGTAGGCAATCGGGgttttagagctagaa) to test that any generated phenotype is specific to disruption of *acbd6*.

To determine indel formation and mosaicism in the crispant embryos, the target region within *acbd6* was amplified from genomic DNA extracts (Lysis Buffer: 50 mM Tris (pH 8.5), 1 mM EDTA, 0.5% [v/v] Tween-20, 100 µg/ml Proteinase K) by polymerase chain reaction, using primers designed in Primer3 (http://primer3.ut.ee; Exon1 forward primer: GGACCTTTGGCGATGCTTTT, Exon1 reverse primer: CAGGTTGATAGCTTCTCCGC). Indel formation was subsequently confirmed using Sanger sequencing (Genewiz). The resulting ab1 trace files were visualised using SnapGene®5.2.4. software and the penetrance of indels in each trace was assessed using ICE analysis.[11]

Phenotypic analysis of F_0 *acbd6* crispant animals

Crispant tadpoles were anaesthetised in 2% MS222 and fixed in 4% PFA following the method described for wholemount *in situ* hybridisation of *X. tropicalis* embryos.[12] For assessment of the cartilaginous structures of the tadpole head, tadpoles were fixed in 4% PFA overnight at 4°C and then immediately placed in the sterile-filtered Alcian Blue solution as described in Young et al. 2017.[13] After staining, samples were washed, de-stained and bleached before soft-tissues were cleared in progressive KOH-glycerol washes, with increasing concentrations of glycerol. Further gross morphological differences between un-injected tadpoles and crispant tadpoles were identified using a Zeiss Axio Zoom.V16 Stereomicroscope and CL9000 LED light source (Carl Zeiss Microscopy). Measurements of the area of the tadpole head were conducted within Zen and followed the external surface of the tadpole head from the snout to the vent, encompassing both eyes. Detailed structural differences were further examined by high-resolution microcomputed tomography (MicroCT) following the protocol previously described in Macken et al.[9]

Tadpole locomotion was assessed at stage NF45 using a Zantiks MWP unit (Zantiks Ltd, Cambridge, UK) in a standard 6-well plate over a 10-minute period (following a 20 second acclimatisation period). Each 6-well plate was filled with 0.05 X MMR and contained a dilute but equally distributed tadpole food mix and lights were maintained on during each trial (to match the rearing conditions of the tadpoles). An infra-red video camera was used to track and record the movement of individual animals with data from each trial output as distance moved in mm in 1 second time-bins.

Data and statistical analysis

Grouped data are shown as the mean ± standard deviation with analysis of measurements of head size and tadpole locomotion conducted using an Independent t-test.

Supplementary method 5: Immunofluorescence and microscopy of peroxisomes (back)

Immunofluorescence and microscopy of peroxisomes

Fibroblasts were grown in high-glucose DMEM supplemented with 10% (v/v) fetal bovine serum, 2 mM glutamine, 5 mM non-essential amino acids and 1% (v/v) MEM vitamins (Thermo Fisher Scientific). COS-7 cells (CRL-1651; ATCC) were cultured in DMEM high glucose (4.5 g/L) supplemented with 10% (v/v) FBS, 100 U/mL penicillin, and 100 µg/mL streptomycin at 37°C with 5% CO_2 and 95% humidity. Cells grown on glass coverslips were fixed for 20 minutes with 4% (v/v) PFA in PBS (pH 7.4), permeabilised with 0.2% Triton X-100 and blocked with 1% BSA. Cells were then incubated with primary and secondary antibodies for 1 hour in a humid chamber. Rabbit anti-PEX14 (1:1400)[14] (generated by D. Crane, Griffith University, Brisbane, Australia), mouse anti-catalase (1:200) (ab179843; Abcam), mouse anti-ATPB (1:500) (ab14730; Abcam) or mouse anti-Myc primary antibody (1:100) (Santa Cruz Biotechnology, Inc (9E10)) were used. Species-specific Alexa Fluor 488 (594) labelled secondary antibodies were applied (1:500) (Thermo Fisher Scientific). Cells were washed 3 times with PBS between each individual step. Finally, coverslips were washed with ddH_2O to remove PBS and mounted on glass slides in Mowiol 4-88-containing n-propyl gallate for anti-fading.[15] Cells were observed using an Olympus IX81 microscope (Olympus) equipped with an UPlanSApo 100×/1.40 oil objective (Olympus) and a CoolSNAP HQ2 CCD camera. Digital images were taken and processed using VisiView software (Visitron Systems). Images were adjusted for contrast and brightness using MetaMorph 7 (Molecular Devices).

For calculation of peroxisomal number in control and patient fibroblasts, an in-house ImageJ[16] macro was used, utilising the Analyze Particles function. A Kruskal-Wallis ANOVA test with Dunn's multiple comparisons was used to determine statistical differences between groups. . Bar graphs are presented as mean ± SD. Analysis was performed from at least three independent experiments.

To determine ACBD6 localisation, COS-7 cells were transfected with a Myc-ACBD6 plasmid using diethylaminoethyl (DEAE)-dextran as described.[15] Cells were processed for

immunofluorescence 24 hours after transfection. To generate the Myc-ACBD6 construct, the coding sequence for human *ACBD6* was amplified with flanking *Bam*HI and *Xho*I restriction sites using the following primers: Forward - CACGGATCCGCTTCATCATTCCTGCCCGCG, Reverse – GTGCTCGAGTTAAGCCTTGCCAGTTGTGT. The PCR product and the vector pCMV-Tag3B (Agilent) were both digested with *Bam*HI and *Xho*I and ligated to generate the plasmid pCMV-Myc-ACBD6, expressing the ACBD6 protein with a Myc tag at the N-terminus from a CMV promoter. The construct was verified by sequencing before use.

Supplementary method 6: YnMyr metabolic labelling and proteomics analysis (back)

YnMyr metabolic labelling of patients' (ACBD6 deficient) and healthy fibroblasts

In triplicate for each condition, fibroblasts derived from a single healthy individual and patient (*ACBD6* deficient) were seeded in 10 cm plates and allowed to grow to ≈ 80% confluence. Cells were incubated for 1 h with DMSO or 100 nM IMP-1088, followed by a metabolic labelling pulse of 20 μM YnMyr for 18 h. Then, cells were washed twice with PBS before they were dissociated by trypsinization. The cells were suspended in culture media and centrifuged at 1500g for 5 min to pellet the cells. The supernatant was removed and the cells were washed by suspending them in PBS followed by another centrifugation step at 1500g for 5 min. Cells were lysed in lysis buffer (50 mM HEPES pH 7.4, supplemented with 0.5% (v/v) NP-40, 0.25% (w/v) SDS, 2 mM $MgCl_2$, Benzonase Nuclease (Merck E1014), and EDTA-free protease inhibitor cocktail (Roche, 11873580001) and allowed to incubate for 10 min at RT. Total protein concentrations were determined by BCA assay and concentrations were adjusted to 2 mg/mL for each sample. Lysates were stored at -80°C until further analysis.

Samples were thawed on ice. Lysates were incubated with premixed CuAAC ('click') ligation reagents (100 μM Azide-PEG3-biotin conjugate (Merck 762024), 1 mM $CuSO_4$, 1 mM TCEP and 100 μM TBTA) while shaking for 1 h at RT. The click reaction was quenched with

10 mM EDTA. Proteins were precipitated ($MeOH/CHCl_3/H_2O$ at 1:0.25:1 final ratio), the protein pellet was washed with MeOH and suspended in 2% (w/v) SDS, 10 mM EDTA in PBS (pH 7.4) at 1 mg/mL protein. Samples were subjected to pull-down. Enrichment of Azide-PEG3-biotin conjugate-labelled YnMyr-labelled proteins was carried out with NeutrAvidin Agarose beads (Pierce, 29201) as described previously.[17-19]

Further proteomics sample preparation, analysis and processing were performed as described previously.[20,21] The mass spectrometry proteomics data have been deposited to the ProteomeXchange Consortium via the PRIDE[22] partner repository with the dataset identifier PXD024957.

YnMyr chemical proteomics and whole proteome analysis of zebrafish and X. tropicalis model systems

YnMyr metabolic labelling of zebrafish

In triplicate for each condition, 12 WT and *acbd6* F_0 crispant zebrafish embryos were incubated with 20 µM YnMyr for 24 h, either between 48-72 hpf or 96-120 hpf. After labelling, zebrafish were washed twice with fresh egg water, deyolked, flash frozen in liquid nitrogen and stored at -80°C until further analysis.

YnMyr metabolic labelling of X. tropicalis

In quadruplicate for each condition, 10 *acbd6* WT, 68 *acbd6* crispant and 71 crispant *X. tropicalis* embryos were incubated with 20 µM YnMyr for 17 h. After labelling, embryos were washed twice with fresh 0.05 x MMR, flash frozen in liquid nitrogen and stored at -80°C until further analysis.

Lysis

Samples were thawed on ice, resuspended in lysis buffer (1% (v/v) Triton X-100, 0.1% (w/v) SDS in PBS, pH 7.4, supplemented with EDTA-free protease inhibitor cocktail (Roche,

11873580001) and homogenized by probe sonication and on ice. Homogenates were centrifuged at 17,000 g for 5 min and supernatant was retained. Total protein concentrations were determined by BCA assay and concentrations were adjusted to 1 mg/mL for each sample.

Chemical proteomics of YnMyr-labelled proteins

Lysates (300 µg) were incubated with premixed CuAAC ('click') ligation reagents (100 µM AzRB[23], 1 mM $CuSO_4$, 1 mM TCEP and 100 µM TBTA) while shaking for 1 h at RT. The click reaction was quenched, proteins precipitated and washed, followed by enrichment of the biotinylated YnMyr-labelled proteins, on-bead reduction, alkylation, digestion by trypsin and peptide desalting, as described previously.[17-19]

Whole proteome analysis

Lysates (30 µg) were precipitated, subjected to reduction, alkylation, digestion by trypsin and peptide desalting, as described previously.[17-19]

Proteomics processing and meta-analysis

Proteomics sample preparation and processing were performed as described previously. [20,21] Zebrafish and *X. tropicalis* proteins with N-terminal glycine (at position 2, behind initiator methionine) were mined from UniProt-deposited proteomes (UP000000437 and UP000008143, respectively). Human orthologues proteins were mapped to zebrafish and *X. tropicalis* proteomes with gprofiler2 R package[24] and finally matched to evidence of co-translational and post-translational *N*-myristoylation of human proteins. Pairwise comparison-generated lists of up- or down-regulated proteins in *acbd6* crispants were used to perform pathway enrichment analysis and the subsequent disease-related network enrichment using Metacore (Clarivate).

Supplementary Methods 7: *Acbd6* Gene Expression in the Adult Mouse Brain (back)

10x Genomics RNA expression in the adult mouse whole cortex and hippocampus were visualized using the gene expression atlas provided by the Allen Institute for Brain Science.[25-27]

SUPPLEMENTARY RESULTS

Supplementary Result 1: *ACBD6* variants (back)

Using WES and homozygosity mapping, we identified 20 homozygous *ACBD6* variants in 27 unrelated families including six frameshift, eight nonsense, three splicing, one in-frame, one large deletion and one missense variants. Affected individuals in family 1 showed a splice acceptor variant (c.574-2A>G) located in intron 5 within ~ 30 Mb stretch of homozygosity (GRCh37/hg19, chr.1: 162 458 412–192 781 639), resulting in an acceptor site loss, with possible cryptic acceptor site activation in exon 6. In silico and RNA studies in fibroblasts of patient and related healthy/WT sibling confirmed cryptic acceptor site activation, deleting 5 nucleotides in exon 6, and introducing a premature stop codon (r.576_580del, p.(Arg193SerfsTer7))(Supplementary Fig. 1). Affected individuals from families 2 and 21 shared the same homozygous c.82dupG, p.(Val28GlyfsTer6) frameshift variant in exon 1. In family 21, the parents denied known consanguinity, but came from a small village. Homozygosity mapping from exome data suggested less than 5th-degree parental relatedness. The probands in families 3, 16 and 17 disclosed a homozygous frameshift variant c.484_488delATATT, p.(Ile162Ter) in exon 5. The homozygous region in family 3 spans13 Mb. The proband in family 4 revealed a homozygous nonsense variant c.760C>T, p.(Arg254Ter) in exon 8. The probands in families 5 and 15 showed a homozygous nonsense variant c.187G>T, p.(Glu63Ter), in exon 1, affecting a conserved ACB domain. This variant resided within a 35.22 Mb region of homozygosity in family 15. Affected individuals from family 6 revealed a homozygous in-frame insertion variant c.654_656dupTAA, p.(Asn219dup) in exon 6 within a 42.6 Mb region of homozygosity. The proband in family 7 disclosed a

homozygous frameshift variant c.474delA, p.(Asp159ThrfsTer16) in exon 5. The cases in family 8 revealed a homozygous frameshift variant c.285delA, p.(Lys95AsnfsTer23) in exon 2, affecting an ACB domain and residing within a 50.93 Mb homozygosity stretch. The proband in family 9 uncovered a homozygous nonsense variant c.594G>A, p.(Trp198Ter) in exon 6. The probands in families 10 and 19 indicated a homozygous missense variant c.602A>G, p.(Asp201Gly) in exon 6. This variant introduces a glycine at this position that is very flexible and can disturb the required rigidity of the protein. The proband in family 11 uncovered a homozygous nonsense variant c.539C>A, p.(Ser180Ter) in exon 5. The proband in family 12 showed a splice variant c.694+1G>A in intron 7. The proband in family 13 identified a splice variant c.664-2A>G, residing within a 34.46 Mb region of homozygosity. *In silico* analysis and RNA studies of the c.694+1G>A and c.664-2A>G variants using an *in vitro* splice assay validated exon skipping of the 31bp exon 7, resulting in a frameshift and introduction of a premature stop codon (p.(Asp222ProfsTer10)). Additionally, the c.694+1G>A variant showed evidence of activation of a cryptic splice donor site (p.(Ala232AspfsTer8)). In family 14, the proband showed a frameshift variant c.719_723delTTGTA, p.(Ile240ArgfsTer9) in exon 8 residing within an 18.06 Mb homozygosity stretch. The proband in family 18 identified a nonsense variant c.217A>T, p.(Lys73Ter)) in exon 1. The probands in families 20 and 25 showed a nonsense variant c.160C>T, p.(Gln54Ter) in exon 1. In family 20, this variant resides within a 15.18 Mb homozygous region. Affected individuals in family 22 identified a nonsense variant c.280C>T, p.(Gln94Ter) in exon 2. The probands in families 23 and 24 identified a large deletion variant (c.664-18556_694+8366del, p.(?)), affecting a large region of the *ACBD6* sequence which resulted in the absence of the 31bp exon 7. The proband in family 26 revealed a homozyougs nonsense variant c.216C>A, p.(Tyr72Ter) in exon 1. The probands in families 27 uncovered a homozygous duplication variant c.360dupA, p.(Leu121ThrfsTer27) in exon 3. The specific and conserved domain of *ACBD6*, Ankyrin, was disrupted in the probands of families 1, 4, 6, 9, 10 and 11, 12, 13, 14, and 19 (Fig. 1B).

Supplementary Results 2: Zebrafish studies (back)

Functional domains of human *ACBD6* are highly conserved across species, including zebrafish (Supplementary Fig. 4A). Our RT-qPCR results indicate that zebrafish *acbd6* mRNA is maternally distributed and continuously expressed at high levels during development (Supplementary Fig. 4B). Additionally, we observed high levels of *acbd6* mRNA in the testis, brain, kidney, and eyes, as well as other tissues, indicating a consistent expression pattern with human *ACBD6* mRNA as reported in FANTOM5 and GTEx expression datasets (Supplementary Fig. 4C-E).

Given the *acbd6* mutants showed reduced VSR, we hypothesized that the mutant was insensitive to sudden light changes rather than completely blind. Therefore, we recorded the locomotion of the mutants during 10-minute time intervals of light-dark cycles. The findings indicated that *acbd6*-/- mutants retained a response to light changes (Fig. 3F) but exhibited as gradual decline in locomotor activity during the dark period (Fig. 3G). Furthermore, homozygous *acbd6* mutants displayed a transient elevation of locomotion at the first minute after light off (Fig. 3H) but not after light on (Supplementary Fig. 5B). A detailed analysis of the light-switching period revealed that *acbd6*-/- mutants demonstrated an exaggerated response during the first 30 seconds after light off (Supplementary Fig. 5C, D), suggesting a hypertonia-like or hyperkinetic disorder-like behavior. Additionally, the mutants showed lower locomotor activity in the first second after light off (Supplementary Fig. 5E), consistent with the lower number of VSR observed in the mutants. As individuals affected by defective *ACBD6* present a progressive disease course, we therefore analyzed the mutants at 12 dpf. The result demonstrated that *acbd6*-/- mutants consistently had lower locomotor activity in dark periods (Fig. 3I, J). However, the hyperactive behavior was no longer present (Supplementary Fig. 6A, B). Surprisingly, the *acbd6*-/- mutants demonstrated an increased distance moved in the light period (Fig. 3I, K) and multiple locomotor bursts were observed in further analysis of the data

(Supplementary Fig. 6C), indicating light-induced seizure-like behavior. To further validate whether these behaviors were consistently observed in different light-dark cycles, we habituated the mutants to light and performed 30-minute light-dark cycles (Supplementary Fig. 7A-F). Similar to the 10-minute light-dark cycles at both 6 and 12 dpf, *acbd6*-/- mutants displayed the same abnormal behaviors confirming the specificity of our observation As the fish developed to 30 dpf, we observed a declining population of *acbd6*-/- mutants (Fig. 3L), and survivors exhibited an extremely small body (Fig. 3M) compared to either *acbd6*+/+ or *acbd6*+/- animals, suggesting that loss of *Acbd6* may cause increased mortality and severe developmental delay. Histological analysis showed an overall reduction in homozygous mutant brain size (Fig. 3N-W) compared to either *acbd6*+/+ or *acbd6*+/-, including telencephalon (Fig. 3O-Q), optic tectum (Fig. 3R-T), cerebellum (Fig. 3U-W) and retina (Supplementary Fig. **8**A-C). Notably, we observed that skeletal muscle fibers in *acbd6*-/- mutants were not only shortened but also exhibited a scattered pattern accompanied by many empty spaces (Supplementary Fig. **8**D-F), suggesting a disrupted muscular phenotype. In contrast to humans, who could receive careful care and attention, the *acbd6*-/- mutants exhibited a general weakness and an inability to compete for food or space, which ultimately leads to reduced chances of survival and delayed overall growth. However, *acbd6*-/- mutants isolated in a separate tanks exhibited favorable survive rates and some fish reach comparable developmental milestones to their control counterparts (data not shown). Interestingly, abnormal social behavior was observed in adult *acbd6*-/- mutants (Supplementary Fig. 9), including spending less time in the defined interaction zone (Supplementary Fig. 9A, B) and having a longer latency to enter the zone (Supplementary Fig. 9C) resulting in more time spent outside of the interaction zone (Supplementary Fig. 9D). In addition, *acbd6*-/- mutants travelled shorter distances within the interaction zone (Supplementary Fig. 9E) and had slightly higher movement outside of zone, although this difference was not statistically significant (Supplementary Fig. 9F). Moreover, *acbd6*-/- mutants travelled a shorter total distance traveled during a 10-minute period, but this

difference was not statistically significant (Supplementary Fig. 9G). Overall, this less social preference behavior is reminiscent of autism spectrum disorder-like behavior.[28]

We hypothesized that the loss of Acbd6 could increase susceptibility to chemical-induced seizures due to erratic locomotor activities in both *acbd6*-/- mutants which may indicate seizure-like behavior. Therefore, we subjected *acbd6* F_0 and control larvae to different doses of PTZ, and found that *acbd6* F_0 larvae displayed similar locomotor activities to the control larvae at doses of less than 10 mM PTZ, but exhibited aggressive hyperexcited behavior with doses over 15 mM PTZ (Fig. 5J). This data suggests that the downregulation of *ACBD6* in patients may contribute to the onset of epilepsy-like seizures as suggested by the increased sensitivity of *acbd6* F_0 larvae to higher doses of PTZ. Since individuals with biallelic *ACBD6* variants showed progressive abnormal movement, we investigated the impact of *acbd6* F_0 knockout on neuronal and skeletal muscle development. We used a transgenic reporter line *Tg(mnx1:GFP;olig2:DsRed)*, that labels motor neurons and oligodendrocytes and found that *acbd6* F_0 larvae displayed excessive axonal arborizations in both motor axons and oligodendrocytes, which worsened as larvae developed (Fig. 4K-N and Supplementary Fig. 13). Additionally, we observed progressive degeneration of muscle fibers during development using phalloidin staining (Fig. 4O-T and Supplementary Fig. 14). We also noted a gradual increase in myelin basic protein a *(mbpa*) expression during development in *acbd6* F_0 knockouts (Supplementary Fig. 15A), which may explain the abnormal axonal development phenotype. Interestingly, upregulated *mbpa* expression was detected in the homozygous mutant as well (Supplementary Fig. 15B). Additionally, the *acbd6* mRNA expression was down-regulated in the *acbd6* F_0 knockouts (Supplementary Fig. 15C). Our zebrafish model replicated many of the clinical features seen in individuals with bi-allelic variants in *ACBD6*, indicating how these variants contribute to disease progression. Our extensive analysis of both *acbd6* mutant and F_0

zebrafish provides insight into the underlying disease mechanisms observed in affected individuals.

Supplementary Result 3: Loss of ACBD6 does not impact on peroxisome function (back)

The localisation of PEX14 and catalase at peroxisomes further indicates that peroxisomal membrane and PTS1 (peroxisomal targeting signal 1)-dependent matrix import are normal. The morphology of mitochondria, which are elongated in fibroblasts, was also not altered when compared to controls (Fig. 3 A-C).

Furthermore, fatty acid analysis after a D3-C22:0 loading test in cultured fibroblasts did not reveal any abnormalities of peroxisomal VLCFA β-oxidation (Supplementary Table 5). Peroxisomal β-oxidation of D3-C22:0 (presented as ratio D3-C16:0/D3-C22:0) was within the reference range (controls), but highly reduced in fibroblasts from a Zellweger Spectrum Disorder (ZSD) patient lacking peroxisomal metabolic functions (Supplementary Table 5). The D3-C26:0 levels were also within reference range (control), but highly elevated in ZSD fibroblasts indicative of fatty acid elongation and accumulation of VLCFA (Supplementary Table 5). In contrast to the loss of ACBD6, ACBD5 deficient fibroblasts show a reduction in VLCFA β-oxidation and an accumulation of VLCFA.[29,30] We can conclude from these studies that ACBD6 deficiency does not cause alterations to peroxisomal VLCFA β-oxidation or peroxisome biogenesis. In addition, expression of a Myc-ACBD6 construct in COS-7 cells confirmed a cytoplasmic and nuclear localisation of Myc-ACBD6[20] but did not provide evidence for a peroxisomal localisation under standard culture conditions (Fig. 3C).

Supplementary Results 4: Proteomics analyses of developing WT and *acbd6* F_0 zebrafish and frog knockouts (back)

To shed light on the potential role of *ACBD6* on *N*-myristoylation during zebrafish development, we employed metabolic labelling with YnMyr and chemical proteomics at

different stages of development. At 72 and 120 hpf, both WT and *acbd6* F_0 zebrafish express >32 significantly enriched *N*-myristoylated proteins, for each of which the human orthologue is a validated co-translationally *N*-myristoylated substrate (Supplemental Fig. 19A-D). In addition, significantly enriched proteins also included >48 proteins with N-terminal glycine, thereby potentially *N*-myristoylated, but where unequivocal evidence of *N*-myristoylation is currently lacking the human orthologue, or where the human orthologue does not possess an N-terminal glycine. At 72 hpf, an increased abundance of YnMyr-labelled proteins is observed in the *acbd6* F_0, including Marcks and Chchd-related proteins, known to be co-translationally *N*-myristoylated in humans (Fig. 7A). Of note, zebrafish express duplications of multiple proteins, including the aforementioned Marcks- and Chchd-related proteins (Fig. 7A). Conversely, several zebrafish proteins with N-terminal glycines, unique for zebrafish and not found with a N-terminal glycine in humans, are significantly reduced in the *acbd6* F_0, including Crygm2d18 (Crystallin, gamma M2D18), predicted to be involved in lens development in camera-type eye and visual perception, Sfpq (Splicing factor proline/glutamine rich), associated with brain development, CNS neuron axonogenesis and midbrain-hindbrain boundary initiation), and various myosin-type proteins (Myh7, Smyhc1), linked to muscle-related diseases (Fig. 7A). Shown in Fig. 7B, at 120 hpf, in addition to the previous, a significant reduction is observed for Fus and Fusl, and further reductions among myosin-related proteins (Myh1, Myh6, A0a8m9ppa1 and A0a8m9pjw6).

We next performed whole proteomics analysis comparing WT and *acbd6* F_0 at 72 and 120 hpf (Supplementary Fig.19E, F, respectively). Meta-analysis of up-regulated proteins in *acbd6* F_0 revealed a significant involvement of translation- and metabolism-related pathways (Supplementary Fig. 20A), and significant enrichments into disease networks, including myopathy, frontotemporal dementia and delayed speech and language development (Supplementary Fig. 20B). Down-regulated proteins are significantly involved in pathways related to nervous system development, as well as neurodegeneration (Fig.7C). Enriched

disease-related networks include myopathy, optic atrophy, dystonia muscle spasticity and movement disorders, a striking similarity with the observations in human patients (Supplementary Fig. 20C). At 120 hpf, meta-analysis of the whole proteome data reveals similar enrichments (Supplementary Fig. 20D-G). Notably, upregulated proteins enrich in translation- and metabolism-related pathways, and significant enrichments in disease-networks of myopathy, whereas downregulated proteins further enrich in pathways of neurological development and disease, including optic atrophy and spasticity (Supplementary Figure 20G).

Similar to the chemical proteomics analyses in zebrafish, we used YnMyr labelling to identify *N*-myristoylated substrates and pathways affected by loss of ACBD6 in developing *X. tropicalis.* Here, WT, crispant 68 or crispant 71 *X. tropicalis* were metabolically labelled from 1 hpf to 18 hpf, due to the previously reported growth arrest. Chemical proteomics of YnMyr labelling revealed >10 *X. tropicalis* proteins which' human orthologues are known to be co-translationally *N*-myristoylated, including a duplication of Marcks, as well as *X. tropicalis* proteins which share the N-terminal glycine with their orthologue in humans (Supplementary Fig. 21A-C). Comparing WT with *acbd6* crispant 68 and 71 (Figs. 7D and E, respectively) reveals a marked depletion of YnMyr-labelled proteins in the crispants, including all identified *X. tropicalis* proteins with co-translationally *N*-myristoylated human orthologues. Both crispants reveal prominent and significant reductions in proteins including Marcks, Ppm1b, Ppm1g, Znf628 (Associated with Fowler syndrome, encephaloclastic proliferative vasculopathy, hydranencephaly-hydrocephaly syndrome), and to a lesser extent, Slc44a2 (Choline transporter, associated with peripheral vertigo and Meniere disease) and Xb5768883 (Neurofilament heavy polypeptide, uncharacterized, inferred from NCBI XP_002933698.2). Whole proteome analysis of WT *X. tropicalis* and the crispants 68 and 71 (Supplementary Figs. 21D, E, respectively) revealed a reduced abundance of myosin-related proteins (Myh2, Myh4, Myh8, Smarcc1), Klhdc4, associated with Huntington Disease-like 2, as well as reductions in Ppm1b, Fus and both forms of Marcks.

Meta-analysis of upregulated proteins in crispants 68 revealed significantly affected pathways include those involved in translation and metabolism (Figure 7F). The 'Parkinson-disease'-specific pathway was highly significantly enriched. Downregulated proteins associate similarly to general translation- and metabolism-related pathways (Supplementary Fig. 22A) and enrich in disease networks encompassing cancer as well as various neurological disorders, including retinitis pigmentosa 13 (leading to eye defects), as well as myelodysplastic-type diseases (Supplementary Fig. 22B). Moreover, mapping the upregulated proteins into disease networks revealed lactic acidosis as the most prominently enriched (Supplementary Fig. 22C), however, Leigh disease and other neurological diseases dominate the top-20 of most confidently identified diseases. Meta-analysis of *acbd6* crispant 71 resulted in highly similar findings (Supplementary Figs. 22D-G), with notably higher significances of retinitis pigmentosa among the most significantly enriched disease networks, as well as myopathy (Supplementary Fig. 22G).

We next analysed the overlap of differentially YnMyr-enriched proteins between human skin fibroblasts (Figure 6D and Supplementary Figure 18) and those identified from similar comparisons in zebrafish (Figure 7A-B and Supplementary Figure 19) and *X. tropicalis* (Figure 7D-E and Supplementary Figure 21). A partial overlap between all three organisms is observed when selecting proteins directly identified by the presence of a N-terminal glycine (Supplementary Figure 23A), which improves when selecting for proteins that have a human orthologue with a N-terminal glycine (Supplementary Figure 23B). The number of co-translationally *N*-myristoylated proteins overlap markedly between *Homo sapiens* and *Danio rerio* (32) as well as between *Homo sapiens* and *X. tropicalis* (15). Human skin fibroblasts, zebrafish and *X. tropicalis* have differential expression of MARCKS, PPM1B, PPM1G and FUS, with *Homo sapiens* and *Danio rerio* additionally differentially expressing CHCHD3 and CHCHD6 proteins, reportedly involved in neurological disorders (Supplementary Figure 23D). No co-translationally *N*-myristoylated proteins overlap specifically between *Danio rerio* and *X.*

tropicalis, most likely caused by different timepoint during development as well as the gastrulation defects observed in *X. tropicalis* at 18 hpf. In terms of post-translational *N*-myristoylation, substantially less proteins were identified (Supplementary Figure 23E), with FUS, HSPA4 and NCL shared between human skin fibroblasts, zebrafish and *X. tropicalis* with FUS reportedly involved in neurological disorders (Supplementary Figure 23F).

Supplementary Figure 1

A

C

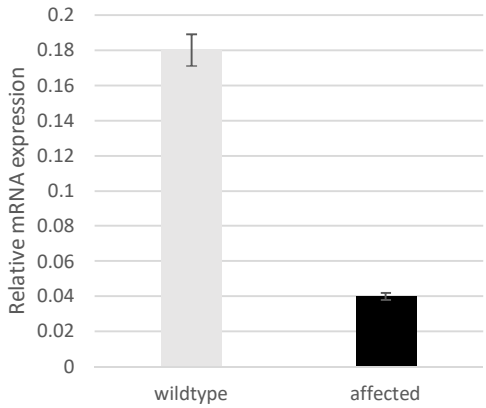

B

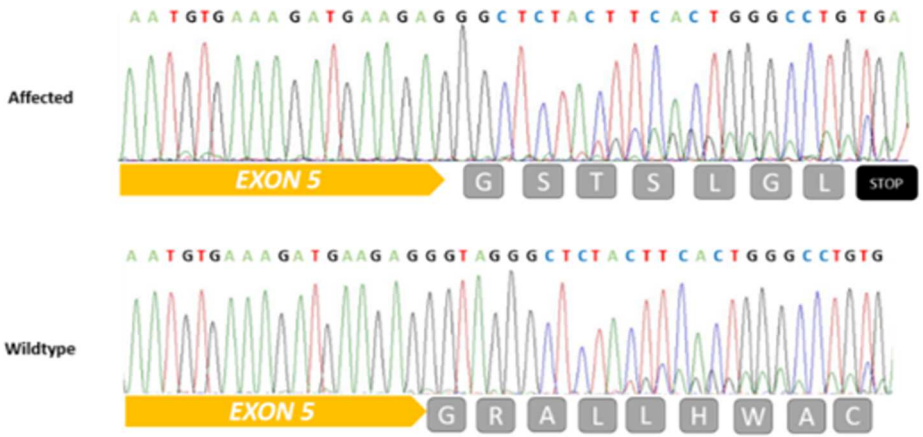

SUPPLEMENTARY FIGURE LEGENDS

Supplementary Figure 1: *In silico* splice prediction and Sanger sequencing on cDNA amplified from patient fibroblasts and relative real-time PCR in patient and wild-type in family 1

(A) Predicted effect of the c.574-2A>G variant on the canonical splice site (visualized with Alamut® Visual). The A>G variant at the canonical splice acceptor site of intron 5 causes a complete loss of the native splice site and activation of a cryptic splice acceptor site. (B) cDNA amplification and Sanger sequencing of patient and control RNA showed that it activated the first cryptic acceptor site in exon 6 and introduced a premature stop codon after 8 amino acids. The effect of the cryptic splice activation causes frameshift variant r.576_580delp.(Arg193SerfsTer7) (C) Relative expression level of *ACBD6* in patient and wildtype control shows significantly decreased level of mRNA in case (p value= 0.0002).

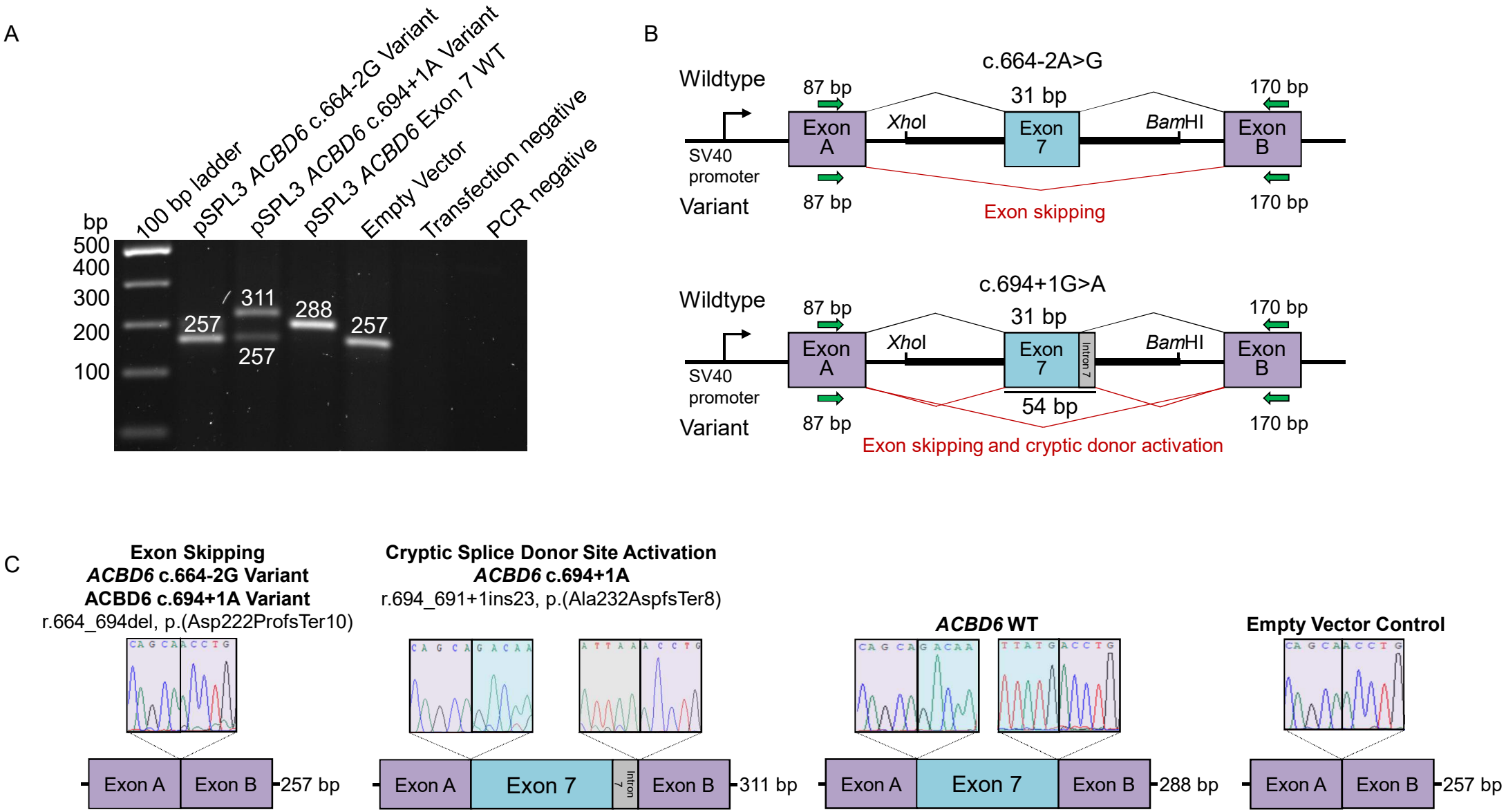
A
100 bp ladder
pSPL3 ACBD6 c.664-2G Variant
pSPL3 ACBD6 c.694+1A Variant
pSPL3 ACBD6 Exon 7 WT
Empty Vector
Transfection negative
PCR negative
bp
500
400
300
200
100
257
311
257
288
257
B
c.664-2A>G
Wildtype
87 bp
31 bp
170 bp
Exon A
XhoI
Exon 7
BamHI
Exon B
SV40 promoter
Variant
87 bp
170 bp
Exon skipping
c.694+1G>A
Wildtype
87 bp
31 bp
170 bp
Exon A
XhoI
Exon 7
Intron 7
BamHI
Exon B
SV40 promoter
54 bp
Variant
87 bp
170 bp
Exon skipping and cryptic donor activation
C
Exon Skipping
ACBD6 c.664-2G Variant
ACBD6 c.694+1A Variant
r.664_694del, p.(Asp222ProfsTer10)
Cryptic Splice Donor Site Activation
ACBD6 c.694+1A
r.694_691+1ins23, p.(Ala232AspfsTer8)
ACBD6 WT
Empty Vector Control
Exon A
Exon B
257 bp
Exon A
Exon 7
Intron 7
Exon B
311 bp
Exon A
Exon 7
Exon B
288 bp
Exon A
Exon B
257 bp

Supplementary Figure 2. RNA analysis of the *ACBD6* c.664-2A>G variant

(A) Gel electrophoresis of the RT-PCR of the *ACBD6* c.664-2G variant, c.694+1A variant, Exon 7 WT, and empty pSPL3 vector amplicons. Transfection negative and PCR negative controls performed as expected.

(B) Vector construct of the *in vitro* splice assay showing exon 7 inserted between vector exons A and B with schematic illustration of splicing outcomes for the c.664-2A>G and c.694+1G>A variants. WT splicing is shown in black in the upper schematic diagram while aberrant splicing outcomes of each variant is shown below in red.

(C) Sanger sequencing of cDNA amplicons are shown from left to right.The c.664-2G and c.694+1A variants show skipping of exon 7, deleting 31 nucleotides (r.664_694del, p.(Asp222ProfsTer10)). The c. 694+1A variant also activates a cryptic splice donor site (r.694_691+1ins23, p.(Ala232AspfsTer8)) causing a frameshift. The wild-type Exon 7 and empty vector controls performed as expected.

Supplementary Figure 3. Mouse whole cortex and hippocampus

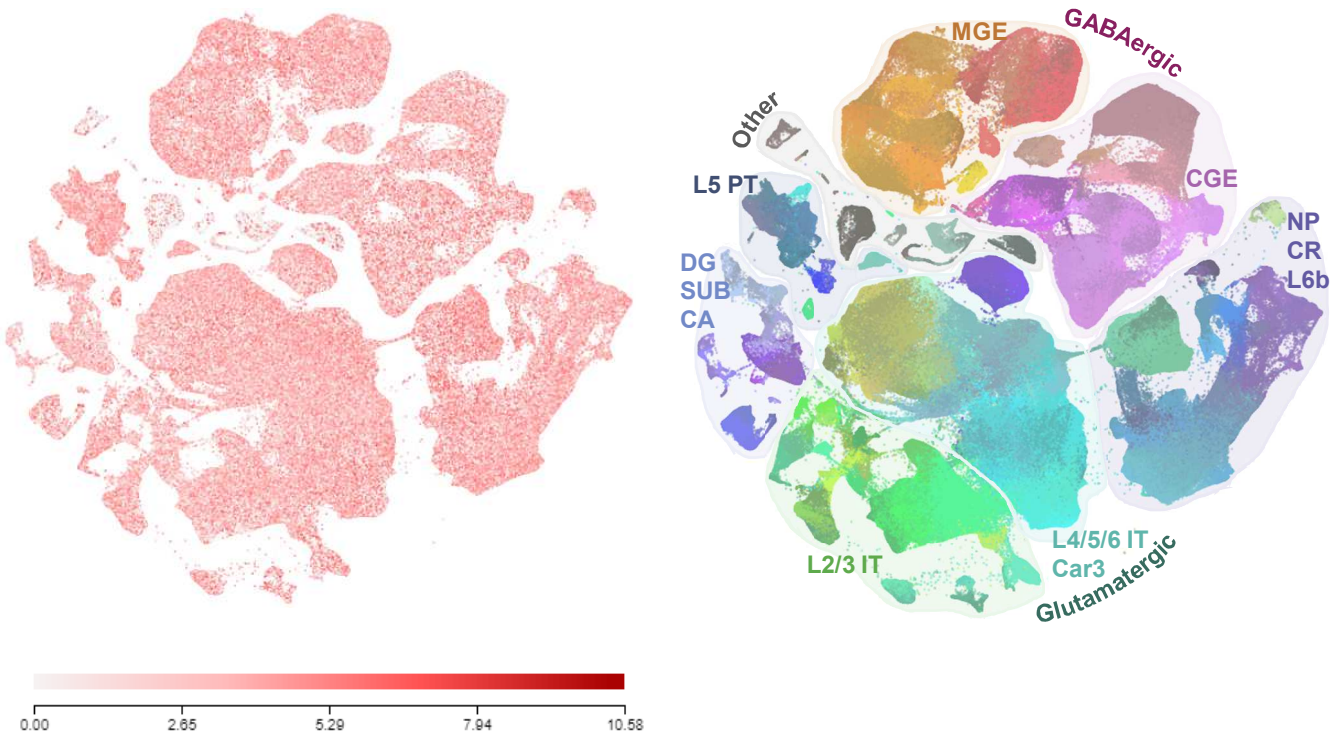

Supplementary Figure 3: *Acbd6* Gene Expression in the Adult Mouse Brain

Visualization of *Acbd6* expression in the adult mouse cortex and hippocampus using single-cell RNA-seq. *Acbd6* expression (red) is nearly ubiquitously shown in most transcriptomic cell regions in the whole cortex and hippocampus (left). [10x Genomics, https://www.sciencedirect.com/science/article/abs/pii/S0092867421005018?dgcid=rss_sd_all]

Abbreviations for the catalog of transcriptomic cell types: CGE, Caudal ganglionic eminence; CA, cingulate area; CR, Cajal Retzius; DG, dentate gyrus; IT, Intratelencephalic; L2, layer 2; L3, layer 3; L4, layer 4; L5, layer 5; L6, layer 6; L6b, layer 6b; MGE, Medial ganglionic eminence; NP, near-projecting; PT, pyramidal tract; SUB, subiculum.

Supplementary Figure 4

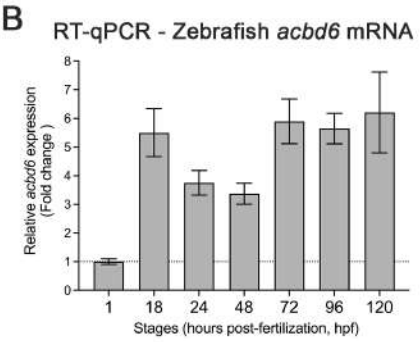

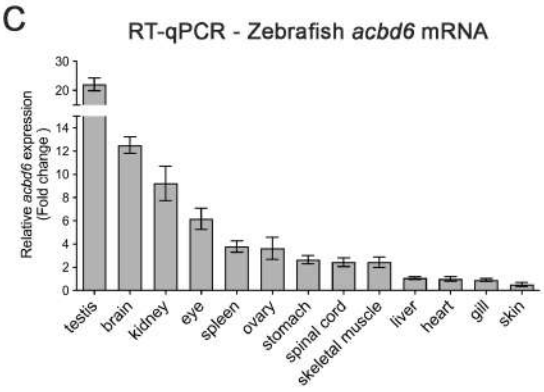

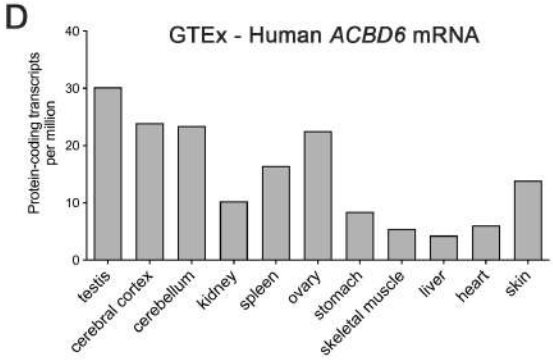

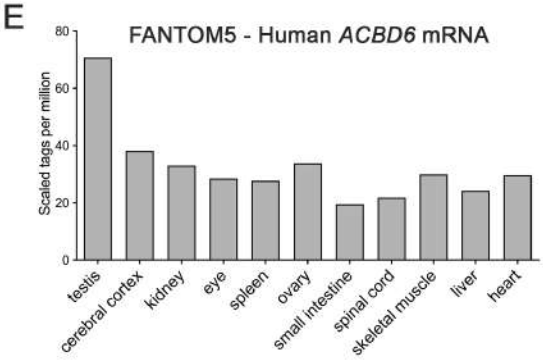

Supplementary Figure 4. *ACBD6* is conserved across species and zebrafish *acbd6* exhibits high expression during development with similar tissue-specific expression patterns to human

(A) Protein sequence alignment of human (*Homo sapiens*) ACBD6 and corresponding orthologs from mouse (*Mus musculus*), chicken (*Gallus gallus*), *Xenopus* (*Xenopus tropicalis*) and zebrafish (*Danio rerio*). Highlighted letters on a yellow background represent identical and conserved amino acid residues between species. Zebrafish and human ACBD6 shared 69.2% identity and 78.2% similarity in the acyl-CoA binding domain and shared 80% identity and 95.4% similarity in the ankyrin-repeat motif. **(B)** The temporal expression of *acbd6* mRNA by RT-qPCR at different developmental stages of zebrafish. Expression levels were normalized to the *18S* housekeeping gene and compared to 1 hpf embryos. Data shown are mean ± SD. **(C)** Expression of *acbd6* mRNA by RT-qPCR at different zebrafish adult tissues. The expression levels were normalized to the *18S* housekeeping gene and compared to heart. Data shown are mean ± SD. **(D, E)** The tissue-specific RNA expression data obtained through Cap Analysis of Gene Expression generated by the FANTOM5 project are reported as Scaled Tags Per Million, and the tissue-specific RNA-seq data generated by the Genotype-Tissue Expression (GTEx) project is reported as protein-coding transcripts per million, corresponding to median values of the different individual samples from each tissue.

Supplementary Figure 5

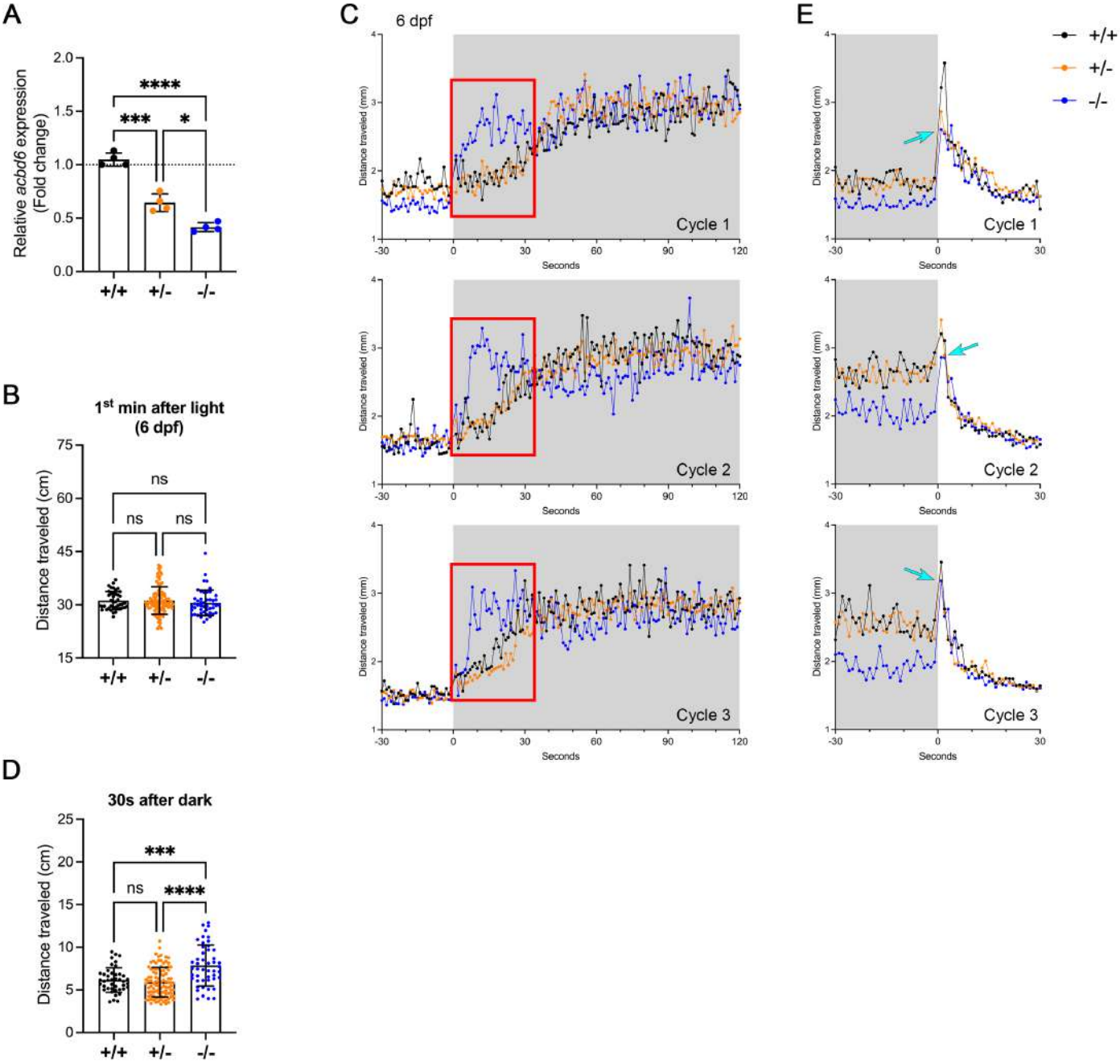

Supplementary Figure 5. Zebrafish *acbd6*-/- exhibited a reduction in mRNA expression, and displayed a hyperactive behavior when changed to dark at 6 dpf

(A) Expression of *acbd6* mRNA in *acbd6* mutants was detected by RT-qPCR. The expression levels were normalized to the *18S* housekeeping gene and compared to *acbd6*+/+. Error bars = mean ± SD. Four biological replicates were performed, with each replicate containing technical triplicates. **(B)** Distance traveled of each larva from 3 cycles of first minute in light period from Fig. 4F. Error bars = mean ± SD. **(C)** Three light to dark transition cycles from Fig. 4F were selected to show locomotor activity and time bin was set up in seconds. Of note, the error bar was removed to reveal the mean value of each time point. Red open box indicates the first 30 seconds of dark period. **(D)** Distance traveled of each larva from 3 cycles of beginning 30 seconds of dark period as indicated by red box in Supplementary Fig. **5**C. Error bars = mean ± SD. **(E)** Three dark to light transition cycles from Fig. 4F were selected to show locomotor activity and time bin was set up in seconds. Error bar was removed to reveal the mean value of each time point. Cyan arrow indicates the distance moved of first second light period of *acbd6*-/-. In (A, B, D), one-way ANOVA with Dunnett's T3 multiple comparisons test. ns, not significant $p \geq 0.05$, *$p < 0.05$, ***$p < 0.001$ and ****$p < 0.0001$.

Supplementary Figure 6

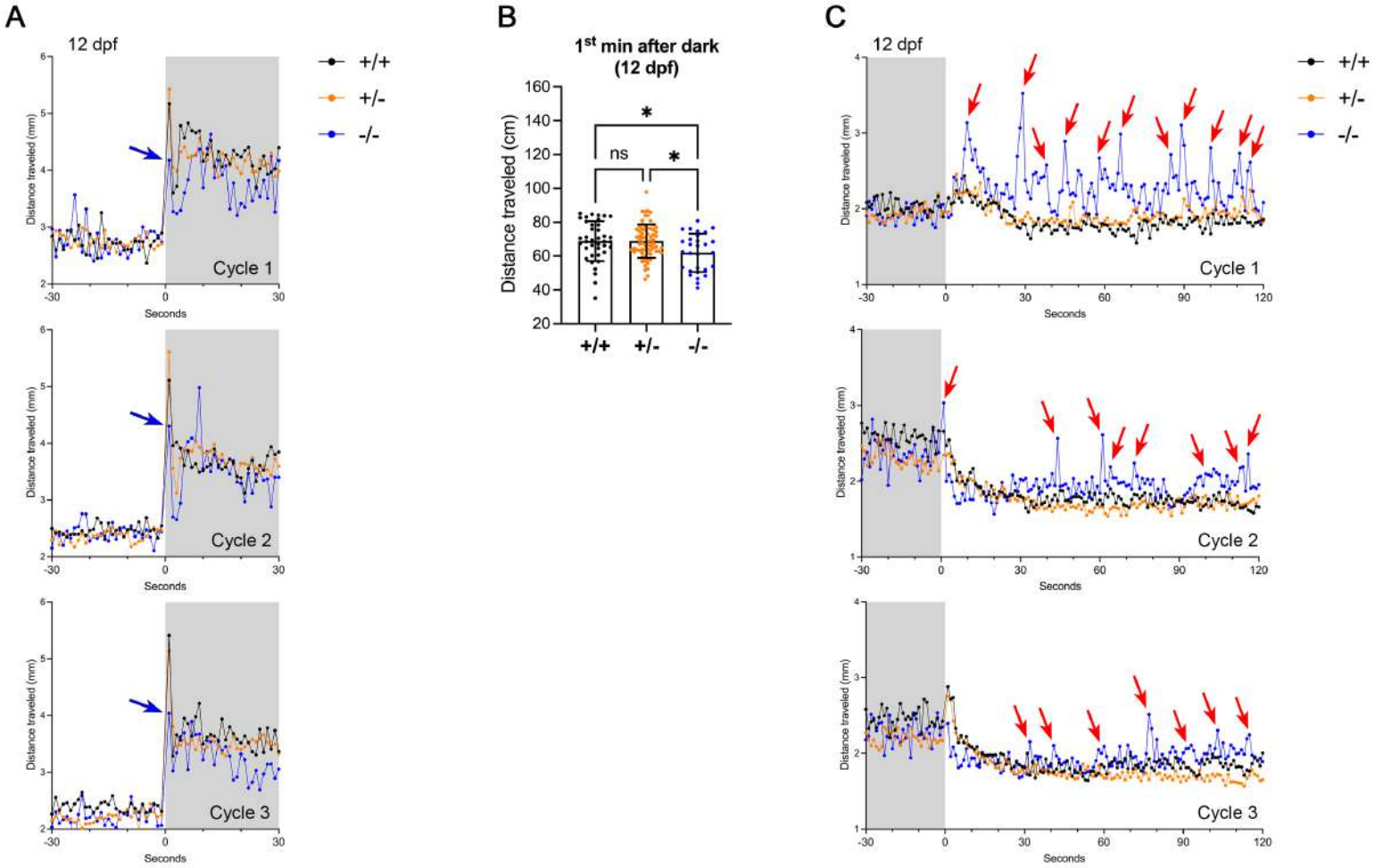

Supplementary Figure 6. Zebrafish *acbd6*-/- displayed hyperactive behavior whith the light on but reduced locomotor activity in the dark period at 12 dpf

(A) Three light to dark transition cycles from Fig. 4I were selected to show locomotor activity and time bin was set up in seconds. The error bar was removed to reveal the mean value of each time point. The blue arrow indicates the distance moved of first second dark period of *acbd6*-/-. **(B)** Distance traveled from each larva from 3 cycles of first minute in dark period from Fig. 4I. Error bars = mean ± SD. One-way ANOVA with Dunnett's T3 multiple comparisons test. ns, not significant $p \geq 0.05$, $*p < 0.05$. **(C)** Three dark to light transition cycles from Fig. 4I were selected to show locomotor activity and time bin was set up in seconds. The error bar was removed to reveal the mean value of each time point. Red arrows indicate some locomotor bursts of *acbd6*-/-.

Supplementary Figure 7

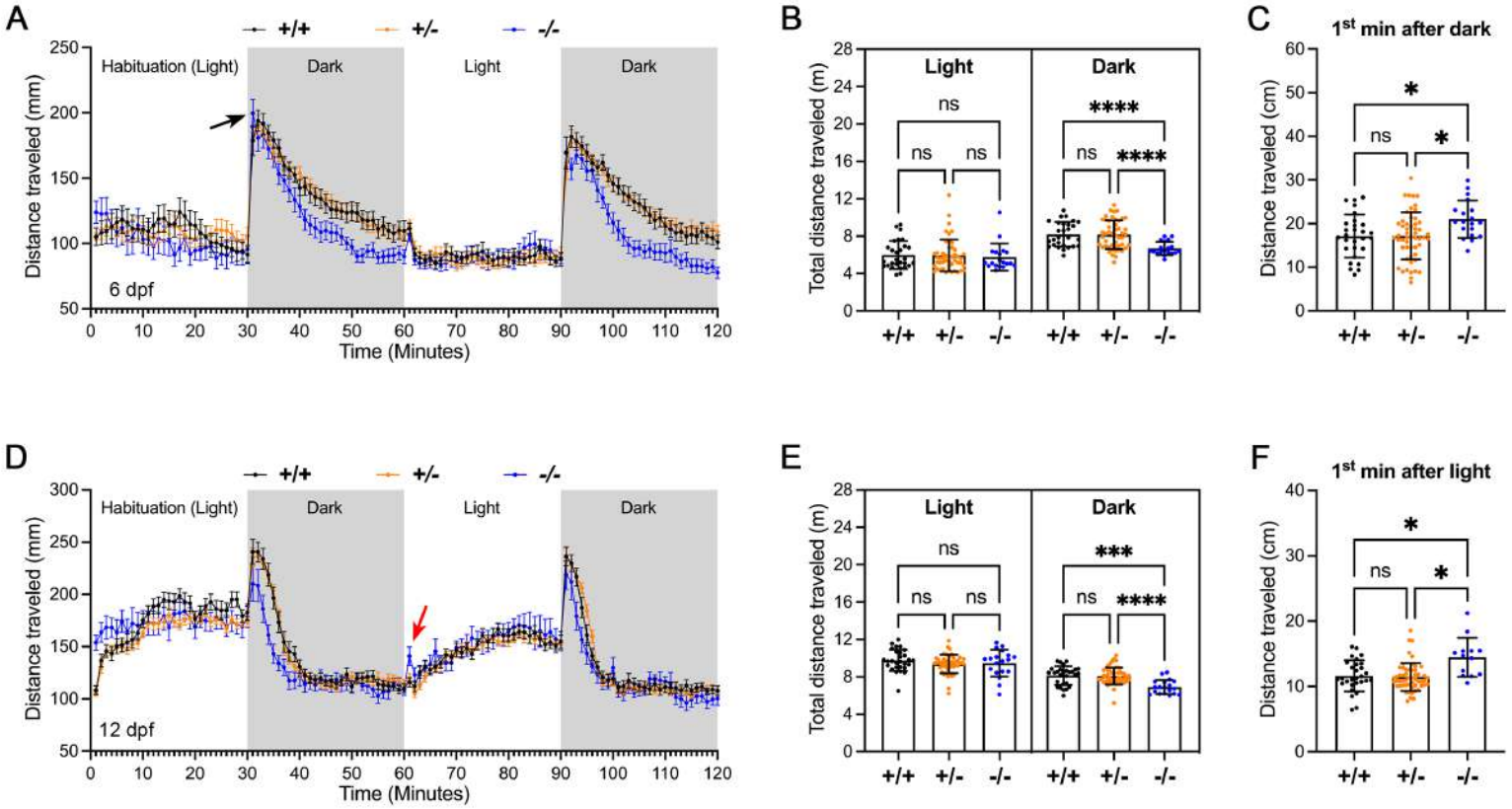

Supplementary Figure 7. Zebrafish *acbd6*-/- displayed abnormal behaviors in 30-minute light-dark cycles at 6 and 12 dpf

(A) Locomotor activities of zebrafish larvae in light and dark condition at 6 dpf. +/+ (n = 28 larvae), +/- (n = 48 larvae) and -/- (n = 19 larvae). Zebrafish larvae were placed in 2 cycles of 30-minute light-dark period. Error bars = mean ± SEM. Black arrow indicates increased movement of homozygous mutants at first minute in dark. **(B)** Cumulative distance traveled of each larva from the second light period or two dark periods from Supplementary Fig. **7**A. Error bars = mean ± SD. **(C)** Distance traveled of each larva from first minute of two dark cycles in Supplementary Fig. 7A. Error bars = mean ± SD. **(D)** Locomotor activities of zebrafish larvae in light and dark condition at 12 dpf. +/+ (n = 28 larvae), +/- (n = 48 larvae) and -/- (n = 19 larvae). Error bars = mean ± SEM. Red arrow indicates increased movement of homozygous mutants at first minute in light period. **(E)** Cumulative distance traveled of each larva from second light period or two dark periods from Supplementary Fig. 7D. Error bars = mean ± SD. **(F)** Distance traveled of each larva from first minute of second light cycle in Supplementary Fig. 7D. Error bars = mean ± SD. In (B, C, E, F), one-way ANOVA with Dunnett's T3 multiple comparisons test. ns, not significant $p \geq 0.05$, *$p < 0.05$ and ****$p < 0.0001$.

Supplementary Figure 8

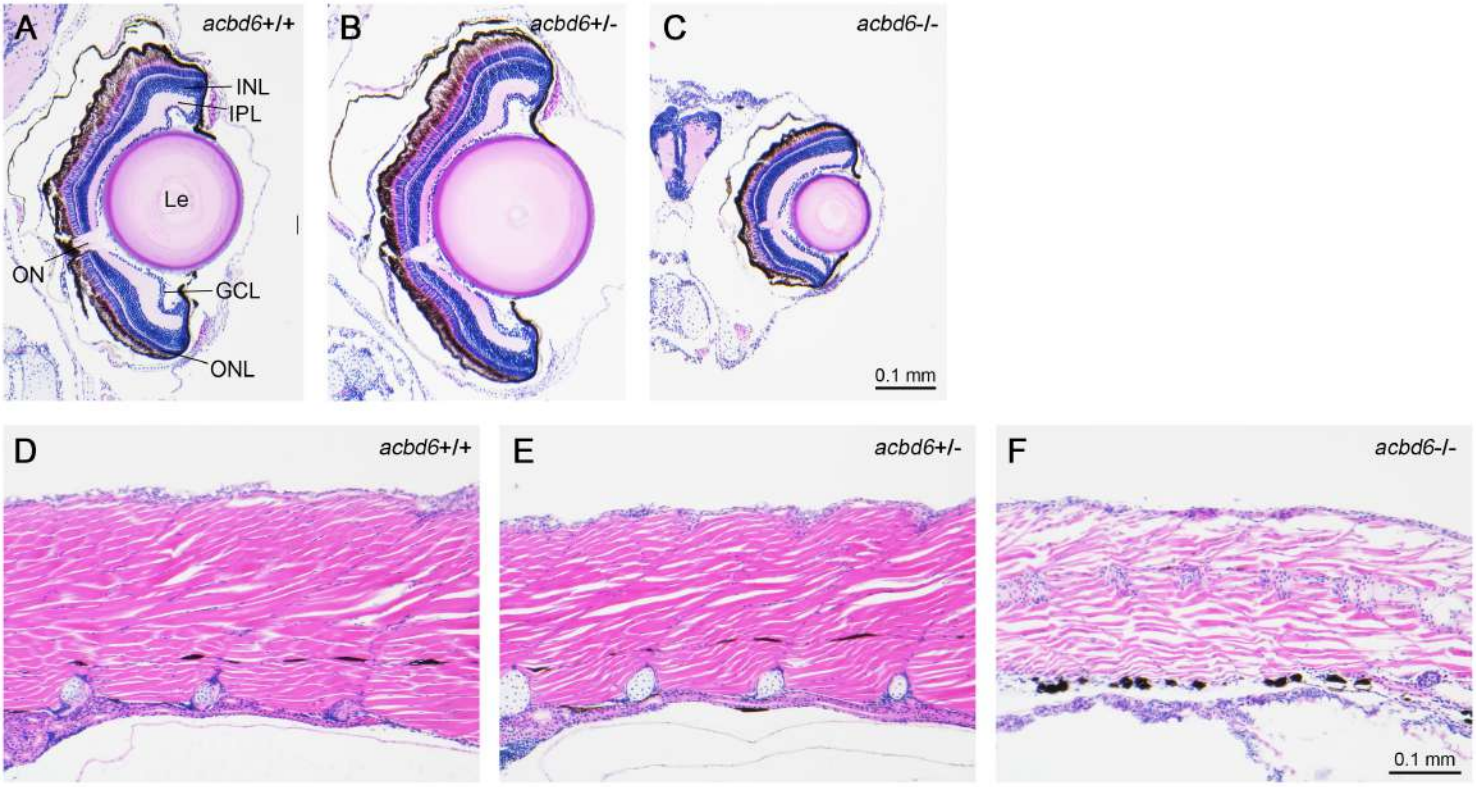

Supplementary Figure 8. Zebrafish *acbd6*-/- displayed abnormal histology in the eye and muscle at 30 dpf

(A-C) Representative images of transverse sections of the eye from *acbd6*+/+, *acbd6*+/- and *acbd6*-/- animals. Optic nerve (ON), inner nuclear layer (INL), inner plexiform layer (IPL), ganglion cell layer (GCL), outer nuclear layer (ONL). **(D-F)** Representative images of transverse section of trunk from *acbd6*+/+, *acbd6*+/- and *acbd6*-/- animal.

Supplementary Figure 9

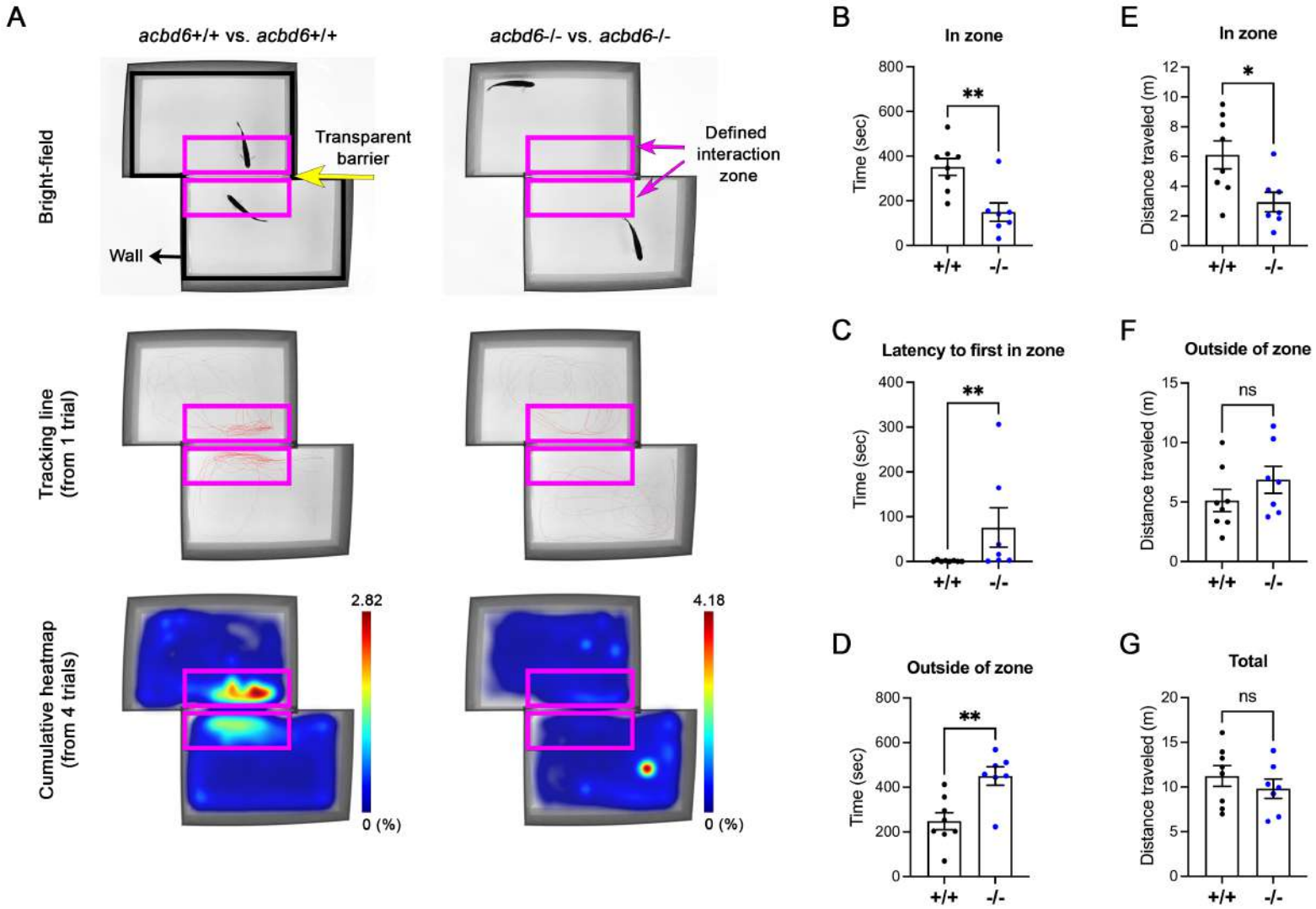

Supplementary Figure 9. Zebrafish adult *acbd6*-/- mutants exhibited autism spectrum disorder-like behavior (back)

(A) Top row of panels in the social behavior test of adult zebrafish displays images of both *acbd6*+/+ (n = 8 animals) and *acbd6*-/- (n = 7 animals). The bright field images are taken from recorded video, with two magenta-colored open boxes indicating the designated spacial interaction zone (see also Supplementary video 17, 18), A transparent glass barrier is present in the middle of the two zones, which is pointed out by a yellow arrow. The middle row shows the reconstructed swim path (drawn in red line) of the fish during a 10-minute trial using the EthoVision XT program. The bottom row exhibits the cumulative heatmap from 4 trials of the social behavior test, where darker red indicates the fish spent more time in that position. The percentage of total time spent is shown at the top of the color bar. **(B)** Total time spent in the interaction zone during a trial. **(C)** Latency for a fish to enter the interaction zone. **(D)** Total time spent outside of the interaction zone during a trial. **(E)** Distance traveled in the interaction zone during a trial. **(F)** Distance traveled outside of the interaction zone during a trial. **(G)** Total distance traveled during a trial. Each dot represents one fish and the error bars represent the mean ± SEM. The Mann-Whitney test was used for (B-D), and an unpaired Student *t*-test with Welch's correction was used for (E-G). ns, not significant $p \geq 0.05$, *$p < 0.05$ and **$p < 0.01$.

Supplementary Figure 10

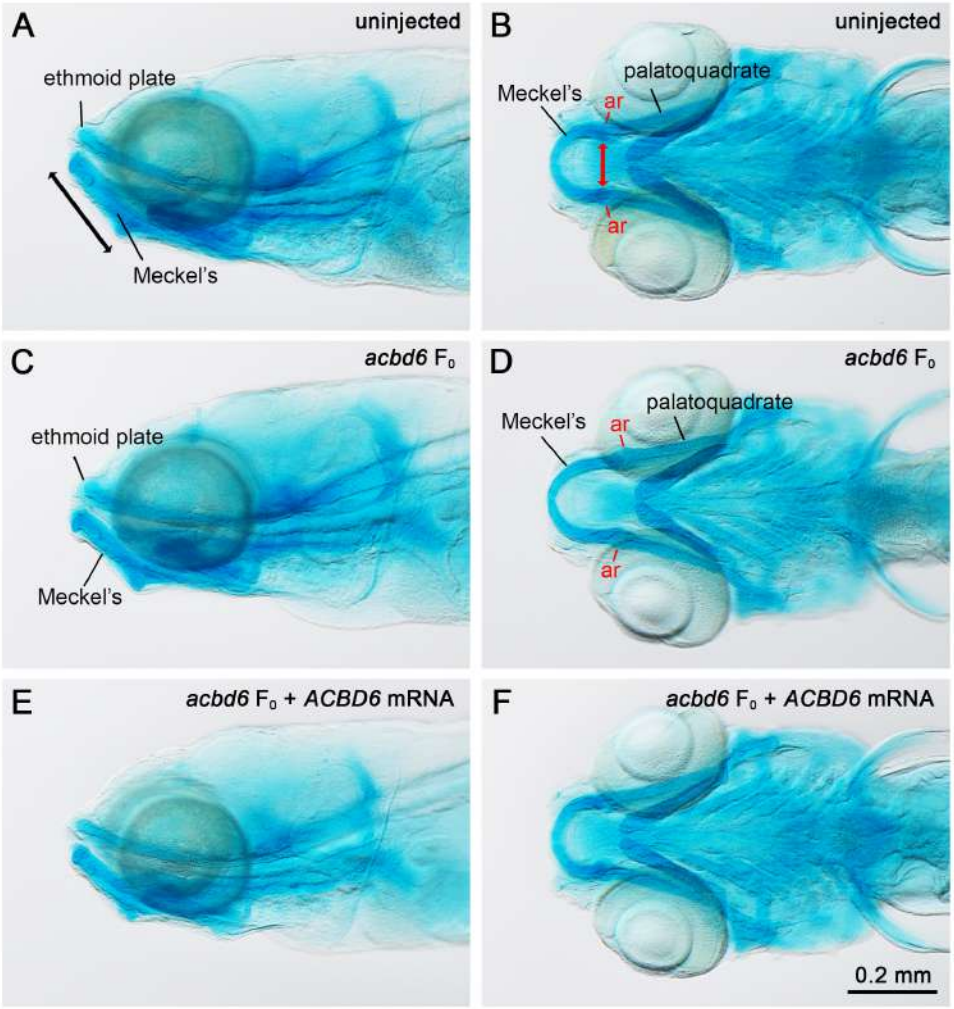

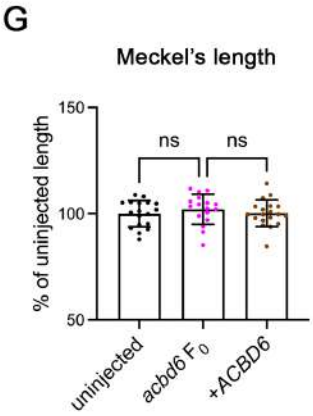

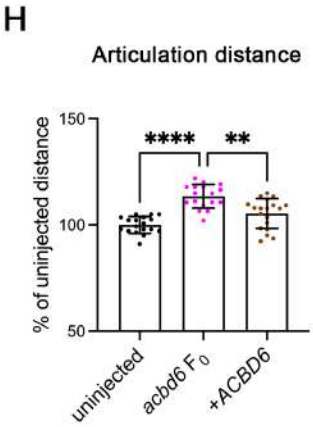

Supplementary Figure 10. Zebrafish *acbd6* F_0 knockout showed craniofacial dysmorphism

Alcian blue staining was performed to reveal the craniofacial cartilage structure of uninjected control **(A, B)**, *acbd6* F_0 **(C, D)** and F_0 rescued with human *ACBD6* mRNA rescue **(E, F)** larvae at 8 dpf. **(G)** Quantification of the length of Meckel's cartilage measurement (indicated by a black line with a double arrowhead in (A)). **(H)** Quantification of distances of the articulation between Meckel's and palatoquadrate (indicated by a red line with a double arrowhead in (B)). In (G, H), each dot represents one animal. Uninjected control = 18 animals, *acbd6* F_0 = 17 animals, rescue = 19 animals. Error bars = mean ± SD. One-way ANOVA with Dunnett's T3 multiple comparisons test. ns, not significant $p \geq 0.05$, ***$p < 0.001$ and ****$p < 0.0001$. ar, articulation.

Supplementary Figure 11

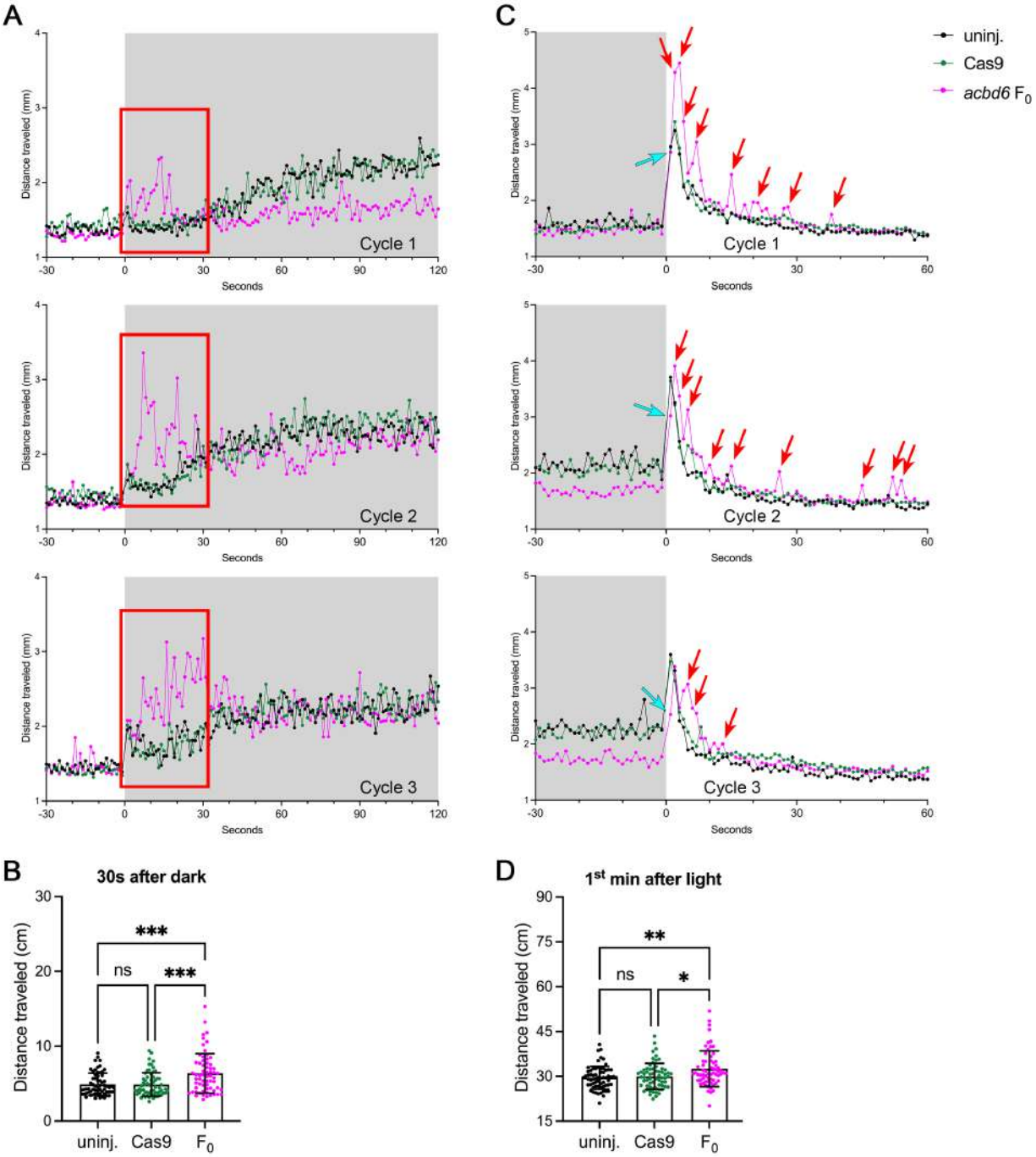

Supplementary Figure 11. Zebrafish *acbd6* F_0 knockouts showed similar but worse abnormal behaviors than stable homozygous mutants at 6 dpf

(A) Three light to dark transition cycles from Fig. 4G were selected to show locomotor activity with the time bin shown in seconds. The error bar was removed to reveal the mean value of each time point. Red open box indicates the first 30 seconds of dark period. **(B)** Average of cumulative distance traveled of each larva from 3 cycles of first 30 seconds of dark period from Supplementary Fig. 11A. Error bars = mean ± SD. **(C)** Three dark to light transition cycles from Fig. 4G were selected to show locomotor activity with the time bin shown in seconds. The error bar was removed to reveal the mean value of each time point. Red arrows indicate some locomotor bursts of *acbd6* F_0 larvae. Cyan arrows indicate the first second of light period. **(D)** Average of cumulative distance traveled of each larva from 3 cycles of first minute in light period as indicated by red arrows in Fig. 4G. Error bars = mean ± SD. In (B, D), one-way ANOVA with Dunnett's T3 multiple comparisons test. ns, not significant $p \geq 0.05$, $*p < 0.05$, $**p < 0.01$ and $***p < 0.001$.

Supplementary Figure 12

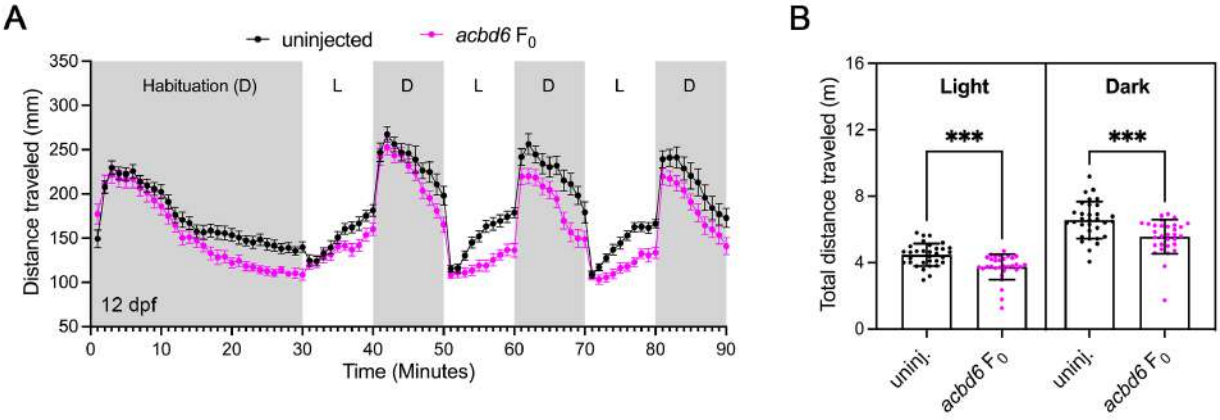

Supplementary Figure 12. Zebrafish *acbd6* F_0 knockout showed an overall reduction of locomotor activities at 12 dpf

(A) Locomotor activities of zebrafish larvae in light and dark condition at 12 dpf. n = 32 larvae for each group. Zebrafish larvae were first habituated under dark for 30 minutes followed by 3 cycles of 10-minute time bins of light and dark periods. Error bars = mean ± SEM. Dark period (D), light period (L). **(B)** Average of cumulative distance traveled of each larva from 3 cycles of light or dark periods from Supplementary Fig. 12A. Error bars = mean ± SD. One-way ANOVA with Dunnett's T3 multiple comparisons test. ***$p < 0.001$.

Supplementary Figure 13

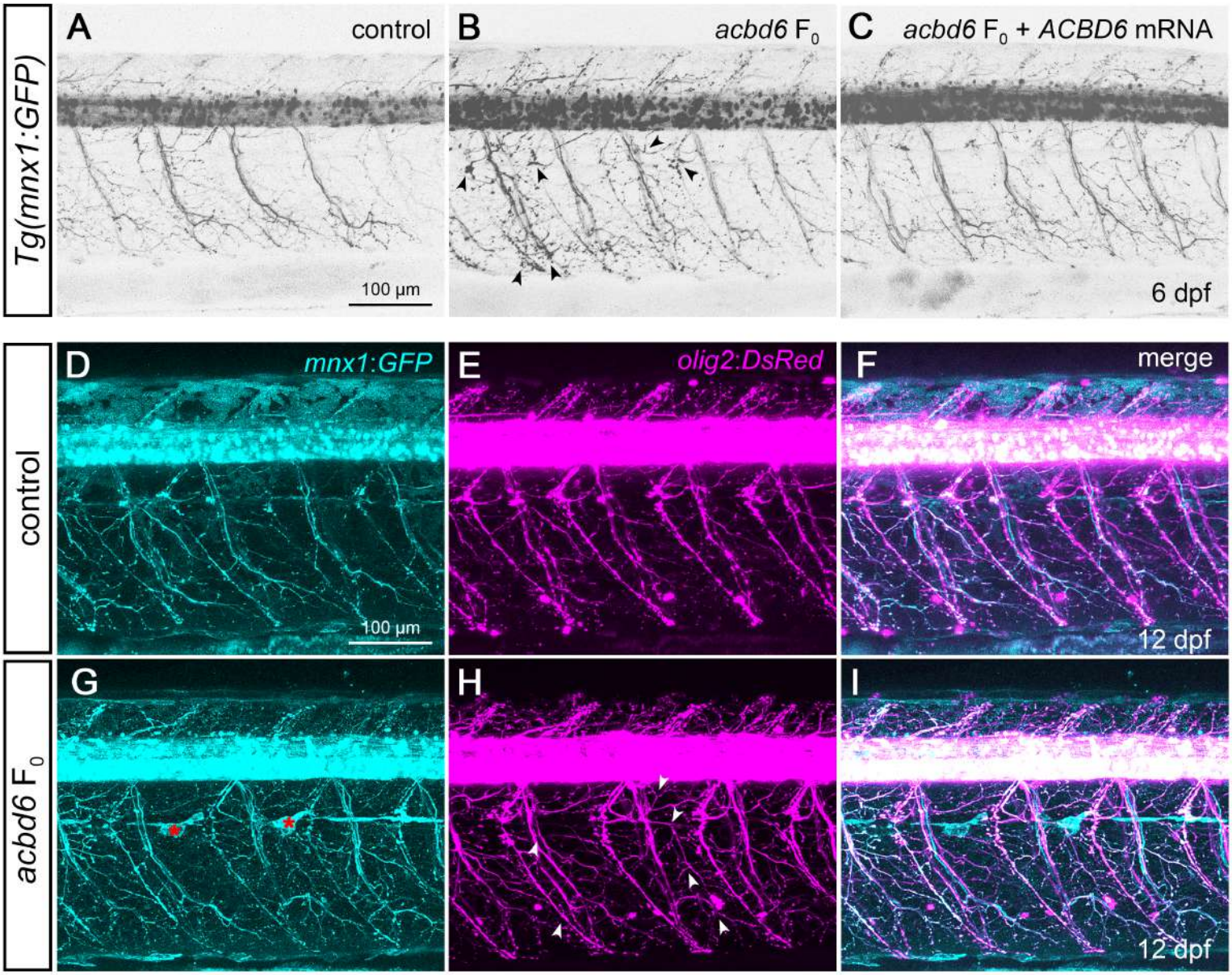

Supplementary Figure 13. The *acbd6* F_0 knockout showed increased motor axonal branches.

The representative confocal images of *slc45a2* sgRNA-injected or *acbd6* + *slc45a2* sgRNAs-injected *Tg(mnx1:GFP;olig2:DsRed)* larva at 6 dpf (A-C) and at 12 dpf (D-I). Lateral view, anterior to the left and dorsal to the top. Black arrowheads (in B) and white arrowheads (in H) indicate excess axonal arborizations. Red asterisks indicate fluorescence from pigment cells.

Supplementary Figure 14

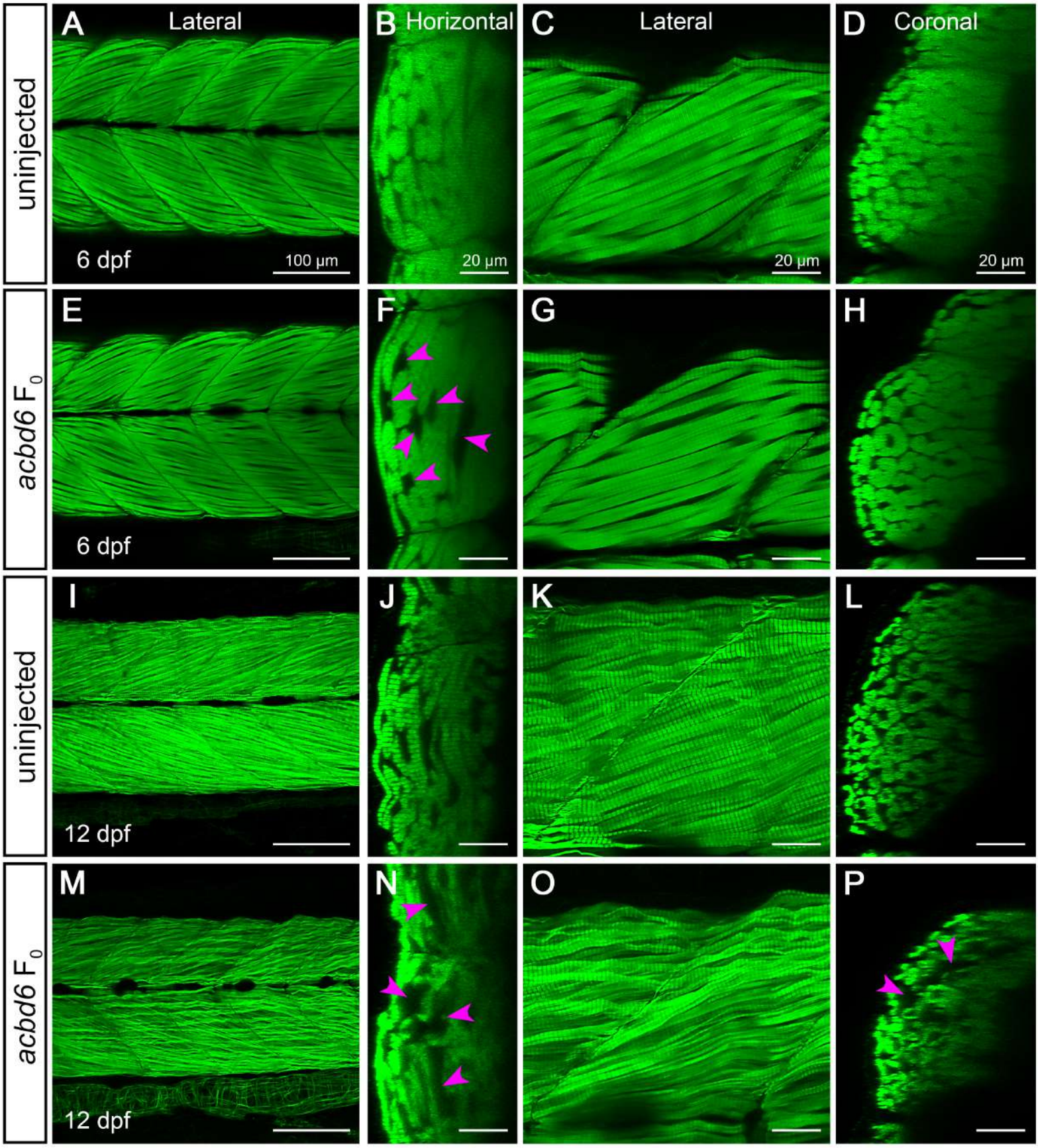

Supplementary Figure 14. The *acbd6* F_0 knockout showed progressive muscle degeneration

The representative confocal images of *slc45a2* sgRNA-injected or *acbd6* + *slc45a2* sgRNAs-injected larva at 6 dpf (A-H) and at 12 dpf (I-P). Lateral view, anterior to the left and dorsal to the top. The images of horizontal and coronal views were generated from (C, G, K, and O) by the Orthogonal views tool in ImageJ. Magenta arrowheads (in F, N, P) indicate abnormal spaces between muscle fibers.

Supplementary Figure 15

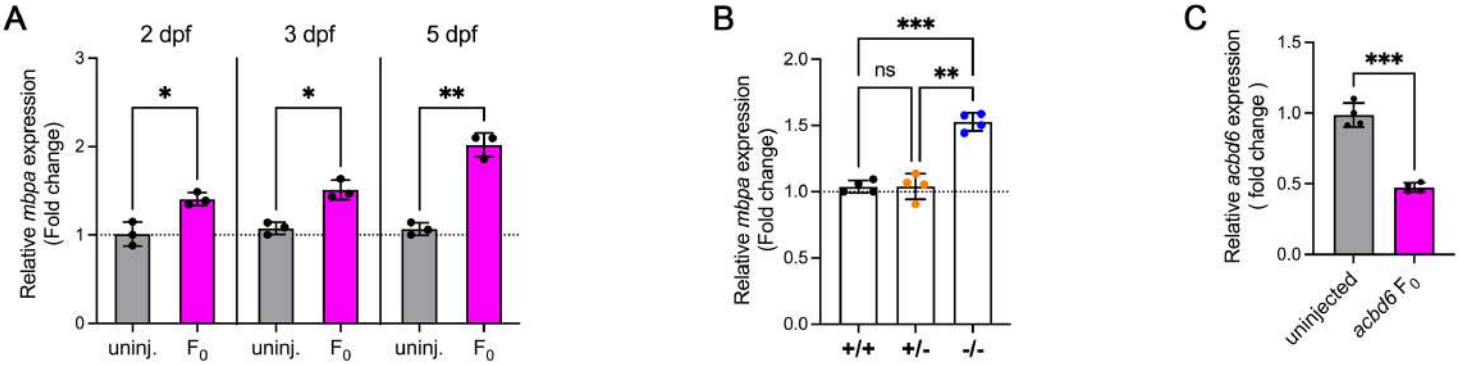

Supplementary Figure 15. Elevated *mbpa* expression was detected in *acbd6* F_0 knockouts as well as in homozygous mutants, and the downregulated expression of *acbd6* mRNA in F_0 knockouts was confirmed using RT-qPCR

(A) The expression levels were normalized to the *18S* housekeeping gene and compared to the uninjected control. Three biological replicates were performed with each replicate containing technical triplicates. **(B)** The expression levels were normalized to the *18S* housekeeping gene and compared to *acbd6*+/+. Four biological replicates were performed with each replicate containing technical triplicates. Error bars = mean ± SD. One-way ANOVA with Dunnett's T3 multiple comparisons test: ns, not significant $p \geq 0.05$, $*p < 0.05$, $**p < 0.01$ and $***p < 0.001$. **(C)** Expression of *acbd6* mRNA in *acbd6* F_0 was detected by RT-qPCR. The expression levels were normalized to the *18S* housekeeping gene and compared to uninjected controls. Error bars = mean ± SD. Four biological replicates and each replicate contained technical triplicates. Unpaired Student *t* test with Welch's correction. $***p < 0.001$

A

```
hs MASSFLPAGAITGDSGGELSSGDDSGEVEFPHSPEIEETSCLAEL---FEKAAAHLQGLIQVASREQLLY 67
xt MAS----PGVLEESSSGEACSGG---------CPEQWEEKTEEELQGQFEQAAKHVQNGASVASTEQLLF 57

hs LYARYKQVKVGNCNTPKPSFFDFEGKQKWEAWKALGDSSPSQAMQEYIAVVKKLDPGWNPQIPEKKGKEA 137
xt LYARYKQVKVGRCNTPKPGFFDYEGKKKWEAWKALGDYSCQQAMNEYIETVKKLDPDWSPQALEEPHKEP 127

hs NTGFGGPVISSLYH-EETIREEDKNIFDYCRENNIDHITKAIKSKNVDVNVKDEEGRALLHWACDRGHKE 206
xt KTTFGGPVVSCLYKVQETLREEDKDIFDYCRENNISRVSHALSTGAIDVNVADDEGRCLLHWACDRGHTQ 197

hs LVTVLLQHRADINCQDNEGQTALHYASACEFLDIVELLLQSGADPTLRDQDGCLPEEVTGCKTVSLVLQR 276
xt LVSVLLFHNAHINMQDSEGQTPLHYASACEFPDIVDLLLDHGADPSLVDNDGFQPHEVTDSKNIAAMLQQ 267

hs HTT-GK------------A 282
xt HASYGEHNKPASLLLEMPQ 286
```

B

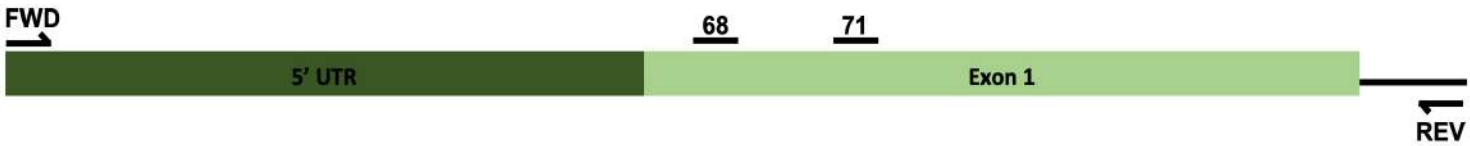

C

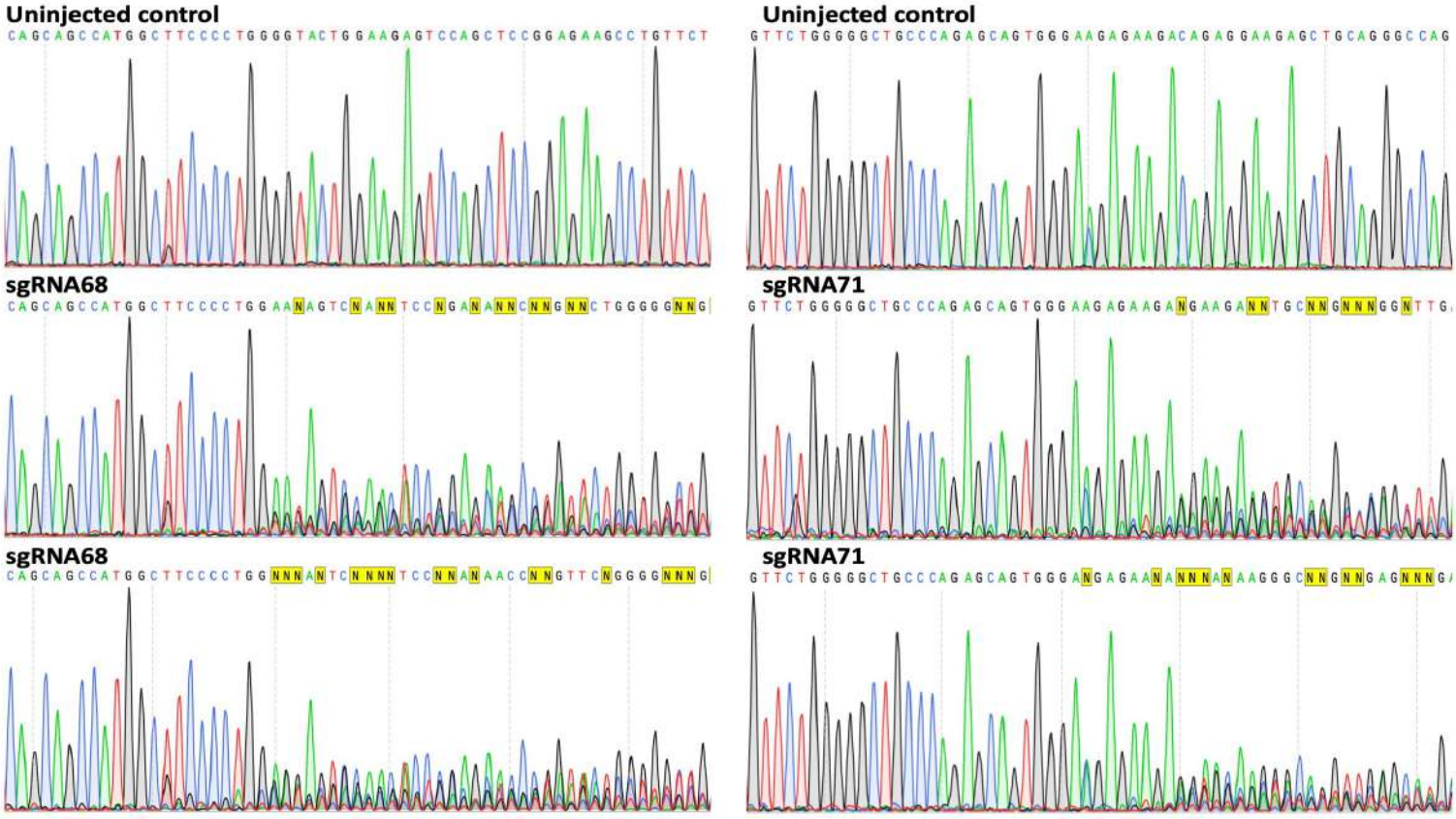

D

Phenotype	Sample	Indel %	KO Score	Predominant indel(s)
Mild	68	64	44	-15bp (20%), -8bp (32%), -11bp (3%)
	71	81	23	-15bp (57%), -4bp (12%), -7bp (10%)
Moderate	68	85	50	-15bp (32%), -4bp (27%), -10bp (18%)
	71	89	89	-21bp (36%), -2bp (24%), -8bp (15%)
Severe	68	90	90	-2bp (44%), -8bp (30%), -21bp (16%)
	71	91	91	-2bp (52%), -8bp (39%), 0bp (3%)

Supplementary Figure 16. Targeted disruption of *acbd6* exon 1 generates F_0 crispants bearing insertion-deletion changes *in vivo*

(A) The *acbd6* amino-acid sequence of *H. sapiens* (NP_115736.1) and *X. tropicalis* (NP_001008065.2) aligned within SnapGene®5.2.4. using a local Smith-Waterman alignment shows modest sequence conservation (66.4%). **(B)** The partial *X. tropicalis* exon schematic depicts the target region within *acbd6*, exon1 and the relative position of the CRISPR/Cas9 sgRNAs and genotyping primers. **(C, D)** Sanger sequencing of the target region from uninjected and crispant embryos reveals both sgRNA-68 (GGACTCTTCCAGTACCCCAG) and sgRNA-71 (GGAGTGGGACGAGAAGACAG) result in consistent levels of CRISPR/Cas9 directed indel formation (ab1 trace files visualised in SnapGene®5.2.4.).

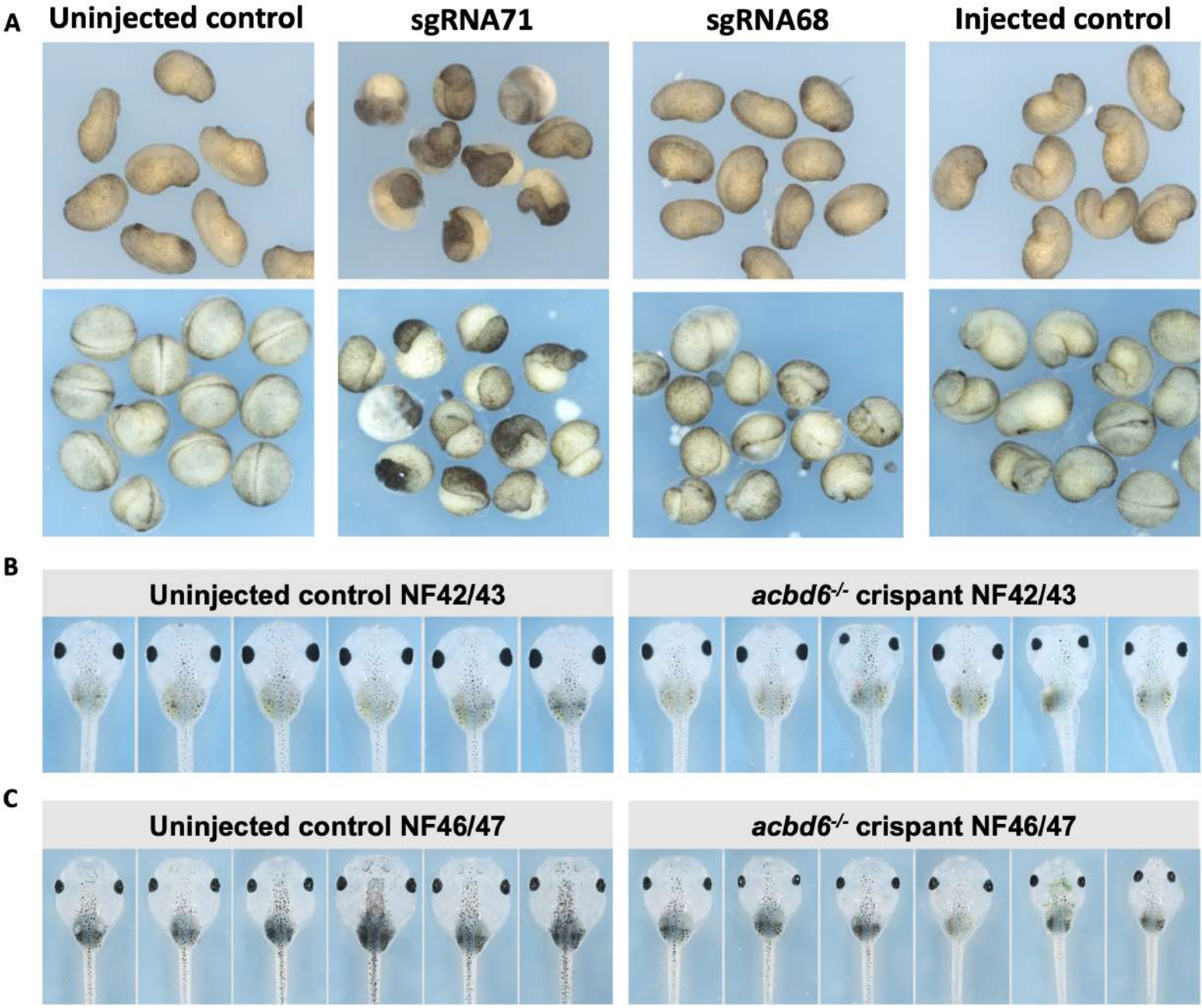
A
Uninjected control
sgRNA71
sgRNA68
Injected control
B
Uninjected control NF42/43
acbd6-/- crispant NF42/43
C
Uninjected control NF46/47
acbd6-/- crispant NF46/47

Supplementary Figure 17. Survival, movement and morphology of *abcd6* cripspant tadpoles

(A) Fertilised X. tropicalis eggs were obtained from two clutches and injected at the one-cell stage with Cas9 protein and 600pg of sgRNA-68 (GGACTCTTCCAGTACCCCAG) or sgRNA-71 (GGAGTGGGACGAGAAGACAG). Substantial numbers of the resulting F_0 X. tropicalis crispant embryos bearing homozygous indels in exon 1 of acbd6 were observed to die at gastrula stages across both experiment. Embryos injected with sgRNA68 that were observed to develop normally compared to both uninjected and tyr-/- control embryos were subsequently found to have a single nucleotide polymorphism affecting the PAM (A, third panel – top row). **(B, C)** Images show tadpole head morphology at two free-feeding stages, crispants were injected with sgRNA-68 (NF42/43 and NF46/47) and the presence of microcephaly, craniofacial defects and eye abnormalities noted.

- *Homo sapiens* protein with N-terminal glycine
- Co-translationally *N*-myristoylated *Hs* protein
- Post-translationally *N*-myristoylated *Hs* protein
- Other *Homo sapiens* protein

Label Post-translationally *N*-myristoylated *Hs* protein implicated in neurological disease
Label Co-translationally *N*-myristoylated *Hs* protein implicated in neurological disease
Label Co-translationally *N*-myristoylated *Hs* protein

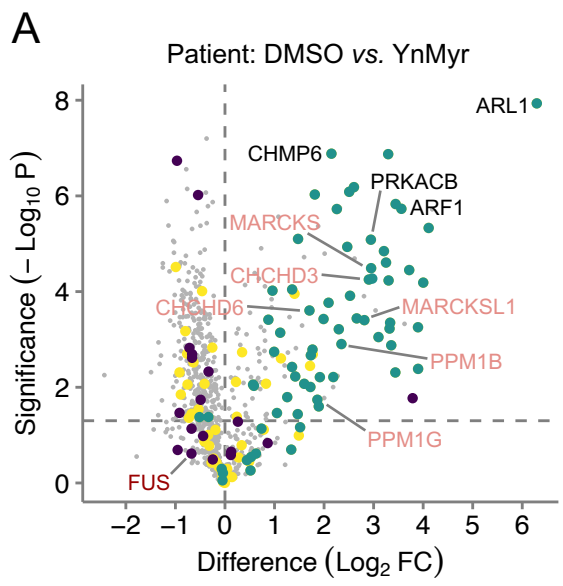

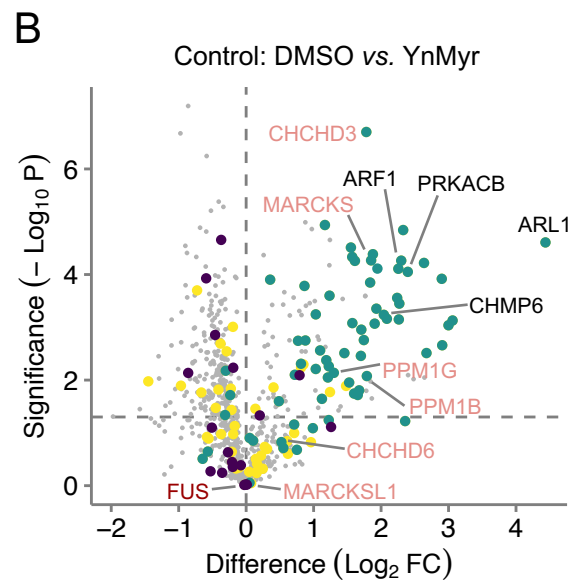

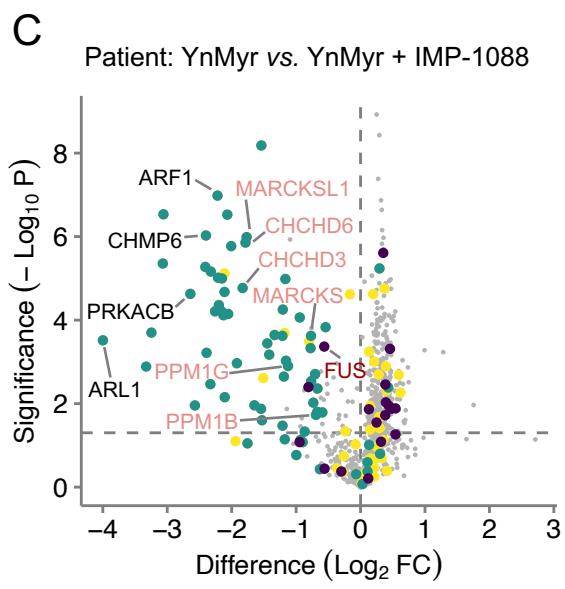

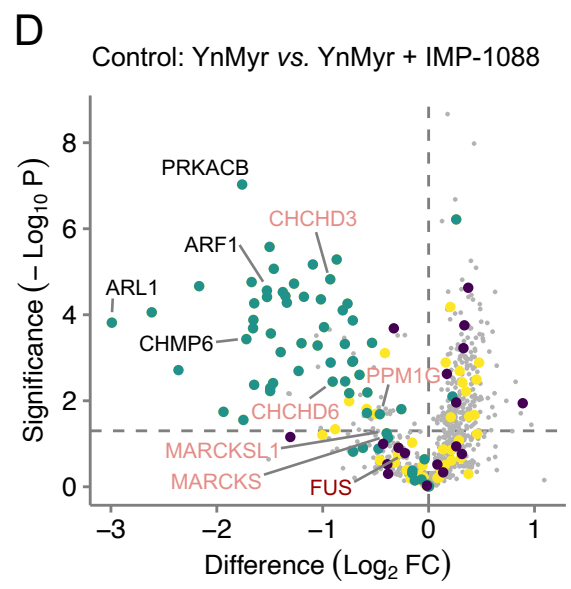

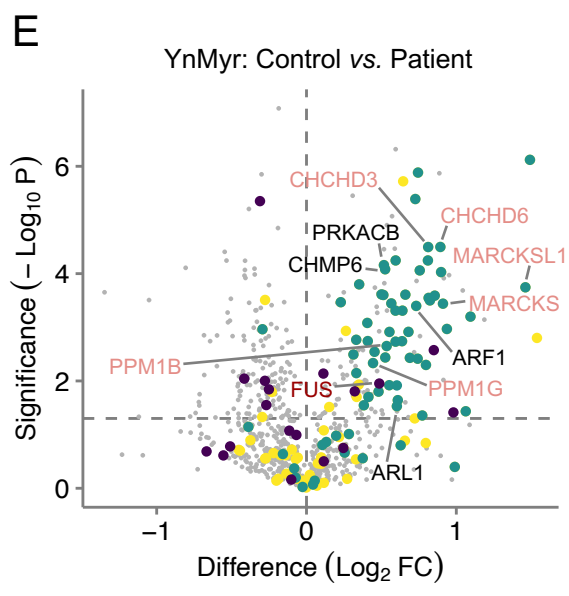

Supplementary Figure 18. Chemical proteomics analysis of *N*-myristoylation in fibroblasts of a ACBD6 deficient patient and a healthy sibling (back)

(A) Volcano plot depicting YnMyr labelling of proteins in ACBD6 deficient fibroblasts derived from F1:S3. Horizontal dotted line: significance threshold (p-value = 0.05). FC: fold-change. Position on the left equals increased in DMSO condition (negative control), position on the right equals increased in YnMyr condition (positive control). Highlighted are two well-validated *N*-myristoylated proteins (black), including those implicated in neurological disorders (orange).

(B) YnMyr labelling of proteins in fibroblasts of healthy sibling of F1:S3. Further description as in (A).

(C) Inhibition of YnMyr labelling of proteins in ACBD6 deficient fibroblasts derived from F1:S3, with *N*-myristoyltransferase inhibitor IMP-1088. Horizontal dotted line: significance threshold (p-value = 0.05). FC: fold-change. Position on the left equals increased in YnMyr condition, position on the right equals increased in YnMyr + IMP-1088 inhibited condition. Highlighted are two well-validated *N*-myristoylated proteins (black), including those implicated in neurological disorders (orange).

(D) Inhibition of YnMyr labelling in fibroblasts of healthy sibling of F1:S3. Further description as in (C).

(E) Volcano plot comparing YnMyr labelling of proteins in ACBD6 deficient fibroblasts of F1:S3 and healthy sibling. Horizontal dotted line: significance threshold (p-value = 0.05). FC: fold-change. Position on the left equals decreased in ACBD6 deficient fibroblasts, position on the right equals increased in ACBD6 deficient fibroblasts.

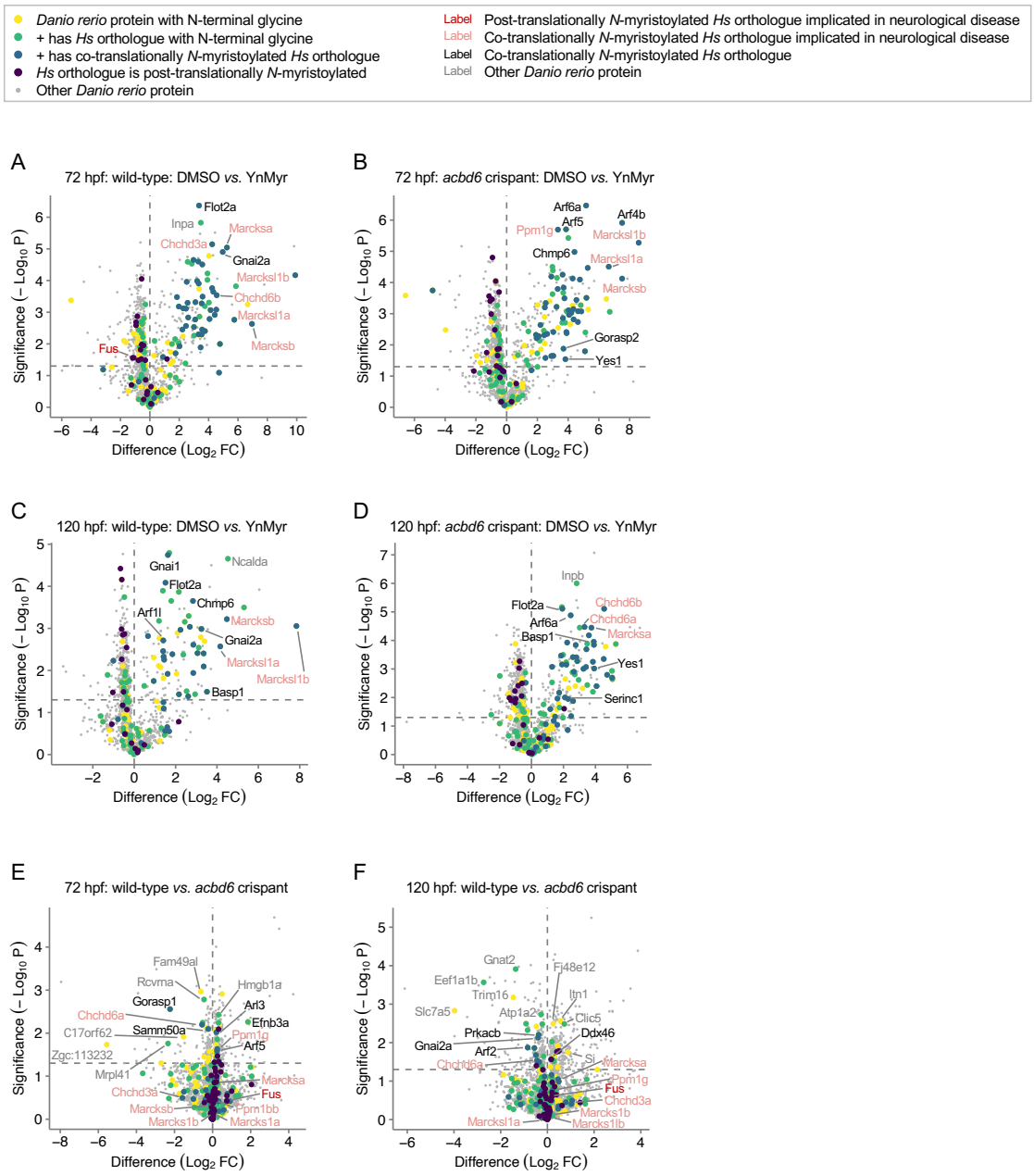
Danio rerio protein with N-terminal glycine
+ has Hs orthologue with N-terminal glycine
+ has co-translationally N-myristoylated Hs orthologue
Hs orthologue is post-translationally N-myristoylated
Other Danio rerio protein
Label Post-translationally N-myristoylated Hs orthologue implicated in neurological disease
Label Co-translationally N-myristoylated Hs orthologue implicated in neurological disease
Label Co-translationally N-myristoylated Hs orthologue
Label Other Danio rerio protein
A
72 hpf: wild-type: DMSO vs. YnMyr
B
72 hpf: acbd6 crispant: DMSO vs. YnMyr
C
120 hpf: wild-type: DMSO vs. YnMyr
D
120 hpf: acbd6 crispant: DMSO vs. YnMyr
E
72 hpf: wild-type vs. acbd6 crispant
F
120 hpf: wild-type vs. acbd6 crispant
Significance (−Log10 P)
Difference (Log2 FC)

Supplementary Figure 19. Chemical and whole proteome analysis of wild-type and *acbd6* F_0 crispant zebrafish (back)

(A) Volcano plot depicting YnMyr labelling of proteins in wild-type zebrafish at 72 hpf. Horizontal dotted line: significance threshold (p-value = 0.05). FC: fold-change. Position on the left equals increased in DMSO condition (negative control), position on the right equals increased in YnMyr condition (positive control). Highlighted are proteins with well-validated *N*-myristoylated orthologues in *Homo sapiens* (black), including those implicated in neurological disorders (orange).

(B) YnMyr labelling of proteins in *acbd6* F_0 crispant zebrafish at 72 hpf. Further description as in (A).

(C) YnMyr labelling of proteins in wild-type zebrafish at 120 hpf. Further description as in (A).

(D) YnMyr labelling of proteins in *acbd6* F_0 crispant zebrafish at 120 hpf. Further description as in (A).

(E) Whole proteome analysis of proteins in wild-type and *acbd6* F_0 crispant zebrafish at 72 hpf. Horizontal dotted line: significance threshold (p-value = 0.05). FC: fold-change. Position on the left equals reduced in crispant, position on the right equals increased in crispant. Highlighted are proteins with well-validated *N*-myristoylated orthologues in *Homo sapiens* (black), including those implicated in neurological disorders (orange).

(F) Whole proteome analysis of proteins in wild-type and *acbd6* F_0 crispant zebrafish at 120 hpf. Further description as in (E).

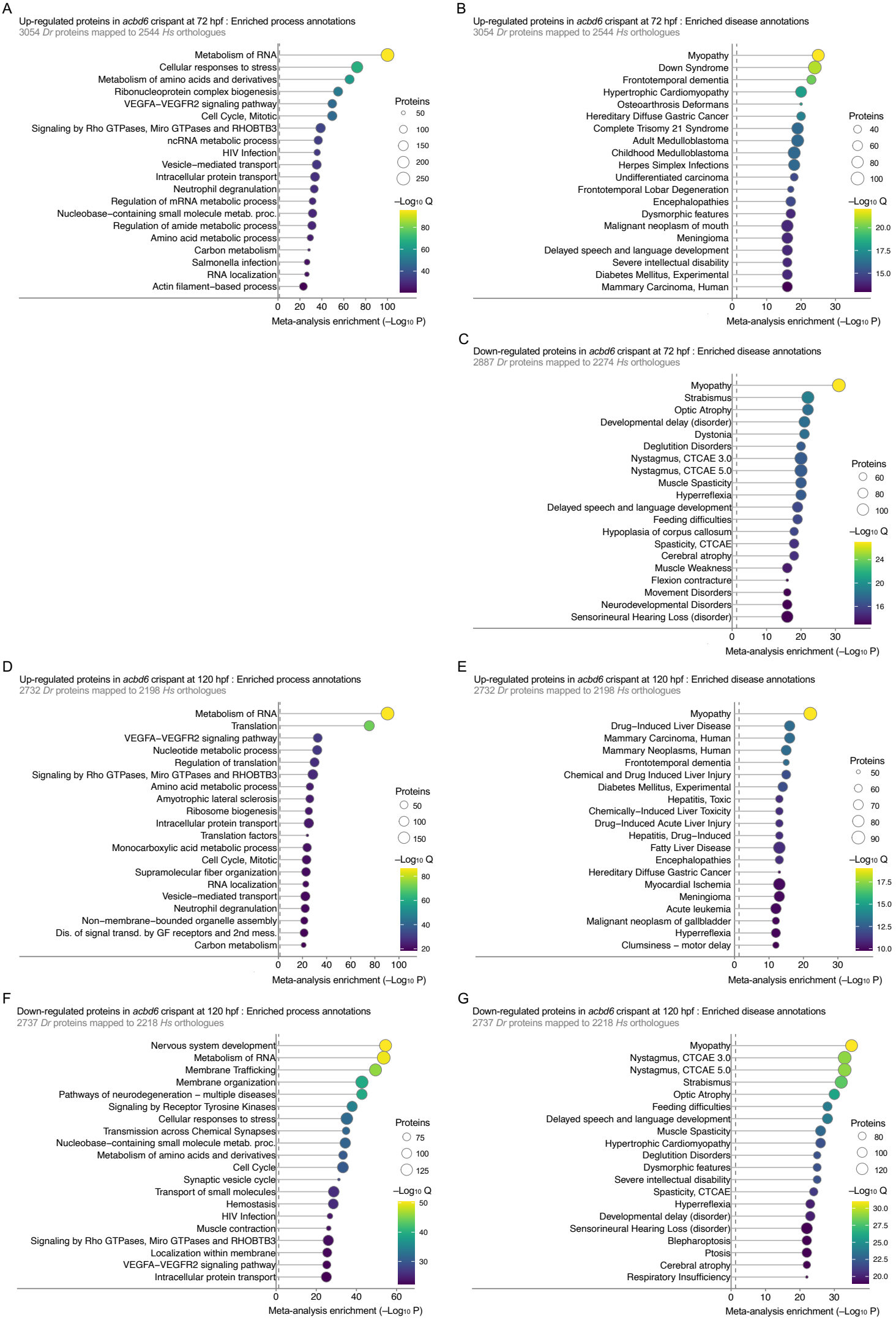
A
Up-regulated proteins in acbd6 crispant at 72 hpf : Enriched process annotations
3054 Dr proteins mapped to 2544 Hs orthologues
Metabolism of RNA
Cellular responses to stress
Metabolism of amino acids and derivatives
Ribonucleoprotein complex biogenesis
VEGFA–VEGFR2 signaling pathway
Cell Cycle, Mitotic
Signaling by Rho GTPases, Miro GTPases and RHOBTB3
ncRNA metabolic process
HIV Infection
Vesicle–mediated transport
Intracellular protein transport
Neutrophil degranulation
Regulation of mRNA metabolic process
Nucleobase–containing small molecule metab. proc.
Regulation of amide metabolic process
Amino acid metabolic process
Carbon metabolism
Salmonella infection
RNA localization
Actin filament–based process
Proteins
50
100
150
200
250
–Log10 Q
80
60
40
0 20 40 60 80 100
Meta-analysis enrichment (–Log10 P)
B
Up-regulated proteins in acbd6 crispant at 72 hpf : Enriched disease annotations
3054 Dr proteins mapped to 2544 Hs orthologues
Myopathy
Down Syndrome
Frontotemporal dementia
Hypertrophic Cardiomyopathy
Osteoarthrosis Deformans
Hereditary Diffuse Gastric Cancer
Complete Trisomy 21 Syndrome
Adult Medulloblastoma
Childhood Medulloblastoma
Herpes Simplex Infections
Undifferentiated carcinoma
Frontotemporal Lobar Degeneration
Encephalopathies
Dysmorphic features
Malignant neoplasm of mouth
Meningioma
Delayed speech and language development
Severe intellectual disability
Diabetes Mellitus, Experimental
Mammary Carcinoma, Human
Proteins
40
60
80
100
–Log10 Q
20.0
17.5
15.0
0 10 20 30
Meta-analysis enrichment (–Log10 P)
C
Down-regulated proteins in acbd6 crispant at 72 hpf : Enriched disease annotations
2887 Dr proteins mapped to 2274 Hs orthologues
Myopathy
Strabismus
Optic Atrophy
Developmental delay (disorder)
Dystonia
Deglutition Disorders
Nystagmus, CTCAE 3.0
Nystagmus, CTCAE 5.0
Muscle Spasticity
Hyperreflexia
Delayed speech and language development
Feeding difficulties
Hypoplasia of corpus callosum
Spasticity, CTCAE
Cerebral atrophy
Muscle Weakness
Flexion contracture
Movement Disorders
Neurodevelopmental Disorders
Sensorineural Hearing Loss (disorder)
Proteins
60
80
100
–Log10 Q
24
20
16
0 10 20 30
Meta-analysis enrichment (–Log10 P)
D
Up-regulated proteins in acbd6 crispant at 120 hpf : Enriched process annotations
2732 Dr proteins mapped to 2198 Hs orthologues
Metabolism of RNA
Translation
VEGFA–VEGFR2 signaling pathway
Nucleotide metabolic process
Regulation of translation
Signaling by Rho GTPases, Miro GTPases and RHOBTB3
Amino acid metabolic process
Amyotrophic lateral sclerosis
Ribosome biogenesis
Intracellular protein transport
Translation factors
Monocarboxylic acid metabolic process
Cell Cycle, Mitotic
Supramolecular fiber organization
RNA localization
Vesicle–mediated transport
Neutrophil degranulation
Non–membrane–bounded organelle assembly
Dis. of signal transd. by GF receptors and 2nd mess.
Carbon metabolism
Proteins
50
100
150
–Log10 Q
80
60
40
20
0 20 40 60 80 100
Meta-analysis enrichment (–Log10 P)
E
Up-regulated proteins in acbd6 crispant at 120 hpf : Enriched disease annotations
2732 Dr proteins mapped to 2198 Hs orthologues
Myopathy
Drug–Induced Liver Disease
Mammary Carcinoma, Human
Mammary Neoplasms, Human
Frontotemporal dementia
Chemical and Drug Induced Liver Injury
Diabetes Mellitus, Experimental
Hepatitis, Toxic
Chemically–Induced Liver Toxicity
Drug–Induced Acute Liver Injury
Hepatitis, Drug–Induced
Fatty Liver Disease
Encephalopathies
Hereditary Diffuse Gastric Cancer
Myocardial Ischemia
Meningioma
Acute leukemia
Malignant neoplasm of gallbladder
Hyperreflexia
Clumsiness – motor delay
Proteins
50
60
70
80
90
–Log10 Q
17.5
15.0
12.5
10.0
0 10 20 30
Meta-analysis enrichment (–Log10 P)
F
Down-regulated proteins in acbd6 crispant at 120 hpf : Enriched process annotations
2737 Dr proteins mapped to 2218 Hs orthologues
Nervous system development
Metabolism of RNA
Membrane Trafficking
Membrane organization
Pathways of neurodegeneration – multiple diseases
Signaling by Receptor Tyrosine Kinases
Cellular responses to stress
Transmission across Chemical Synapses
Nucleobase–containing small molecule metab. proc.
Metabolism of amino acids and derivatives
Cell Cycle
Synaptic vesicle cycle
Transport of small molecules
Hemostasis
HIV Infection
Muscle contraction
Signaling by Rho GTPases, Miro GTPases and RHOBTB3
Localization within membrane
VEGFA–VEGFR2 signaling pathway
Intracellular protein transport
Proteins
75
100
125
–Log10 Q
50
40
30
0 20 40 60
Meta-analysis enrichment (–Log10 P)
G
Down-regulated proteins in acbd6 crispant at 120 hpf : Enriched disease annotations
2737 Dr proteins mapped to 2218 Hs orthologues
Myopathy
Nystagmus, CTCAE 3.0
Nystagmus, CTCAE 5.0
Strabismus
Optic Atrophy
Feeding difficulties
Delayed speech and language development
Muscle Spasticity
Hypertrophic Cardiomyopathy
Deglutition Disorders
Dysmorphic features
Severe intellectual disability
Spasticity, CTCAE
Hyperreflexia
Developmental delay (disorder)
Sensorineural Hearing Loss (disorder)
Blepharoptosis
Ptosis
Cerebral atrophy
Respiratory Insufficiency
Proteins
80
100
120
–Log10 Q
30.0
27.5
25.0
22.5
20.0
0 10 20 30
Meta-analysis enrichment (–Log10 P)

Supplementary Figure 20. Whole proteome meta-analysis of wild-type and *acbd6* F_0 crispant zebrafish

(A) Top-20 of biological processes most significantly enriched in proteins up-regulated in *acbd6* F_0 crispant zebrafish at 72 hpf. Most significantly enriched process at the top. Colour indicates Q-value as secondary significance indicator. Size of circles indicates number of proteins enriched in depicted process. Dr: Danio rerio. Hs: Homo sapiens.

(B) Top-20 of disease networks most significantly enriched in proteins up-regulated in *acbd6* F_0 crispant zebrafish at 72 hpf. Further description as in (A).

(C) Top-20 of disease networks most significantly enriched in proteins down-regulated in *acbd6* F_0 crispant zebrafish at 72 hpf. Further description as in (A).

(D) Top-20 of biological processes most significantly enriched in proteins up-regulated in *acbd6* F_0 crispant zebrafish at 120 hpf. Further description as in (A).

(E) Top-20 of disease networks most significantly enriched in proteins up-regulated in *acbd6* F_0 crispant zebrafish at 120 hpf. Further description as in (A).

(F) Top-20 of biological processes most significantly enriched in proteins down-regulated in *acbd6* F_0 crispant zebrafish at 120 hpf. Further description as in (A).

(G) Top-20 of disease networks most significantly enriched in proteins down-regulated in *acbd6* F_0 crispant zebrafish at 120 hpf. Further description as in (A).

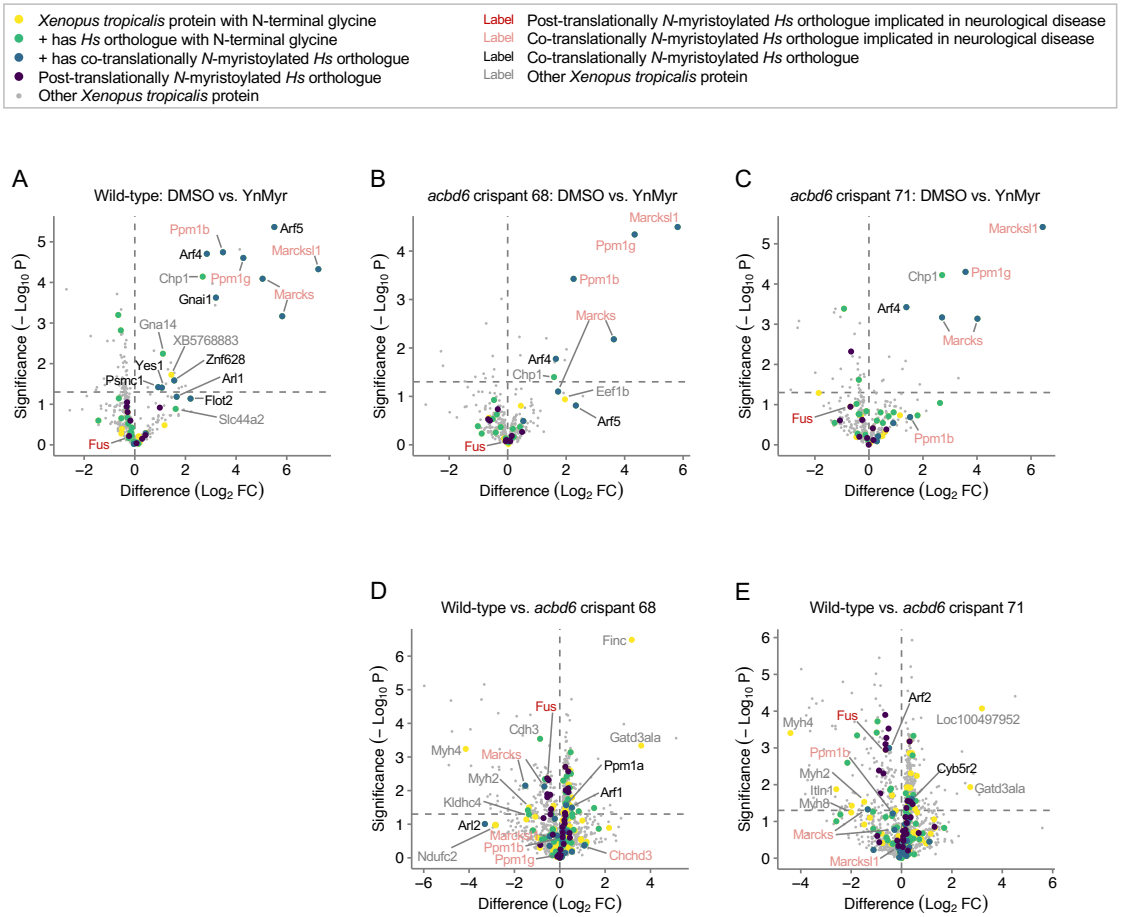
Xenopus tropicalis protein with N-terminal glycine
+ has Hs orthologue with N-terminal glycine
+ has co-translationally N-myristoylated Hs orthologue
Post-translationally N-myristoylated Hs orthologue
Other Xenopus tropicalis protein
Label Post-translationally N-myristoylated Hs orthologue implicated in neurological disease
Label Co-translationally N-myristoylated Hs orthologue implicated in neurological disease
Label Co-translationally N-myristoylated Hs orthologue
Label Other Xenopus tropicalis protein
A
Wild-type: DMSO vs. YnMyr
B
acbd6 crispant 68: DMSO vs. YnMyr
C
acbd6 crispant 71: DMSO vs. YnMyr
D
Wild-type vs. acbd6 crispant 68
E
Wild-type vs. acbd6 crispant 71
Significance (– Log10 P)
Difference (Log2 FC)
Arf5
Ppm1b
Arf4
Marcksl1
Chp1
Ppm1g
Gnai1
Marcks
Gna14
XB5768883
Yes1
Znf628
Psmc1
Arl1
Flot2
Slc44a2
Fus
Eef1b
Finc
Cdh3
Gatd3ala
Myh4
Ppm1a
Myh2
Kldhc4
Arl2
Ndufc2
Chchd3
Arf2
Loc100497952
Cyb5r2
Itln1
Myh8

Supplementary Figure 21. Chemical and whole proteome analysis of wild-type and *acbd6* crispant *X. tropicalis* (back)

(A) Volcano plot depicting YnMyr labelling of proteins in wild-type *X. tropicalis*. Horizontal dotted line: significance threshold (p-value = 0.05). FC: fold-change. Position on the left equals increased in DMSO condition (negative control), position on the right equals increased in YnMyr condition (positive control). Highlighted are proteins with well-validated *N*-myristoylated orthologues in *Homo sapiens* (black) including those implicated in neurological disorders (orange).

(B) YnMyr labelling of proteins in *acbd6* crispant 68 *X. tropicalis*. Further description as in (A).

(C) YnMyr labelling of proteins in *acbd6* crispant 71 *X. tropicalis*. Further description as in (A).

(D) Whole proteome analysis of proteins in wild-type and *acbd6* crispant 68 *X. tropicalis*. Horizontal dotted line: significance threshold (p-value = 0.05). FC: fold-change. Position on the left equals reduced in crispant, position on the right equals increased in crispant. Highlighted are proteins with well-validated *N*-myristoylated orthologues in *Homo sapiens* (black) including those implicated in neurological disorders (orange).

(E) Whole proteome analysis of proteins in wild-type and *acbd6* crispant 71 *X. tropicalis*. Further description as in (D).

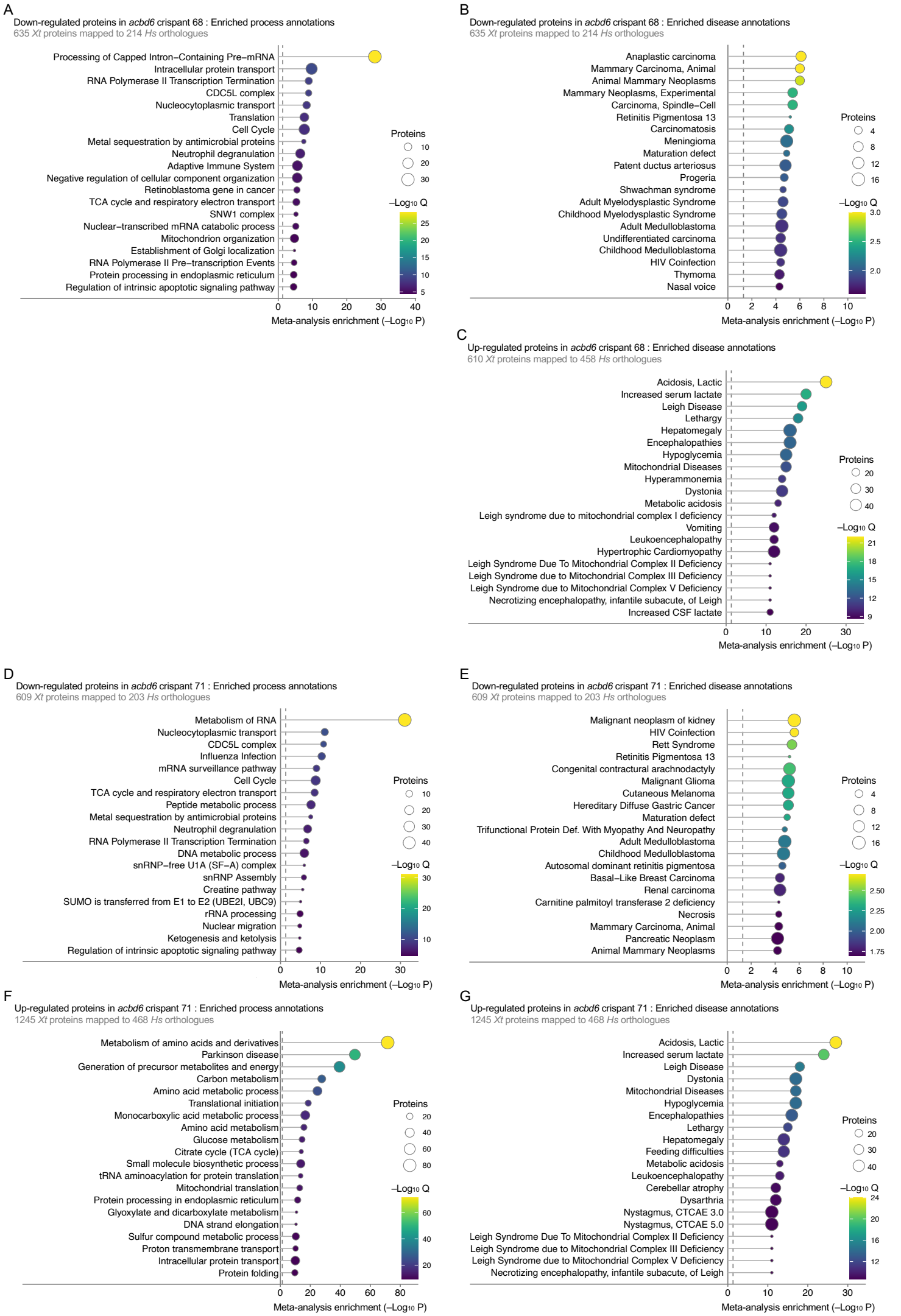
A
Down-regulated proteins in acbd6 crispant 68 : Enriched process annotations
635 Xt proteins mapped to 214 Hs orthologues
Processing of Capped Intron−Containing Pre−mRNA
Intracellular protein transport
RNA Polymerase II Transcription Termination
CDC5L complex
Nucleocytoplasmic transport
Translation
Cell Cycle
Metal sequestration by antimicrobial proteins
Neutrophil degranulation
Adaptive Immune System
Negative regulation of cellular component organization
Retinoblastoma gene in cancer
TCA cycle and respiratory electron transport
SNW1 complex
Nuclear−transcribed mRNA catabolic process
Mitochondrion organization
Establishment of Golgi localization
RNA Polymerase II Pre−transcription Events
Protein processing in endoplasmic reticulum
Regulation of intrinsic apoptotic signaling pathway
Proteins
10
20
30
−Log10 Q
25
20
15
10
5
0
10
20
30
40
Meta-analysis enrichment (−Log10 P)
B
Down-regulated proteins in acbd6 crispant 68 : Enriched disease annotations
635 Xt proteins mapped to 214 Hs orthologues
Anaplastic carcinoma
Mammary Carcinoma, Animal
Animal Mammary Neoplasms
Mammary Neoplasms, Experimental
Carcinoma, Spindle−Cell
Retinitis Pigmentosa 13
Carcinomatosis
Meningioma
Maturation defect
Patent ductus arteriosus
Progeria
Shwachman syndrome
Adult Myelodysplastic Syndrome
Childhood Myelodysplastic Syndrome
Adult Medulloblastoma
Undifferentiated carcinoma
Childhood Medulloblastoma
HIV Coinfection
Thymoma
Nasal voice
Proteins
4
8
12
16
−Log10 Q
3.0
2.5
2.0
0
2
4
6
8
10
Meta-analysis enrichment (−Log10 P)
C
Up-regulated proteins in acbd6 crispant 68 : Enriched disease annotations
610 Xt proteins mapped to 458 Hs orthologues
Acidosis, Lactic
Increased serum lactate
Leigh Disease
Lethargy
Hepatomegaly
Encephalopathies
Hypoglycemia
Mitochondrial Diseases
Hyperammonemia
Dystonia
Metabolic acidosis
Leigh syndrome due to mitochondrial complex I deficiency
Vomiting
Leukoencephalopathy
Hypertrophic Cardiomyopathy
Leigh Syndrome Due To Mitochondrial Complex II Deficiency
Leigh Syndrome due to Mitochondrial Complex III Deficiency
Leigh Syndrome due to Mitochondrial Complex V Deficiency
Necrotizing encephalopathy, infantile subacute, of Leigh
Increased CSF lactate
Proteins
20
30
40
−Log10 Q
21
18
15
12
9
0
10
20
30
Meta-analysis enrichment (−Log10 P)
D
Down-regulated proteins in acbd6 crispant 71 : Enriched process annotations
609 Xt proteins mapped to 203 Hs orthologues
Metabolism of RNA
Nucleocytoplasmic transport
CDC5L complex
Influenza Infection
mRNA surveillance pathway
Cell Cycle
TCA cycle and respiratory electron transport
Peptide metabolic process
Metal sequestration by antimicrobial proteins
Neutrophil degranulation
RNA Polymerase II Transcription Termination
DNA metabolic process
snRNP−free U1A (SF−A) complex
snRNP Assembly
Creatine pathway
SUMO is transferred from E1 to E2 (UBE2I, UBC9)
rRNA processing
Nuclear migration
Ketogenesis and ketolysis
Regulation of intrinsic apoptotic signaling pathway
Proteins
10
20
30
40
−Log10 Q
30
20
10
0
10
20
30
Meta-analysis enrichment (−Log10 P)
E
Down-regulated proteins in acbd6 crispant 71 : Enriched disease annotations
609 Xt proteins mapped to 203 Hs orthologues
Malignant neoplasm of kidney
HIV Coinfection
Rett Syndrome
Retinitis Pigmentosa 13
Congenital contractural arachnodactyly
Malignant Glioma
Cutaneous Melanoma
Hereditary Diffuse Gastric Cancer
Maturation defect
Trifunctional Protein Def. With Myopathy And Neuropathy
Adult Medulloblastoma
Childhood Medulloblastoma
Autosomal dominant retinitis pigmentosa
Basal−Like Breast Carcinoma
Renal carcinoma
Carnitine palmitoyl transferase 2 deficiency
Necrosis
Mammary Carcinoma, Animal
Pancreatic Neoplasm
Animal Mammary Neoplasms
Proteins
4
8
12
16
−Log10 Q
2.50
2.25
2.00
1.75
0
2
4
6
8
10
Meta-analysis enrichment (−Log10 P)
F
Up-regulated proteins in acbd6 crispant 71 : Enriched process annotations
1245 Xt proteins mapped to 468 Hs orthologues
Metabolism of amino acids and derivatives
Parkinson disease
Generation of precursor metabolites and energy
Carbon metabolism
Amino acid metabolic process
Translational initiation
Monocarboxylic acid metabolic process
Amino acid metabolism
Glucose metabolism
Citrate cycle (TCA cycle)
Small molecule biosynthetic process
tRNA aminoacylation for protein translation
Mitochondrial translation
Protein processing in endoplasmic reticulum
Glyoxylate and dicarboxylate metabolism
DNA strand elongation
Sulfur compound metabolic process
Proton transmembrane transport
Intracellular protein transport
Protein folding
Proteins
20
40
60
80
−Log10 Q
60
40
20
0
20
40
60
80
Meta-analysis enrichment (−Log10 P)
G
Up-regulated proteins in acbd6 crispant 71 : Enriched disease annotations
1245 Xt proteins mapped to 468 Hs orthologues
Acidosis, Lactic
Increased serum lactate
Leigh Disease
Dystonia
Mitochondrial Diseases
Hypoglycemia
Encephalopathies
Lethargy
Hepatomegaly
Feeding difficulties
Metabolic acidosis
Leukoencephalopathy
Cerebellar atrophy
Dysarthria
Nystagmus, CTCAE 3.0
Nystagmus, CTCAE 5.0
Leigh Syndrome Due To Mitochondrial Complex II Deficiency
Leigh Syndrome due to Mitochondrial Complex III Deficiency
Leigh Syndrome due to Mitochondrial Complex V Deficiency
Necrotizing encephalopathy, infantile subacute, of Leigh
Proteins
20
30
40
−Log10 Q
24
20
16
12
0
10
20
30
Meta-analysis enrichment (−Log10 P)

Supplementary Figure 22. Whole proteome meta-analysis of wild-type and *acbd6* crispant *Xenopus*

(A) Top-20 of biological processes most significantly enriched in proteins down-regulated in *acbd6* crispant 68 *X. tropicalis*. Most significantly enriched process at the top. Colour indicates Q-value as secondary significance indicator. Size of circles indicates number of proteins enriched in depicted process. Xt: *Xenopus tropicalis*. Hs: Homo sapiens.

(B) Top-20 of disease networks most significantly enriched in proteins down-regulated in *acbd6* crispant 68 *X. tropicalis*. Further description as in (A).

(C) Top-20 of disease networks most significantly enriched in proteins up-regulated in *acbd6* crispant 68 *X. tropicalis*. Further description as in (A).

(D) Top-20 of biological processes most significantly enriched in proteins down-regulated in *acbd6* crispant 71 *X. tropicalis s*. Further description as in (A).

(E) Top-20 of disease networks most significantly enriched in proteins down-regulated in *acbd6* crispant 71 *X. tropicalis*. Further description as in (A).

(F) Top-20 of biological processes most significantly enriched in proteins up-regulated in *acbd6* crispant 71 *X. tropicalis*. Further description as in (A).

(G) Top-20 of disease networks most significantly enriched in proteins up-regulated in *acbd6* crispant 71 *X. tropicalis*. Further description as in (A).

A All proteins identified with a N-terminal glycine

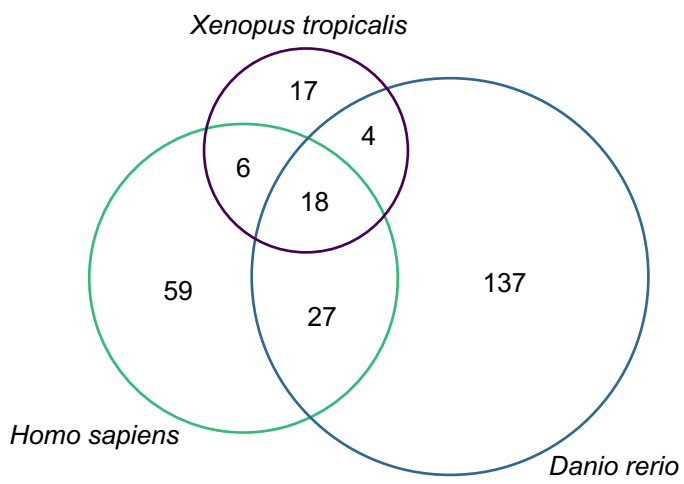

B Known proteins with N-terminal glycine in *Homo sapiens*

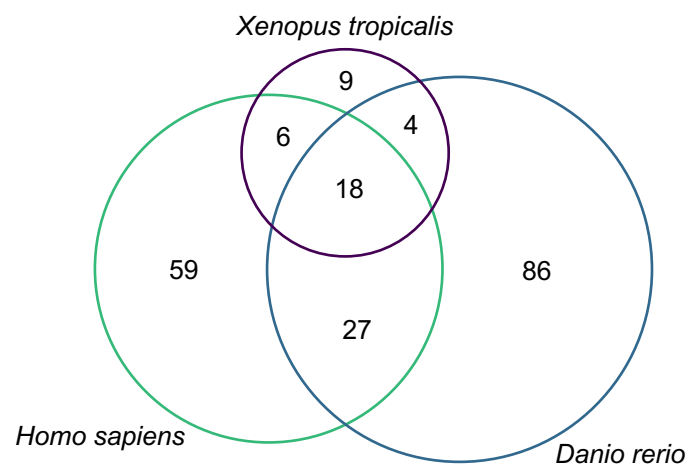

C Known co-translationally *N*-myristoylated proteins in *Homo sapiens*

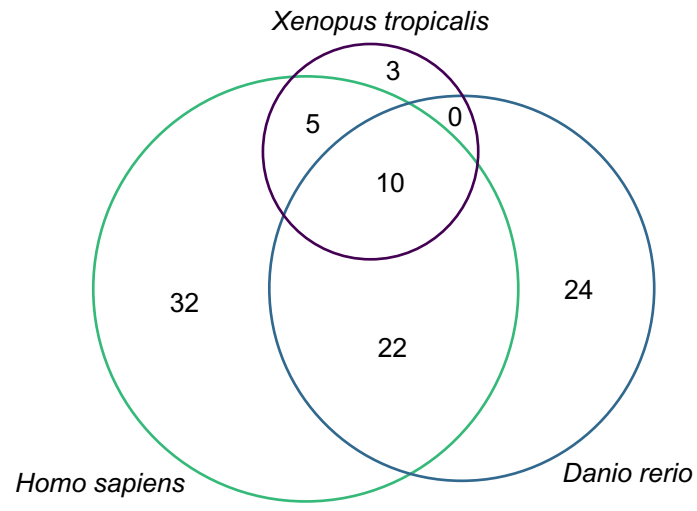

D

Overlap between *Homo sapiens, Danio rerio* and *Xenopus tropicalis* proteins
Co-translationally *N*-myristoylated protein in *Homo sapiens*
N-terminal glycine in *Homo sapiens*

Homo sapiens *Danio rerio* *Xenopus tropicalis*	*Homo sapiens* *Danio rerio*	*Homo sapiens* *Xenopus tropicalis*
EEF1A	AKAP12	ARF1
EEF1B	ARF6	ARF3
FLOT2	ATP1A1	ARL1
GNAI1	BASP1	CHP1
GNAI2	CAV2	RPS17
GORASP2	CHCHD3	SAMM50
HMGB2	CHCHD6	
MARCKS	CHMP6	
MARCKSL1	DUSP22	
PPM1B	FAM49A	
PPM1G	FMNL3	
PSMC1	GNAI3	
RPL10	LAMTOR1	
RPL18	LNP	
RPL5	LRRC57	
RPL8	MGRN1	
RPS23	NCS1	
SLC44A1	NDUFAF4	
	PPM1A	
	PPP3R1	
	PRKACB	
	PRMT1	
	RP2	
	RPS8	
	SRC	
	TLDC1	
	TMEM106B	

E Known post-translationally *N*-myristoylated proteins in *Homo sapiens*

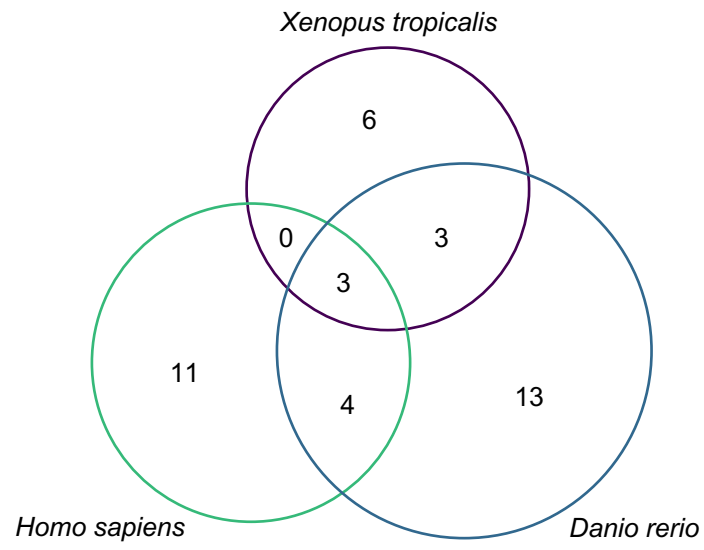

F

Identified orthologues of post-translationally *N*-myristoylated *Homo sapiens* proteins in *Danio rerio* and *Xenopus tropicalis*.

Homo sapiens *Danio rerio* *Xenopus tropicalis*	*Homo sapiens* *Danio rerio*	*Homo sapiens* *Xenopus tropicalis*
FUS	BCAP31	*No overlap*
HSPA4	HNRNPA0	
NCL	ILF3	
	MYL6	

Supplementary Figure 23. Comparison of overlap in identified (potential) N-myristoylated proteins between *Homo sapiens*, *Danio rerio* and *Xenopus tropicalis*

(A) Venn diagram depicting overlap between proteins identified in *Homo sapiens*, *Danio rerio* and *Xenopus tropicalis* containing a N-terminal glycine.

(B) Venn diagram depicting overlap between proteins with a N-terminal glycine identified in *Homo sapiens*, *Danio rerio* and *Xenopus tropicalis*, which have an orthologue with a N-terminal glycine in *Homo sapiens*.

(C) Venn diagram depicting overlap between proteins with a N-terminal glycine identified in *Homo sapiens*, *Danio rerio* and *Xenopus tropicalis*, which have a co-translationally *N*-myristoylated orthologue in *Homo sapiens*.

(D) List of potential co-translationally *N*-myristoylated proteins overlapping between *Homo sapiens*, *Danio rerio* and *Xenopus tropicalis*. *Danio rerio* and *Xenopus tropicalis* proteins with an orthologue in *Homo sapiens* with a N-terminal glycine are depicted in gray, with a co-translationally *N*-myristoylated orthologue in *Homo sapiens* in orange.

(E) Venn diagram depicting overlap between proteins identified in *Homo sapiens*, *Danio rerio* and *Xenopus tropicalis*, which have a post-translationally *N*-myristoylated orthologue in *Homo sapiens*.

(F) List of potential post-translationally *N*-myristoylated proteins overlapping between *Homo sapiens*, *Danio rerio* and *Xenopus tropicalis*.

SUPPLEMENTARY TABLES

Supplementary Table 1. Detailed clinical description and *ACBD6* variant characteristics are *Available as a separate Excel file.* **(back)**

Supplementary Table 2. *ACBD6* variants details including pathogenicity prediction and presence in genomic databases**.** *Available as a separate Excel file.* **(back)**

Legend: GERP score calculated using ``varsome.com``. GERP++ track with the average value for the specific nucleotide genomic position presented.

Supplementary Table 3. The frequency of facial dysmorphic features. Available as a separate Excel file. **(back)**

Supplementary Table 4. Detailed dysmorphic features of the *ACBD6* cohort members with available facial photographs. Available as a separate Excel file. **(back)**

Supplementary Table 5. Peroxisomal VLCFA β-oxidation is normal in ACBD6-deficient patient fibroblasts. **(back)**

D3-C22 loading test (nmol/mg protein)	Patient 1	Patient 2	Brother Patient 1	Control 1	Control 2	ZSD
D3-C26 (chain elongation)	0.09	0.17	0.09	0.13	0.2	2.01
D3-C16/D3C22 ratio (beta-oxidation)	2.23	1.70	1.77	1.54	1.64	0.01

Peroxisomal β-oxidation parameters were determined in two ACBD6-deficient patient fibroblast cell lines (patient 1 and 2). Fibroblasts from the healthy brother of patient 1 as well as fibroblasts from healthy individuals and a patient with peroxisomal Zellweger Spectrum Disorder (ZSD) served as controls. VLCFA metabolism (D3-C22:0 loading test) was measured.

Note that peroxisomal VLCFA β-oxidation and chain elongation is normal in ACBD6-deficient patients and healthy controls but altered in ZSD cells. Data present mean of duplicate measurements.

Supplementary Table 6. Primer list for zebrafish studies. Available as a separate Excel file. **(back)**

Supplementary Table 7. Disorders to consider in the differential diagnosis of *ACBD6*-related disease. Available is a separate Word file. **(back)**

SUPPLEMENTARY CASE REPORTS (back)

Family 1

The proband (F1:S1) from Family 1 is a 37-year-old female who was born full-term to consanguineous Iranian parents. Her parents are healthy with an unremarkable family history. The proband has two affected brothers (F1:S2 and F1:S3) currently aged 22 and 20 years old, and two healthy siblings. The affected brothers were also born full-term following an uneventful pregnancy and delivery. All affected siblings in this family were noted to have severe global developmental delay (GDD), intellectual disability (ID), and impaired speech. The index case started independent walking only after 4.5 years but her youngest brother (F1:S3) failed to acquire autonomous ambulation and has severe congenital clubfoot. All of them have aggressive behavior and fighting responses to each other with self-injury and sleep disturbance. They also had some dysmorphic facial features including high-set arched eyebrows (F1:S1 and F1:S2), mild proptosis (F1:S1 and F1:S2), broad nasal bridge (all siblings), thin upper lip (F1:S1 and F1:S2), small mouth (F1:S1 and F1:S2), prominent jaw (all siblings), prominent supraorbital ridges (F1:S2), and low set eyebrows (F1:S3). The index case and the youngest affected sibling (F1:S3) had developed complex partial seizures from age 35 and two years old,

respectively. Electroencephalogram (EEG) in the proband showed right spike wake discharge and in the sibling, it revealed bilateral poly spike discharges. The latter has been managed with valproic acid.

Upon examination at current ages, they all had a severe ID, a suggestion of reduced upgaze, dystonia, and short stature. The index case and the older affected sibling (F1:S2) had little expressive speech with dysarthria and likely preserved perceptive language. Their gait was broad-based, suggestive of gait ataxia. The index case had episodes of gait freezing and a suggestion of left lower limb dystonia. Dystonia presented with a prominent stooped posture in all affected siblings. While the older affected siblings seemed to have a paucity of movements, the non-ambulant younger brother (F1:S3) had frequent jerky movements in the upper limbs, head, and face (including simple motor tics) periodically accompanied by simple vocal tics. This sibling was non-verbal and had additional urinary incontinence. Psychomotor regression and signs of premature aging were reported in all affected siblings along the course of their disease. Post-contrast brain magnetic resonance imaging (MRI) in the index case performed at 35 years of age showed hypoplasia of the posterior corpus callosum, agenesis of the anterior commissure, short midbrain, and cerebellar vermis hypoplasia. Moreover, there were multiple ring-enhancing abscesses with surrounding vasogenic edema in the right temporoparietal lobes associated with signs of ventriculitis and hydrocephalus. Brain MRI of the older affected sibling (F1:S2) showed partial agenesis of the corpus callosum, anterior commissure hypoplasia, short midbrain, small cerebellar vermis, and focal periventricular white matter lesions.

Family 2

The affected individual F2:S1 is a 7-year-old girl from a consanguineous Lebanese family with first-degree cousin marriage. She has three unaffected elder siblings. Her occipitofrontal circumference (OFC) at birth was 33 cm/ -1.4 z, her birth weight 3.1 kg/ -0.9 z, height at birth 47 cm/ -2.1 z. The height at the last examination was 102.5 cm/ -4.3 (below average) and weight

23.2 kg/ -0.2 z. She had severe GDD and currently is unable to sit independently. Her neurological examination was remarkable with spasticity, ataxia, spastic-ataxic gait, and tremor. She is non-verbal and has a severe ID. From the age of 3 years, she started experiencing myoclonic seizures with multifocal spike-wave complexes on EEG. Brain MRI showed hypoplastic corpus callosum and incomplete hippocampal rotation. She had no behavioral abnormalities but similar to other patients with *ACBD6* variants, she had a coarse face, deep-set eyes, a broad nose with a depressed nasal bridge, and an everted lower lip.

Family 3

Family 3 has two affected males F3:S1 and F3:S2 currently aged 27 and 20 years, respectively. Both were born borderline pre-term at the gestational age of 37 weeks to a consanguineous Turkish family. Early postnatal measurements were unremarkable in both. Currently, the older sibling (F3:S1) has a slightly short height, which is 160 cm (-2.91 z). The disease manifested with severe GDD in both. On examination, they had truncal dystonia with a stooped posture, spasticity, broad-based ataxic gait, and tremor. The older sibling is more affected than the younger brother. Their receptive language seems to be less affected, but they could express only a few words. The degree of ID was moderate. Both were reported to have high myopia, muscular hypotonia at early ages, anxiety, and hyperactivity. The older sibling (F3:S1) had gradually developed parkinsonism with hypomimia, a moderate degree of lateral body flexion, anteflexion, head tremor, and drooling. His spasticity was asymmetric, predominating on the right side, and on walking, he had some foot dystonia. In addition to this, the older sibling had nystagmus and arterial hypertension, while the younger sibling had cryptorchidism and hypospadias. Both siblings seemed to regress in motor skills after the initial delayed acquisition. Regarding facial dysmorphism, as a child, F3:S1 had medial eyebrow flare, hypertelorism, small nose, depressed nasal bridge, full nasal tip, short and smooth philtrum, thin upper lip, and broad chin. As an adult, he currently has widow's peak, right convergent squint, prominent

supraorbital ridges, thick eyebrows, a high nasal ridge, a small mouth with a full lower lip, and a broad chin. His younger brother (F3:S2) as a child showed bi-frontal narrowing, up-slanting palpebral fissures, hypertelorism, broad nasal bridge, full nasal tip, short philtrum, small mouth, full lips, and a broad chin. In adulthood, he had a squint, widow's peak, bifrontal narrowing, laterally sparse eyebrows, up-slanting palpebral fissures (USPFs), thin nasal ridge, full nasal tip, small mouth, full lower lip, and a broad chin. Brain MRI performed on the older affected brother (F3:S1) at the age of 20 years showed hypoplasia of the corpus callosum and anterior commissure, associated with the mild reduction of periventricular white matter and ventricular dilatation. Brain MRI performed in the younger brother (F3:S2) at the age of 11 years was unremarkable.

Family 4

The affected boy F4:S1, currently aged 1 year, is a product of an uneventful pregnancy born to a first-cousin couple from Bangladesh. His OFC at birth was normal. His disease manifested with severe GDD, neonatal generalized tonic-clonic seizures (GTCS), and occasional difficulty. He was spastic and showed some elements of ataxia and tremor. By the age of one year, he had expressed no behavioral abnormalities. Recently, he has developed repeated vomiting and has been found to have hepatomegaly. MRI brain and EEG were unavailable.

Family 5

The affected siblings (F5:S1 and F5:S2) are female and male currently aged 17 and 6 years old, respectively. They were born to a consanguineous Egyptian family with a first-degree cousin marriage. Both had unremarkable prenatal history and normal postnatal measurements but currently, have short stature. The disease manifested in both with moderate GDD. The older sibling (F5:S1) sat independently at the age of 2 years and was able to walk only from the age of 6 years. The younger sibling (F5:S2) started sitting independently from 18 months of age

and acquired walking from the age of 5.5 years. Both had velocity-dependent spasticity in the lower limbs, ataxia, and spastic-ataxic gait, together with the head and upper limb rest and postural tremor. The older sibling had undergone tendon surgery for her lower limb spasticity. They had broken pursuit and limited upgaze. They did not express parkinsonism or limb dystonia; however, truncal dystonia was present in both leading to forward stooped posture and lateral flexion of the body. A moderate degree of ID was common for both siblings and they were able to express only a few words. While the older sibling developed generalized tonic-clonic seizures from the age of 2 years, the younger sibling started experiencing atonic seizures from the age of 6 months. The seizures were infrequent with a good response to antiepileptic medication. Their EEG showed multifocal spikes and generalized discharges, respectively. Self-aggression, sleep disturbances together with dysmorphic features including a coarse face, broad nose with a depressed nasal bridge, and USPFs were among the shared symptoms in both affected individuals. Prognathia, breathing difficulty, and hepatomegaly associated with organic acidaemia were reported in the older sibling. Brain MRI performed in the older sibling (F5:S1) at the age of 12 years showed short midbrain and inferior vermis hypoplasia. Brain MRI performed in the younger sibling (F5:S2) at the age of 5 months revealed a marked reduction of periventricular white matter with moderate dilatation of the lateral ventricles, hypoplasia of the corpus callosum, and incomplete hippocampal rotation.

Family 6

The affected cousins are a 20-year-old male (F6:S1) and a 10-year-old female (F6:S2), respectively, born full-term to consanguineous parents of Pakistani origin. Their parents are unaffected first-degree cousins. Clinical presentation in the affected cousins was remarkable with GDD, significantly delayed walking until the age of 5 years, and ID. They had a pseudobulbar smile, expressive language impairment, progressive spasticity, and ataxic gait. Both cousins did not express seizures. The elder male cousin (F6:S1) had gradually developed

a whole-body jerky tremor predominating on the right side combined with limited upgaze, hypomimia, negative myoclonus in the limbs, and dystonia. He had cervical dystonia with head posturing and jerky head tremor. Lateral flexion of the body and the right foot and arm dystonia with asymmetric limb spasticity were also present. His gait was particularly spastic-ataxic. He was reported to have night blindness, breathing difficulties, urinary incontinence, and premature aging. Behaviorally, there was aggression with temper tantrums. His EEG showed signs suggestive of neuronal dysfunction and his brain MRI performed at the age of 20 years showed short midbrain and small inferior cerebellar vermis. The younger female cousin (F6:S2), in addition to similar symptoms to her cousin, had twitching movements on the angle of her mouth, and sleep disturbances. She has also gradually developed a stooped posture with flexion of the body to one side. Her brain MRI performed at the age of 10 years revealed hypoplasia of the posterior corpus callosum, anterior commissure agenesis, short midbrain, small inferior vermis, and hypertrophy of the clava. EMG and nerve conduction studies in both siblings were normal. In terms of dysmorphic features, both cousins shared common signs such as short stature, hypertelorism, arched eyebrows, thin upper lip, and a broad chin. In addition to this, F6:S2 had USPFs, left divergent squint, prominent supraorbital ridges, depressed nasal bridge, and full nasal tip. F6:S1 additionally had a long face, blue irises, triangular nose, high nasal ridge, flared nasal alae, low-set columella, and short philtrum. The disease course in both affected individuals was remarkable with dystonia, progressive ataxic gait impairment, and slowness of movements. Noticeably, both affected cousins seemed to regress after the initial acquisition of walking skills as well as expressed the signs of cognitive regression.

Family 7

The proband (F7:S2) is a 16-year-old male born to a distant cousin couple of Pakistani origin. The disease manifested with moderate GDD/ID. Presently, he presents with short stature, language impairment, hand posturing, and spasticity coupled with a broad-based clumsy gait.

He has not developed seizures but experiences sleep disturbances and frequently becomes aggressive. From dysmorphic features, he had prominent supraorbital ridges, a high nasal ridge, a full nasal tip, a thin upper lip, and a broad chin. He has gradually developed a stooped posture. Brain MRI performed at the age of 7 years showed agenesis of the corpus callosum and anterior commissure, colpocephaly, and inferior vermis hypoplasia. His older sibling (F7:S1), currently aged 25 years, presented with similar features, gradually developing bradykinesia, stooped posture, and gradual psychomotor regression. He had a tall forehead, high anterior hairline, prominent supraorbital ridges, squint, triangular nose with high ridge and low columella, small mouth, thin upper lip, full lower lip, and a broad chin. His brain MRI performed at the age of 12 years revealed hypoplasia of the posterior corpus callosum, anterior commissure agenesis, incomplete hippocampal rotation, short midbrain, and hypoplasia of the inferior cerebellar vermis. This affected individual (F7:S1) showed signs of premature aging.

Family 8

Two affected siblings (F8:S1 and F8:S2) are an 8-year-old girl and a 6-year-old boy from a consanguineous Tajik family where parents are first-degree cousins. The affected girl was born pre-term and both siblings had normal early post-natal measurements. They could sit independently only from the age of 3 years and started walking at 4 years. Currently, both of them are non-verbal and have spasticity combined with an ataxic gait. They have moderate-to-severe ID, stereotypic mouth dyskinesia, simple motor and vocal tics, some aggression, hand stereotypies, and elements of hyperactivity. Short stature, frontal upsweep of hair, bi-frontal narrowing, squint, high set arched eyebrows, hypertelorism, and broad and depressed nasal bridge combined with a small nose, short columella, triangular nares, broad chin were present in both siblings. Both of them had slightly stooped posture on standing and walking. Up to the current age, no seizures have been reported. Brain MRI of the older sibling (F8:S1) showed

agenesis of the anterior commissure, short midbrain, and inferior vermis hypoplasia. Brain MRI of the younger sibling (F8:S2) was unremarkable.

Family 9

The index (F9:S1) case is an 8-year-old girl born to consanguineous Iranian parents at a normal gestational age with normal post-natal measurement. Her current height is normal for her age. She had moderate to severe GDD/ID, language impairment, suspected partial seizures from the age of 6 months, and poor vision. Currently, she can ambulate independently. Her brain MRI and EEG are unavailable.

Family 10

The affected siblings (F10:S1 and F10:S2) are a 6-year-old girl and a 3-year-old boy born full-term to a healthy first-cousin couple of Egyptian origin. They had unremarkable birth weight, height, and OFC. The disease manifested with moderate GDD in the female, and the male expressed mild motor delay. Currently, they are able to walk with support and their gait is ataxic. Both had undergone tendon surgery due to lower limb spasticity. They have a severe ID and can express only a few words. There was not a history of seizures but EEG showed focal epileptogenic activity with secondary generalization in both siblings. On examination, they had dysmorphic facial features including a tall forehead (F10:S1), high anterior hairline (both siblings), hypertelorism (both siblings), USPFs (F10:S1), and high nasal bridge (F10:S1) combined with flared nasal alae (F10:S1), thin upper lip (both siblings), curly hair (F10:S2), and high anterior hairline (F10:S2) and associated with sparse lateral half of the eyebrows (F10:S2), depressed nasal bridge (F10:S2), full nasal tip (F10:S2), long and smooth philtrum (F10:S2). Neurological examination showed broken pursuit, limited upgaze, upper limb, and truncal ataxia in both siblings. The muscle tone in the upper limbs was normal and mild hypertonia was present in the lower limbs. There were head tremor and jerky upper limb tremor

at rest and posture. No parkinsonism signs were found but mild upper limbs dystonia on pronation/supination was present. Both siblings had a stooped posture and lateral flexion of the body. The lower limbs were not dystonic. They had postural instability, and urinary incontinence with no orthostatic hypotension. Behaviorally, they were reported to have temper tantrums with sleep disturbances but no aggression. Autistic spectrum disorder with hand stereotypies and hyperactivity were shared features between the two siblings. Brain MRI performed in the sister (F10:S1) at the age of 2 years depicted mild reduction of periventricular white matter and ventricular dilatation, hypoplasia of posterior corpus callosum, anterior commissure agenesis, incomplete hippocampal rotation, short midbrain, and inferior vermis hypoplasia. Brain MRI performed in the younger brother (F10:S2) at the age of 3 years showed hypoplasia of the posterior corpus callosum, agenesis of the anterior commissure, and short midbrain with normal cerebellar vermis.

Family 11

The proband is a 20-year-old man (F11:S1) born at term to a consanguineous Turkish family. He manifested severe GDD in all domains. Independent sitting was acquired by 4-year-olds, started walking with support from 7 years old, and was found to have a severe ID. Currently, his speech is limited to single words, and he is unstable with a broad-based gait. Upon examination, he was found to have a small head circumference with short stature, cerebellar ataxia with the head and upper limb tremor, hand dysmetria, stooped, and laterally flexed body posture with postural instability. Muscle tone in the limbs was reported to be normal and he had not exhibited any epileptic seizures until his current age. Behaviorally, he is hyperactive with hand stereotypes and incontinence. Concerning facial dysmorphism, as a child, he had high-set arched eyebrows, a narrow nose with a high nasal bridge, a thin upper lip, a small mouth, and a broad chin. As an adult, he has a long face, hypertelorism, USPFs, high nasal ridge, small mouth, and broad and tall chin. Brain MRI performed at the age of 13 years showed partial

agenesis of the corpus callosum, incomplete hippocampal rotation, agenesis of the anterior commissure, ventriculomegaly, short midbrain, and inferior vermis hypoplasia.

Family 12

This family presents with 2 affected female siblings (F12:S1 and F12:S2) currently aged 2.5 and 4 years old. Their parents are neurologically healthy consanguineous Native Americans (Choctaw). Both affected siblings were born at term with a history of intrauterine growth restriction. Both presented with failure to thrive (small, poor weight gain), hypotonia, and moderately severe GDD. They started walking independently by the age of 2 years with unsteady clumsy gait. Speech acquisition is also delayed as currently, the younger sibling is non-verbal and the older sibling can use only single words. There was no history of epileptic seizures. At the recent follow-up examination, they had ID, impaired pursuit with normal saccades, mild truncal ataxia with no limb spasticity, and hyperkinetic movement disorders. Both siblings were found to have urinary incontinence and dysmorphic features including lateral USPFs, and a thin upper lip. Additionally, everted lower lip, prognathia, cleft palate, and telecanthus were present in the younger sibling. Brain MRI scans were unavailable.

Family 13

The index case is an 11-year-old Egyptian boy (F13:S1) born full-term to consanguineous neurologically healthy parents. His physical measurements were unremarkable at birth: however, at age 11 years he was found to have small head size (-2.2SD) and low body weight (-2.9SD). He manifested moderate GDD/ID and currently can only say a few words. Independent sitting and walking were delayed until the ages of 2 and 3 years, respectively. Myoclonic-tonic seizures started at the age of 2 years, and they were controlled with valproate, lamotrigine, and levetiracetam. EEG showed bitemporal epileptogenic focus. On neurological examination, he had impaired saccades with limited upgaze. Muscle tone revealed velocity-

dependent mild hypertonia in the upper and lower limbs. At the age of 10, he had a tendon release surgery related to spasticity in his lower limbs. He was mildly ataxic in his limbs and his gait was impaired. Head and limb tremor together with truncal dystonia leading to forward and lateral flexion of the body and postural instability were present. A trial of levodopa provided a minimal benefit. Urinary incontinence was present. Behaviorally, he was reported to have autistic features, temper tantrums, sleep disturbances, hand stereotypic movement, excessive laughing, hyperactivity, and polyphagia. Dysmorphological review of his facial photos shows squint, thick eyebrows, bifrontal narrowing, mild hypertelorism, and a prominent nose with a high nasal ridge and full tip coupled with low-set and posteriorly rotated ears, tented upper lip, full lower lip, and broad chin. Brain MRI performed at 10 years of age revealed a small anterior commissure, mild white matter volume loss, bilateral incomplete hippocampal rotation, and hypertrophy of the clava.

Family 14

The affected individual is a 4-year-old boy (F14:S1) born after an uneventful pregnancy and delivery to consanguineous parents from Iran. He presented with failure to thrive and moderate GDD. His speech is currently limited to only a few words and he failed to acquire independent ambulation. At age 4 years, his head circumference was below the 13th percentile, and his weight and height were below the 0.4th percentile. On examination, he had velocity-dependent upper and lower limb spasticity, limb ataxia with head and had tremor, and truncal dystonia (stooping and lateral flexion of the body) with scoliosis. Urinary incontinence, episodes of aggressive and hyperactive behaviour, and sleep problems were reported by parents. Dysmorphological review of his facial photos shows a high anterior hairline, frontal prominence, and USPFs combined with a full nasal tip, small mouth, full and everted lower lip, as well as a pointed chin. Brain MRI performed at 1 year of age showed posterior corpus callosum hypoplasia, absent anterior commissure, minimal white matter volume loss, bilateral

incomplete hippocampal rotation, slightly short midbrain, T2 hyperintensity of the central tegmental tracts, and hypertrophy of the clava.

Family 15

This family presents with a 7-year-old affected boy (F15:S1) born to first-degree cousins from Egypt. His neonatal and current physical measurements were within normal limits. He manifested moderate GDD with delayed sitting and walking up to the ages of 2 and 3 years, respectively. He currently presents with ID and speech limited to single words. Upon examination, he had impaired saccades with limited upgaze. Mild hypertonia in lower limbs, limb and gait ataxia, as well as head and arm tremor with truncal dystonia, were among the conspicuous movement abnormalities. He was reported to have behavioral problems mainly encompassing autistic features, temper tantrums, and sleep disturbances. A dysmorphological review of his facial photos showed bifrontal narrowing, flat anterior facies, depressed nasal bridge, full nasal tip, full lips and cheeks, and broad chin. His brain MRI scan performed at 6 years of age demonstrated a small anterior commissure with normal corpus callosum.

Family 16

The proband is a 15-year-old female (F16:S1) born after an uneventful pregnancy to consanguineous Brazilian parents. She does not have any siblings. She presents with moderate to severe GDD/ID with the acquisition of independent gait by age 7 years and significantly delayed speech. She is dependent on daily activities, is nonverbal, and cannot communicate. From the age of 11, she started experiencing tonic-clonic seizures recurring weekly. Her seizures were controlled with two antiepileptic medications, phenobarbital, and carbamazepine. She later needed to use oxcarbazepine and currently only uses phenobarbital to control her seizures. Examination revealed impaired smooth eye movements, limb spasticity and ataxia, and unsteady gait with limb and head tremor. Generalized dystonia involving upper and lower limbs and trunk leading to lateral flexion of the body was present. She had postural instability

and urinary incontinence. Her gait was described as parkinsonian and her parkinsonism did not respond to levodopa after 6 months. She had self-injurious behavior with temper tantrums and autistic features. Her facial dysmorphism was reported to include coarse facial features with lateral USPFs, a broad nose with a depressed nasal bridge, a thin upper lip, and an everted lower lip. Brain MRI showed corpus callosum hypoplasia.

Family 17

In this family, there are affected male and female siblings, aged 50- and 37-years-old, respectively (F17:S1 and F17:S2). Their parents are consanguineous and originated from Portugal. For the index (male sibling), the initial clinical record dated back to the age of 12 years old, with spastic diplegia, ataxia, profound ID, coarse facial features, and inappropriate laugh noted. Later, he presented parkinsonism, tremor, and gait disturbances. A brain MRI performed at 39 years of age revealed agenesis of the corpus callosum. Currently, at 50 years old he has suffered a regression, has lost his speech, and is confined to a wheelchair. His sister was born at term after an uneventful pregnancy, with a normal birth weight (3.4 kg). She has been followed by the Clinical Genetics department since she was 7 months old. She was referred to us for evaluation of GDD and dysmorphic features, resembling her older brother. At that time, she had a normal ophthalmological evaluation, normal metabolic screening, and normal karyotype (46, XX), and a mild epiphyseal dysplasia on radiographs. She has similar clinical findings with severe ID, very limited language (speaks only a few words), tremor, gait disturbance, inappropriate laughing, kyphoscoliosis, and small hands and feet. Their dysmorphic facial features included coarse facies (adult), thick eyebrows, full nasal tip, broad chin, and wide mouth. Brain MRI showed agenesis of the corpus callosum. They have one unaffected brother. Their father is said to have parkinsonism and psychosis, suggestive of Lewy Body dementia.

Family 18

Proband is a 7-year-old girl born in a consanguineous Saudi family (F18:S1). She was evaluated for GDD, and walked at age 3-years-old. A brain MRI scan is not available.

Family 19

This family presents with affected twins (F19:S1 and F19:S2) born prematurely via Cesarean section to consanguineous Palestinian Arab parents. Upon birth, they had small head circumference and body weight, and currently, at the age of 5.5 years, their weight is within the 50-75th percentile, whereas their height is below the 10th percentile. Both presented with severe GDD/ID and both are currently unable to walk independently. On examination, they had limited speech, upper and lower limb spasticity, ataxia, head tremor with forward stooped posture, and lower limb dystonia. Parents reported urinary incontinence and behavioral issues. Facial dysmorphic features included high anterior hairline, bifrontal narrowing, fullness over the forehead in the midline, and laterally arched eyebrows coupled with USPFs, high nasal ridge, full nasal tip, full lower lip, and a broad chin. Brain MRI showed partial agenesis of the corpus callosum and mild hypertrophy of the clava in both twins.

Family 20

This is a consanguineous family from Iraq that presents with affected siblings currently aged 8 (F20:S2) and 17 years old (F20:S1). They present with failure to thrive (currently they have short stature and low weight) and moderate GDD/ID. They failed to acquire independent ambulation and exhibited cerebellar ataxia, upper and lower limb dystonia, and urinary incontinence together with temper tantrums. On examination, F20:S1 showed an inability to stand independently, foot deformities, lower limb hypotonia with periodic myoclonic jerks, stooped body posture, drooling, a pseudobulbar smile, and preserved perceptive language. F20:S2 showed an inability to stand independently, foot deformities, lower limb hypotonia, stooped body posture, simple vocal and motor tics, stereotypies in the upper limbs, and a

pseudobulbar smile. The review of their facial images showed a long face, thick and arched eyebrows, USPFs, and full nasal tip coupled with low-set columella, broad chin, hypertelorism, and full cheeks. Head computed tomography (CT) scans were normal in both siblings.

Family 21

The index case (F21:S1) is a 10-year-old female from a European non-consanguineous family. She was born at term after an unremarkable pregnancy and delivery with normal birth measurements. She manifested severe GDD and has still not acquired an independent gait. From the age of 6-7 months, she had frequent epileptic spasms that were controlled with valproic acid. EEG showed slow background activity with temporal-occipital spikes, increased during sleep. Upon the most recent examination, her speech was limited to a few words. Cranial nerve examination revealed strabismus. She was reported to have neither spasticity nor ataxia; however, she did have dyskinetic movements, mainly involving the mouth and limbs. Her facial dysmorphic features included long columella, high-arched eyebrows, thin upper lip, USBFs, and tapered fingers. Brain MRI report showed mild cerebellar atrophy and dysmorphic corpus callosum (two MRIs at 6 and 9 years did not show any sign of progression). Brain MRI performed at 6 and 9 years of age demonstrated corpus callosum hypoplasia and non-progressive mild cerebellar atrophy.

Family 22

This family presents with 2 affected female siblings currently aged 29 (F22:S1) and 33 (F22:S2). Very limited clinical details were obtainable from this family mainly described as having GDD/ID and autism spectrum disorders.

Family 23

This family has two affected male siblings aged 6 (F23:S1) and 4 (F23:S2) years old, respectively. Both of them a born full-term to consanguineous Arab parents. The disease

manifested with moderate GDD with the later precipitation of lower limb spasticity in the older affected sibling who started walking on tiptoes only at the age of 3 years. At the age of 2 years, the older affected sibling developed epileptic seizures. The younger sibling currently has GDD only with a prominent speech delay. Brain MRIs are not available for review.

Family 24

This is a 1.5-year-old male (F24:S1) from Saudi Arabia who was born full-term to consanguineous parents after an uneventful pregnancy and delivery. Until now he has displayed moderate GDD.

Family 25

This family presented with an 11-year-old female (F25:S1) born full tern to consanguineous parents from Saudi Arabia. She has severe GDD with no speech and no walking. At the age of 11 years, she is able only to crawl and she reported having seizures.

Family 26

F26 has 2 affected siblings aged 9 (F26:S1) and 6 (F26:S2) years old born to a consanguineous Iraqi family. Their mother had a history of two spontaneous abortions. Currently, limited clinical details are available from this family. It is known that both affected siblings have severe GDD/ID, gait disturbances associated with cerebellar ataxia, generalized spasticity, and muscle rigidity. Both affected are reported to have obesity. No diabetes, hearing, or visual impairment was reported.

Family 27

This family has 2 affected male siblings (F27:S1 and F27:S2) currently aged 15 and 11.5 years old, born to consanguineous parents of Punjabi origin. Both affected siblings were born full-

term after uneventful pregnancies. They both had severe GDD with independent walking acquired only at age 4 (F27:S1) and 3 (F27:S2), severe speech delay, and infantile hypotonia. Sibling F27:S2 developed epileptic seizures from age 9. His seizures recurred 1-2 times a month and have been well-controlled by antiepileptic medication. Their disease is reported to have a progressive course.

On examination at the ages of 15 and 11.5 years, they had moderate-to-severe ID, cerebellar ataxia signs, hypomimia, and hyperkinetic movement disorders. They had impaired smooth pursuit and saccades, upper limb ataxia, lower limb spasticity, and broad-based ataxic gait. The prominent hyperkinetic movement disorder was dystonia involving the neck (antero-laterocollis and torticollis), trunk (camptocormia and Pisa sign), and limbs (predominant dystonia in the right upper and lower limbs). They also had some choreo-dystonic movements in their hands, jerky upper limb tremor, and head titubation. F27:S2 has motor tics involving shoulder shrugging and upper limbs flexion at the elbows accompanied by vocalizations. They both had increased tendon reflexes and upgoing plantar response. Autistic features, aggressive behavior, and obesity were reported in both siblings. Their facial dysmorphic features included bi-frontal narrowing, peri-orbital fullness, arched eyebrows, depressed nasal bridge, full nasal tip, thin upper lip, tall and broad chin in F27:S1, and low anterior hairline, bi-frontal narrowing, strabismus, arched eyebrows, full nasal tip, small mouth, full upper lip, tall and broad chin in F27:S2. Brain MRI in F27:S1 showed callosal hypoplasia with prevalent involvement of the posterior sections, persistent caves verage/cavum septum pellucidum. Anterior commissure hypoplasia, and mild WM volume reduction. Brain MRI in F27:S2 showed callosal hypoplasia with prevalent involvement of the posterior sections and anterior commissure hypoplasia.

Family 28

This family presents with two affected siblings originating from a non-consanguineous Thai family. The older affected sibling is a 25-year-old female (F27:S1) who was born at term and

later presented with GDD/ID, speech impairment, spastic-ataxic gait, and truncal dystonia. She has behavioral abnormalities including autism, aggression, and temper tantrums. She has coarse facial features with deep-set eyes, USPFs, a broad nose with a depressed nasal bridge, and an everted lower lip. Her current body weight is 111 kg. CT brain report showed mild diffuse brain atrophy and diffuse thickened cranial vault. Her 22-year-old affected brother (F27:S2) had a similar developmental history and clinical presentation. Additionally, he had an asymmetric spastic-dystonic gait.

SUPPLEMENTARY VIDEO FROM PATIENTS (back)

Legends

Available for 21/35 affected individuals as mp4 files via this link: https://www.dropbox.com/scl/fo/cwy1eqwgqxhcltrknd0f8/h?dl=0&rlkey=zmvm36wrpxmio2z7liu10mpa6 and https://doi.org/10.6084/m9.figshare.25436116.v1

Supplementary video 1.

This video shows the affected siblings from Family 1.

Segment 1. The video shows the proband F1:S1, a 37-year-old female. She has signs of progeria, a pseudobulbar smile, limited speaking, mild hypomimia, dysarthria, and preserved perceptive language. Her eye movement is suggestive of a slow and reduced upgaze.

Segment 2. The video displays a 22-year-old affected sibling from Family 1 (F1:S2). He has intact perceptive language, impaired speech, mild hypomimia, and stooped posture upon sitting.

Segment 3. The video shows F1:S3, the 20-year-old youngest affected sibling. He is wheelchair-bound and has excessive drooling, stooped posture, involuntary head twitching, and

jerky movements in the right shoulder and upper limb (simple motor tics) accompanied by simple vocal tics. He has urinary incontinence; hence he is in his nappies.

Segment 4. Shows the ambulation of all siblings from Family 1. They have short stature. F1:S3 ambulates in the wheelchair with a stooped body posture. F1:S1 and F1:S2 have significantly stooped body postures and broad-based clumsy gait. F1: S1 has additional lateral body flexion and some freezing of the gait upon passing through the doorway with a suggestion of left lower limb dystonia.

Supplementary video 2

This video shows the affected siblings from Family 3.

F3:S1 shows significant camptocormia and body flexion to the right, mild hypomimia, some dystonic head tremor, slow movements, right leg dystonia, shuffling, and unstable gait.

F3:S2 shows a forward-bent posture with a broad-based gait and tic-like vocalizations.

Supplementary video 3

The video shows the 6-year-old proband from Family 5 (F5:S1) who has a broad-based gait.

Supplementary video 4

This video shows affected cousins from Family 6 (F6:S1 and F6:S2).

For case F6:S1

Segment 1 shows mild retro- and torticollis with dystonic head tremor, preserved perceptive language, a pseudobulbar smile, mild hypomimia, and dysarthric speech.

Segment 2 shows dystonic head tremor and right upper limb dystonic posturing with jerky myoclonic tremor, and signs of negative myoclonus.

Segment 3 shows broad-based walking with right foot dystonia, foot dragging, and a mild episodic dystonic tremor in the right leg.

For case F6:S2

Segment 1 shows some unsteady gait.

Segments 2-4 show F6:S2 2 years later.

Segment 2 shows twitching of the left angle of the mouth and a pseudobulbar smile.

Segment 3 shows stooped and slightly laterally flexed body posture.

Segment 3 shows progressed gait impairment: a broad-based slow and unstable gait, suggestion of head titubation.

Supplementary video 5

This video shows the affected siblings F7:S2 and F7:S1 from Family 7.

F7:S2 shows mild head titubation, perioral dyskinesia, choreo-dystonia in the upper limbs, and a clumsy gait.

F7:S1 has hypomimia.

Supplementary video 6

The video displays the affected 8-year-old girl (F8:S1) and the 6-year-old boy (F8:S2) from Family 8. F8:S1 shows a broad-based clumsy gait, slow movements, simple motor (shoulder shrugging) tics accompanied by vocal tics, and hand stereotypies. The boy has a stooped body posture, clumsy gait, vocal tics, and hand stereotypies (including head touching).

Supplementary video 7

This video shows the affected siblings from Family 10 (F10:S1 and F10:S2)

For case F10:S1

Segment 1 shows a pseudobulbar smile and a suggestion of reduced upgaze.

Segment 2 shows a broad-based clumsy gait upon assistance with dragging her left foot most, likely due to asymmetric lower limb dystonia, and a suggestion of mild lower limb spasticity.

For F10:S2

Segment 1 shows a jerky right upper limb myoclonic tremor and a whole-body jerky tremor.

Segment 2 shows a broad-based gait with a slightly stooped body posture.

Supplementary video 8

This video shows the 20-year-old proband from Family 11 (F11:S1).

Segment 1. He looks older than his biological age, has limited speech, and does not follow verbal instructions. He has a dystonic head tremor, cerebellar tremor in the upper limbs, myoclonic jerks in the right upper limb, and opisthotonic movement.

Segment 2. The video shows a broad-based clumsy gait and jerky movements in the upper limbs. His body is stooped and flexed laterally.

Supplementary video 9

This video shows the 11-year-old proband from Family 13 (F13:S1).

Segment 1 shows strabismus, generalized fine jerky tremor in the upper (more prominent) and lower limbs, very asymmetric lower limb dystonia (left lower limb dystonia with dystonic posturing in the left foot) dragging of the left foot on walking, short probable voluntary flexion of the body, vocal tics accompanied with jerky shoulder abduction, some hand stereotypies, and clumsy gait.

Segment 2 shows stooped body posture, jerky upper limb tremor, and hand stereotypies (touching the head).

Segment 3 shows jerky tremor in all limbs, slightly increased muscle tone, dystonia in the big toes, and increased deep tendon reflexes at the knee in the left leg.

Supplementary video 10

This video shows the 7-year-old proband from Family 15 (F15:S1).

The video shows laterocollis, slight head tremor, unsteady gait, and hand stereotypies

Supplementary video 11

This video shows twins from Family 19 (S1 and S2), currently aged 5.5 years old. F19:S1 has a slightly hypomimic face and mild hypokinesia. They are non-verbal and very subtle perioral twitching can be noticed in F19:S2.

Supplementary video 12

This video shows the affected siblings from Family 20 F20:S1 and F20:S2 aged 17 and 8 years old, respectively.

For F20:S1 the video shows an inability to stand independently due to postural instability and hypotonia, foot deformities, lower limb hypotonia with periodic myoclonic jerks, predominantly in the lower limbs, stooped body posture, drooling, a pseudobulbar smile, preserved perceptive language.

For F20:S2 the video shows an inability to stand independently, foot deformities, lower limb hypotonia, stooped body posture, simple vocal and motor tics, stereotypies in the upper limbs and body rocking stereotypies, and a pseudobulbar smile.

Supplementary video 13

This video shows the proband of family 16 who has choreo-dystonia in her hands, she is unable to stand up independently and has a wide-based clumsy gait.

Supplementary video 14

Shows siblings from Family 27

F27:S1. Segment 1 shows mild hypomimia, head tremor, torticollis to the left, antero-laterocollis when sitting, and jerky movements in the left arm. He needs to use his left arm to stand up from the chair.

Segment 2 shows F27:S1 a few years later. He has marked hypomimia, camptocormia, broad-based ataxic gait, chorea-dystonic movements in both hands, some posturing of the right arm, and dystonic right leg. There is probable spasticity in the right leg.

F27:S1. Segment 1 shows mild hypomimia, antero-laterocollis, stopped posture with a slight lateroflexion of the body to the right, some posturing of the right hand on walking, head tremor, and broad-based gait.

Segment 2. F27:S1 a few years later shows broad-based ataxic gait, stooped posture, head titubation, probable motor tics in the upper limbs accompanied by vocalization, jerks in the right upper limbs, dystonia in the right upper and lower limbs with dystonic posturing of the right hand and foot. There is a suggestion of a tight Achilles tendon on the right foot.

Supplementary video 15

The video shows the affected siblings from Family 12.

F12:S1 shows dysmorphic facial features, slightly stooped body posture, and motor tics in shoulders accompanied by vocalization.

F12:S2 shows dysmorphic facial features, obesity, hyperlordosis in the lower back, and left leg spasticity with probable dystonia.

Supplementary video 16

Shows the affected siblings from Family 28

F27:S1 is walking with a stopped posture and lateroflexion to the left. She slightly drags her left foot. Some hypomimia could be appreciated from the lower part of the face. The position of her left-hand fingers is suggestive of dystonia.

F27:S2 is showing vocal tics, leg spasticity upon walking which is more prominent on the left, impaired hand dexterity on the right, probably due to dystonia, and arm waiving stereotypies.

SUPPLEMENTARY VIDEO RECORDINGS FROM ZEBRAFISH MODELS

Legends

Supplementary videos 17 and 18

These videos show the social behavior of a pair of 8-month-old zebrafish with either *acbd6*+/+ (Supplementary video 17) or *acbd6*-/- (Supplementary video 18) genotypes.

SUPPLEMENTARY VIDEO RECORDINGS FROM *X. TROPICALIS* MODELS

Legends

Supplementary videos 19 and 20 show wild-type tadpoles movements and Supplementary videos 21 and 22 shows *acbd6* crispant tadpole movements.

Wild-type or acbd6 crispant tadpoles were placed into 6-well plates and their movement tracked for 10 minutes using a Zantiks MWP. Comparing the movement of control and *acbd6* crispant

tadpoles showed that the crispants to move less over a 10-minute period (average 2.37 mm/s for controls and 1.01 mm/s for crispants, n = 50). The difference was statistically significant ($t(78)=4.9$, $p=<0.001$)

SUPPLEMENTARY REFERENCES (back)

Literature for WES analysis and variant filtering in Supplementary Table 1

Bertoli-Avella AM, Beetz C, Ameziane N, et al. Successful application of genome sequencing in a diagnostic setting: 1007 index cases from a clinically heterogeneous cohort. Eur J Hum Genet. 2021;29(1):141-153.

Makrythanasis P, Maroofian R, Stray-Pedersen A, et al. Biallelic variants in KIF14 cause intellectual disability with microcephaly. Eur J Hum Genet. 2018;26(3):330-339.

Soupene E, Schatz UA, Rudnik-Schöneborn S, Kuypers FA. Requirement of the acyl-CoA carrier ACBD6 in myristoylation of proteins: Activation by ligand binding and protein interaction. PLoS One. 2020;15(2):e0229718

Mitani T, Isikay S, Gezdirici A, et al. High prevalence of multilocus pathogenic variation in neurodevelopmental disorders in the Turkish population. Am J Hum Genet. 2021;108(10):1981-2005.

Vetro A, Nielsen HN, Holm R, et al. ATP1A2/A3-collaborators. ATP1A2- and ATP1A3-associated early profound epileptic encephalopathy and polymicrogyria. Brain. 2021; 144(5):1435-1450

Mahler EA, Johannsen J, Tsiakas K, et al. Exome Sequencing in Children. Dtsch Arztebl Int. 2019;116(12):197-204. doi:10.3238/arztebl.2019.0197

Literature Supplementary Table 7

Ebrahimi-Fakhari D, Behne R, Davies AK, Hirst J. AP-4-Associated Hereditary Spastic Paraplegia. 2018 Dec 13. In: Adam MP, Ardinger HH, Pagon RA, Wallace SE, Bean LJH, Gripp KW, Mirzaa GM, Mamiya A, editors. GeneReviews® [Internet]. Seattle (WA): University of Washington, Seattle; 1993–2022

Abdollahpour H, Alawi M, Kortüm F, et al. An AP4B1 frameshift mutation in siblings with intellectual disability and spastic tetraplegia further delineates the AP-4 deficiency syndrome. Eur J Hum Genet. 2015;23(2):256-9.

Abou Jamra R, Philippe O, Raas-Rothschild A, et al. Adaptor protein complex 4 deficiency causes severe autosomal-recessive intellectual disability, progressive spastic paraplegia, shy character, and short stature. Am J Hum Genet. 2011;88(6):788-795.

Moreno-De-Luca A, Helmers SL, Mao H, et al. Adaptor protein complex-4 (AP-4) deficiency causes a novel autosomal recessive cerebral palsy syndrome with microcephaly and intellectual disability. J Med Genet. 2011;48(2):141-4.

Hirst J, Madeo M, Smets K, et al. Complicated spastic paraplegia in patients with AP5Z1 mutations (SPG48). Neurol Genet. 2016;2(5):e98.

Depienne C, Stevanin G, Brice A, Durr A. Hereditary spastic paraplegias: an update. Curr Opin Neurol. 2007;20(6):674-80.

Hedera P. Hereditary Spastic Paraplegia Overview. 2000 Aug 15 [updated 2021 Feb 11]. In: Adam MP, Ardinger HH, Pagon RA, Wallace SE, Bean LJH, Gripp KW, Mirzaa GM, Amemiya A, editors. GeneReviews® [Internet]. Seattle (WA): University of Washington, Seattle; 1993–2022.

Vermeer S, van de Warrenburg BP, Kamsteeg EJ, Brais B, Synofzik M. ARSACS. 2003 Dec 9 [updated 2020 Jan 2]. In: Adam MP, Ardinger HH, Pagon RA, Wallace SE, Bean LJH, Gripp KW, Mirzaa GM, Amemiya A, editors. GeneReviews® [Internet]. Seattle (WA): University of Washington, Seattle; 1993–2022.

Gregory A, Kurian MA, Maher ER, Hogarth P, Hayflick SJ. PLA2G6-Associated Neurodegeneration. 2008 Jun 19 [updated 2017 Mar 23]. In: Adam MP, Ardinger HH, Pagon RA, Wallace SE, Bean LJH, Gripp KW, Mirzaa GM, Amemiya A, editors. GeneReviews® [Internet]. Seattle (WA): University of Washington, Seattle; 1993–2022

Hayflick SJ, Kurian MA, Hogarth P. Neurodegeneration with brain iron accumulation. Handb Clin Neurol. 2018;147:293-305.

Xiromerisiou G, Dadouli K, Marogianni C, et al. A novel homozygous SACS mutation identified by whole exome sequencing-genotype phenotype correlations of all published cases. J Mol Neurosci. 2020;70(1):131-141.

Chelban V, Alsagob M, Kloth K, et al. Genetic and phenotypic characterization of NKX6-2-related spastic ataxia and hypomyelination. Eur J Neurol. 2020;27(2):334-342.

Guo YP, Tang BS, Guo JF. PLA2G6-Associated Neurodegeneration (PLAN): Review of Clinical Phenotypes and Genotypes. Front Neurol. 2018;9:1100.

Padmakumar M, Jaeken J, Ramaekers V, et al. A novel missense variant in SLC18A2 causes recessive brain monoamine vesicular transport disease and absent serotonin in platelets. JIMD Rep. 2019;47(1):9-16.

Weissbach A, Wittke C, Kasten M, Klein C. 'Atypical' Parkinson's disease - genetic. Int Rev Neurobiol. 2019;149:207-235.